Particle models in connection with Kuramoto-Sivashinsky equation

Thanh Tam Phung

PUCVL
Pôle Universités
Centre Val de Loire

UNIVERSITÉ D'ORLÉANS

UNIVERSITE D'ORLEANS

ÉCOLE DOCTORALE Mathématiques, Informatique, Physique Théorique et Ingénierie des Systèmes

LABORATOIRE : MAPMO & GREMI

THÈSE présentée par :

PHUNG Thanh Tam

soutenue le : **06 Juillet 2012**

pour obtenir le grade de : **Docteur de l'université d'Orléans**

Spécialité : **Mathématiques**

Vers un modèle particulaire de l'équation de Kuramoto-Sivashinsky

THÈSE dirigée par :

François JAMES	Professeur, MAPMO, Orléans
Pascal BRAULT	Directeur de Recherche CNRS, GREMI, Orléans

RAPPORTEURS :

Christophe JOSSERAND	Directeur de Recherche CNRS, IJLRDA, Paris 6
Frédéric LAGOUTIERE	Professeur, Laboratoire de Mathématiques, Orsay

---

JURY :

Michel ZINSMEISTER	Professeur, MAPMO, Orléans
Laurent BOUDIN	Maître de Conférence, HDR, LJLL, Paris 6
Christophe JOSSERAND	Directeur de Recherche CNRS, IJLRDA, Paris 6
Frédéric LAGOUTIERE	Professeur, Laboratoire de Mathématiques, Orsay
François JAMES	Professeur, MAPMO, Orléans
Pascal BRAULT	Directeur de Recherche CNRS, GREMI, Orléans

Particle models in connection with Kuramoto-Sivashinsky equation

PHUNG Thanh Tam

December 17, 2012

Contents

Notations and Abbreviations

KS : Kuramoto-Sivashinsky
KPZ : Kardar-Parisi-Zhang
RD : Random deposition
RDR : Random deposition with surface relaxation
BD : Ballistic deposition
$\mathbb{R}$: the set of all real numbers
$\mathbb{Z}$: the set of all integer numbers
$\mathbb{N}$: the set of all natural numbers
L : system size
k : wave number
l_c : typical length scale
$\overline{h}(t)$: mean high of surface
$w(L,t), W(L,t)$: interface width
$h(x,t)$: the height of interface at position x and time t
$u(x,t)$: the velocity field
$\rho(x,t)$: density field
$\rho^{in}(x)$: initial density
$u^{in}(x)$: initial velocity
$m_i(t)$: mass of i-th particle
$x_i(t)$: position of i-th particle
$u_i(t), v_i(t)$: velocity of i-th particle
$p_i(t)$: momentum of i-th particle
$\xi_i(t)$: distance between two particles
N : number of time steps
I : number of particles
$f(x,t), g(X,\tau)$: scaling function

Chapter 1

Introduction to the problem

1.1 Motivation

In this PhD thesis we deal with finding a model of interacting particles on the line that exhibits spatiotemporal chaos and evolution of Kuramoto-Sivashinky (KS) equation. Essentially, the thesis is made up of two parts.

In the first part (Chapter 2 and Chapter 3), we introduce the Rost-Krug model that hold some symmetry and elementary microscopic properties of the one-dimensional KS equation. From this model, simulations are carried out and we consider evolution and average of number of particles. The point is that after considering Rost-Krug model, we can not obtain evidently KS equation. Then we propose the new particle model for KS equation. In Chapter 3 we construct the model and scaling functions then using continuum limit to lead to KS equation. Moreover, we investigate various interesting properties by taking simulation of the model on power spectrum, variance of velocity, interface width, mean square displacement.

In the second part (Chapter 4), we would like to investigate the sticky particle model for viscous pressureless gases. With a discrete system of a finite particles, we obtain estimates of solution in terms of initial velocity.

Let us now review introduction about the root of physical problem of interacting interface and also about Kuramoto-Sivashinsky equation.

1.2 The physical problem

1.2.1 Surface and interface evolutions

Studying the interface in nature has been considered for a long time by various fields of science. It is the essence of growth/evolution of a dynamical system. The following section will introduce a view of surface growth studies with some concepts and examples (refer to [1]).

1.2.1.1 Some examples

Some surfaces are formed as a result of a deposition, propagation or erosion process. Let us see some simple examples [1].
+ Propagation of water: Immersing one paper into color water, water will spread the paper until balance.
+ Propagation of flame fronts: Burning a part of paper, the considered interface is between the burned and unburned parts of paper.
+ Flux lines in a superconductor: In clear superconductor, the flux lines form ordered lattice. In impurity one, the flux lines stretch to get close the impurity sites.
+ Atom deposition: Coating substrate is an important technological issue. Up to date technique vapor phase deposition allows atom by atom film growth.
+ Bacterial growth: The bacterial colonies multiply and become growth with various shape and rough surfaces.

1.2.1.2 Growth process models

In this part, we will introduce some simple growth process models that are described by stochastic equations. Let us consider the surface $h(i,t)$ to be the set of particles that are at highest position in each column i. To quantitatively describe the growth and how rough is the interface, we define two functions
- The *mean height* of surface $\overline{h}(t)$

$$\overline{h}(t) \equiv \frac{1}{L}\sum_{i=1}^{L} h(i,t)$$

where $h(i,t)$ is the height of column i at time t and L is the size of surface.
- The $interface\ width\ w(L,t)$

$$w(L,t) \equiv \sqrt{\frac{1}{L}\sum_{i=1}^{L}[h(i,t) - \overline{h}(t)]^2}.$$

As deposition is going on, the interface is roughening and displays some specific scaling behavior as follows
(a) $w(L,t) \sim t^{\beta}$ where $t \ll t_x$, t_x is *crossover time*, β is *growth exponent*.
$w(L,t_x) \approx w_{sat}(L)$ where $w_{sat}(L)$ is saturation value.
(b) $w_{sat}(L) \sim L^{\alpha}$, α is *roughness exponent*.
(c) $t_x \sim L^z$, $z = \frac{\alpha}{\beta}$ is *dynamic exponent*.
(d) $w(L,t) \sim L^{\alpha} f(\frac{t}{L^z})$, $f(u)$ is *scaling function*, $f(u) \sim u^{\beta}$, if $u \ll 1$ and $f(u) = const$ if $u \gg 1$.
α, β, z characterize the roughness of surface are the important exponents which we expect to determine, for instance, in following models of deposition. We note that the notations α, β here are different from the parameters used in later model for KS equation.

In remaining part of this section, we would like to review three popular simple models issued from the deposition of many particles with typical laws. For each model, there is the experiment that highlights the position of interface at successive time intervals, so that the growth process can be followed qualitatively.

Random deposition(RD): In this model, position of particle is chosen random above the surface. Then it fall vertically and is deposited on the top of column under it. Let $h(i,t)$ be the height of the interface of site $i(i = 1, 2, ..., L)$ at the time t, we have the discrete formula

$$h(i,0) = 0 \quad \text{for all} \quad i$$
$$h(i,t+1) = h(i,t) + 1.$$

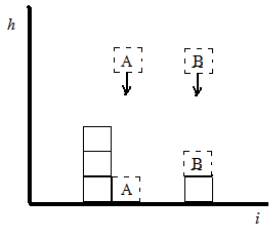

Figure 1.1: Random deposition model

For this model, the growth exponents are determined that $\alpha = \infty, \beta = \frac{1}{2}$ which is suitable with continuum equation

$$\frac{\partial h(x,t)}{\partial t} = F + \eta(x,t)$$

where F is average number of particles arriving at site x. $\eta(x,t)$ is random fluctuations in deposition process such that

$$< \eta(x,t) >= 0$$

$$< \eta(x,t)\eta(x',t') >= 2D\delta^d(x-x')\delta(t-t')$$

Figure 1.2: Random deposition model after depositing 16000 particles on a substrate of size $L = 100$.

Random deposition with surface relaxation (RDR): We choose a random position above the surface and allow a particle to fall vertically toward it. The particle does not stick irreversibly, but rather it can relax to nearest neighbor which has lower height. So, we have the discrete formula

$$h(i,0) = 0 \quad \text{for all} \quad i$$
$$h(i,t+1) = \min\{h(i,t), h(i-1,t), h(i+1,t)\} + 1.$$

The growth exponents of this model are $\alpha = \frac{1}{2}, \beta = \frac{1}{4}, z = 2$. The Edwards-Wilkinson

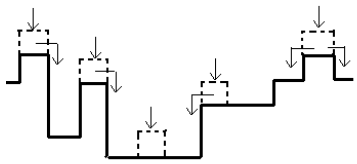

Figure 1.3: Random deposition with surface relaxation model.

equation is the stochastic growth equation that describes this model.

$$\frac{\partial h(x,t)}{\partial t} = \nu \nabla^2 h(x,t) + \eta(x,t)$$

where ν is surface tension and $\nabla h << 1$.

Figure 1.4: The interface after depositing 35000 particles on substrate with size $L = 100$.

Ballistic deposition (BD): A random position above the surface is chosen that allows a particle to fall vertically toward it. The particle sticks to the first side along it trajectory that has an occupied nearest neighbor. So, we have the discrete formula

$$h(i,0) = 0 \quad \text{for all} \quad i$$
$$h(i,t+1) = \max\{h(i,t), h(i-1,t), h(i+1,t)\}.$$

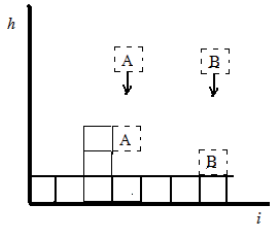

Figure 1.5: Ballistic deposition model.

The growth exponents of this model are $\alpha = \frac{1}{2}, \beta = \frac{1}{3}, z = \frac{3}{2}$. The Kardar-Parisi-Zhang (KPZ) equation is the stochastic growth equation that describes this model.

$$\frac{\partial h(x,t)}{\partial t} = \nu \nabla^2 h(x,t) + \frac{\lambda}{2}(\nabla h(x,t))^2 + \eta(x,t)$$

where ν is surface tension and $\nabla h << 1$.

Figure 1.6: Ballistic deposition model with 35000 particle and length size $L = 200$.

1.2.2 Kuramoto-Sivashinsky equation

1.2.2.1 Introduction

Numerous phenomena are exhibiting self-organisation of structures eventually coupled to some space-time chaotic behavior. Among them, we can cite surface nanostructuration under ion bombardment [22, 23, 24, 25, 26] (see figure 1.7) or flame front evolution [27] (see figure 1.8).

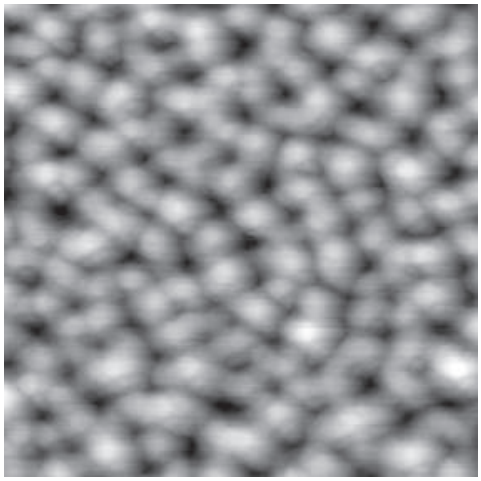

Figure 1.7: Scanning Tunneling Microscopy image of nanostructured Pd surface after ion sputtering. Reproduced from Ref. [22]

For describing such phenomena, the non-linear Kuramoto-Sivashinsky (KS) was first proposed by Kuramoto, Tsizuki, Sivashinsky in the '70s [9, 10, 11, 12, 13, 14]. In one dimension, it takes the form:

$$\partial_t h = \frac{\lambda}{2} |\partial_x h|^2 + \nu_2 \partial_{xx} h + \nu_4 \partial_{xxxx} h, \qquad x \in [0, L], \quad \nu_2, \nu_4 < 0 \tag{1.1}$$

and in the velocity form :

$$\partial_t u = \lambda u \partial_x u + \nu_2 \partial_{xx} u + \nu_4 \partial_{xxxx} u, \qquad x \in [0, L], \quad \nu_2, \nu_4 < 0 \tag{1.2}$$

where $u = -\partial_x h$, and the solutions satisfy periodic boundary conditions. L is the system size.

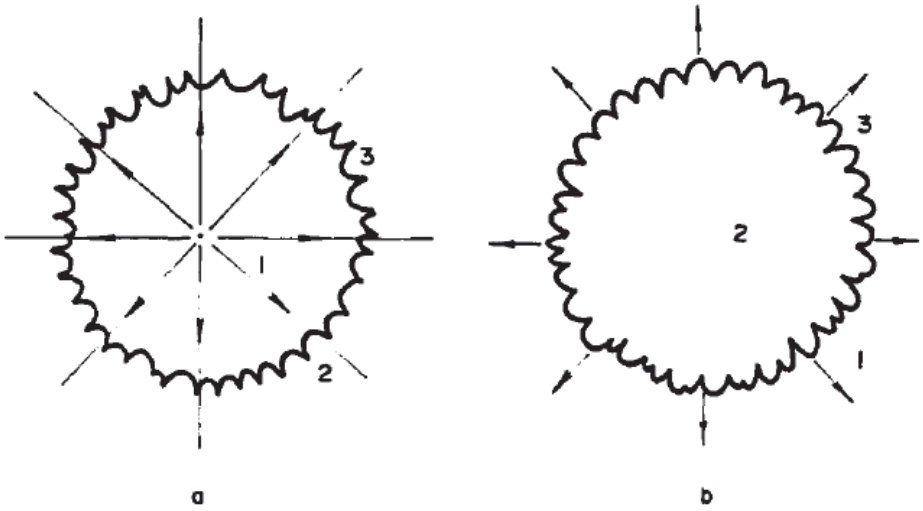

Figure 1.8: (a) Flame stabilized on point source. Arrows indicate direction of gas streamlines. (b) Freely expanding flame. Arrows indicate main direction of motion of front. (1)combustible mixture region; (2) combustion products region; (3) surface of disturbed flame front. Reproduced from Ref. [27]

KS equation is considered as the simplest model that can describe spatio-temporal chaotic systems. 2-dimensional simulation of this equation is reported in figure 1.9.

The KS equation have been studied with various space and time scaling. It can describe instabilities of dissipative trapped ion modes in plasma, instabilities in laminar flame front, phase dynamics in reaction-diffusion systems and fluctuations in fluid films on tilted supports, oscillatory chemical reactions, flow of a thin viscous film along a wall. Moreover, it describes the long-wavelength dynamics [15] at the large length and time scales.

In KS equation, u_{xx} term carries an instability at large scales, u_{xxxx} term makes damping at small scales and the nonlinear term uu_x (the same term as in one-dimensional Navier-Stokes, KPZ and Burgers equation) is crucial for the global stability of the solution and transport energy between large and small scales.Indeed, with periodic boundary condition, the zero solution $u(x,t) = 0$ is linearly unstable growing at rate $\sigma = k^2 - k^4$ to modes with $|k| < k_c = \sqrt{\frac{\nu_2}{\nu_4}}$ [2].

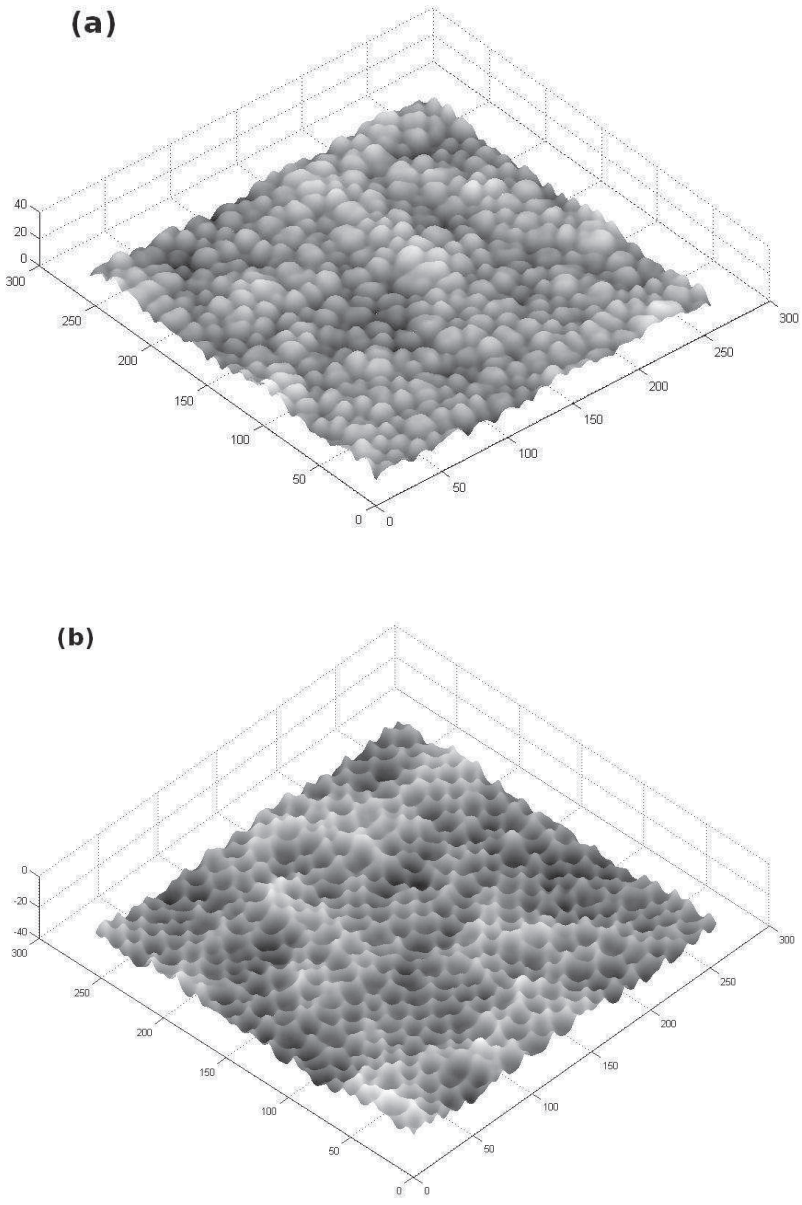

Figure 1.9: (a) KS equation for h(x,y,t) for deposition $\lambda > 0$ (b) KS equation for h(x,y,t) for erosion $\lambda < 0$

1.2.2.2 Solutions of Kuramoto-Sivashinsky equation

The solution of KS equation has two main symmetries. First, it is invariant under arbitrary shifts $h \to h + const$ that is if $h(x,t)$ is the solution of KS equation, then $\widetilde{h}(x,t) = h(x,t) + const$ is also the solution of KS equation. It is easy to see because all terms in equation are the derivative terms. Second, the important symmetry is *Galilean invariance* which is obtained by the nonlinear term. For any constant u_0, if $h(x,t)$ is the KS equation's solution, then the new function defined by

$$\widetilde{h}(x,t) = h(x - u_0 t, t) - u_0 x - \frac{1}{2}u_0^2 t$$

is also the solution of (1.1). The derivatives with respect to t and x for $\widetilde{h}$ are obtained as following

$$\begin{aligned}
\widetilde{h}_t(x,t) &= -u_0 h_x(x - u_0 t, t) + h_t(x - u_0 t, t) - \frac{1}{2}u_0^2 \\
\widetilde{h}_x(x,t) &= h_x(x - u_0 t, t) - u_0 \\
\widetilde{h}_{xx}(x,t) &= h_{xx}(x - u_0 t, t) \\
\widetilde{h}_{xxxx}(x,t) &= h_{xxxx}(x - u_0 t, t).
\end{aligned}$$

Then, let sum these in the form of the KS equation :

$$\begin{aligned}
&\widetilde{h}_t(x,t) + \frac{1}{2}\widetilde{h}_x^2(x,t) + \widetilde{h}_{xx}(x,t) + \widetilde{h}_{xxxx}(x,t) \\
&= -u_0 h_x(x - u_0 t, t) + h_t(x - u_0 t, t) - \frac{1}{2}u_0^2 + \frac{1}{2}(h_x(x - u_0 t, t) - u_0)^2 \\
&+ h_{xx}(x - u_0 t, t) + h_{xxxx}(x - u_0 t, t) \\
&= h_t(x - u_0 t, t) + \frac{1}{2}h_x^2(x - u_0 t, t) + h_{xx}(x - u_0 t, t) + h_{xxxx}(x - u_0 t, t) \\
&= 0.
\end{aligned}$$

In the velocity form, the *Galilean invariance* for $u(x,t)$ is , $\widetilde{u}(x,t) = u(x - u_0, t)$. Physically it means that viewing the fluid from a system of coordinates that moves with velocity u_0 does not change the law of physics.

In Fourier transform, (for example, we take $\nu_2 = \nu_4 = 1$) the equation with periodic boundary condition may be written as

$$\frac{d}{dt}\widehat{u}_k + (k^4 - k^2)\widehat{u}_k + \sum_{k'} ik'\widehat{u}_{k'}\widehat{u}_{k-k'} = 0 \tag{1.3}$$

where

$$\widehat{u}_k(t) = \frac{1}{L}\int_0^L u(x,t)\exp(-ikx)dx, q = \frac{2\pi}{L}, k = nq, n \in \mathbb{Z}, i = \sqrt{-1}$$
$$u(x,t) = \sum_k \widehat{u}_k(t)\exp(ikx).$$

The Fourier transform solutions of (1.1) also satisfy

$$\frac{d}{dt}\widehat{h}_k + (k^4 - k^2)\widehat{h}_k + \frac{1}{2}\sum_{k'} k'(k-k')\widehat{h}_{k'}\widehat{h}_{k-k'} = 0. \tag{1.4}$$

With periodic boundary condition, the zero solution $u(x,t) = 0$ is linearly unstable growing at rate

$$\sigma = k^2 - k^4$$

to modes with $|k| < 1$. However, if system of size $L < 2\pi$, then $k_{min} = \frac{2\pi}{L} > 1$. These modes are so damped modes and $u = 0$ is stable. As the size L increase, the zero solution is unstable leading to bifurcations.

For large scales, the solution has cellular structure with motion of appearing and vanishing cells and cell radius is depending on L [25, 19]. In figure 1.8 and 1.9, the apparence of cell structure is clearly visible. The turbulence in KS essentially is weaker than in Navier-Stokes equation for fluids, that means its time or space averages are not too different from former values.

KS equation is non-integrable. There is no explicit general analytical solution. However, there are many numerical solutions have been studied. It is shown the bounded solutions $u(x,t)$, that is the L^∞ norm $||u||_\infty$ is bounded independent of L which can imply the existence of finite energy density

$$||u||_2^2 = \int_0^L u^2(x,t)dx.$$

For power spectrum,

$$S(k) = L\,\langle||\widehat{u}_k||\rangle$$

where the angular brackets denote average over time t, there are three distinct regimes of the dynamics. It is flat for large scale (small k) and recalls that the solution at this scaling is well-described by a noise-driven Burgers equation or Kardar-Parisi-Zhang (KPZ)

equation for kinetic roughening. There is a hump around $k_c = 1/\sqrt{2}$ which is the most linearly unstable mode and has the spatio-temporal disorder. The Fourier spectrum of those fluctuation is decaying quickly at small scales (large k) an in exponential way. This is related to the dissipative provide by linear terms.

Beside the results are mentioned, there are many extended studies on dynamics and analysis of the Kuramoto-Sivashinsky equation in different length scales, generalization to higher space dimensions , non-periodic boundary condition and the effect of additional terms in equation.

1.2.2.3 Particle models connecting with Kuramoto-Sivashinsky equation

By many important properties of KS equation, it is interesting and useful to find a particle model that exhibits these characteristics. It is interesting, for understanding KS associated phenomena to connect the KS equation with a particle model as suggested by rost and Krug [2]: they follow particle evolving in the velocity field u. They propose a system of interacting particles in an harmonic potential limited to first neighbours in one dimension :

$$\dot{x_i} = u_i, \quad \dot{u_i} = (x_{i-1} - 2x_i + x_{i+1}), \tag{1.5}$$

with collision rules which are not allowing mass conservation, but allowing particle creation when two adjacent particle becomes more separated than a defined length. This length might connected to the typical length of 1.1 $l_c = \frac{2\pi}{k_c} = 2\pi\sqrt{\frac{2\nu_4}{\nu_2}}$.

Moreover, this length is related to the coefficient of equation (1.1) as resulting from balance from unstable erosion ($\nu_2\partial_{xx}u$) and diffusion ($\nu_4\partial_{xxxx}u$) terms when considering, for example, a deposition/erosion process in surface physics. As pointed out by the authors, this particle form is faling in reproducing the partial derivative equation, especially the forth derivative term. Nevertheless, it is reproducing some qualitative macrosopic properties of the KS equation.Moreover using such harmonic potential rather leads to a wave equation rather than KS equation, when using a scaling of the form : $\varepsilon x_i(t) = X(\varepsilon t, \varepsilon i)$ with $\varepsilon \to 0$, ε being the inverse of particle number in the system.

When considering early stages of thin film growth there can exist some typical length associated with clustering phenomena or leading to pattern growth [28, 29]. To recover the quasi-periodic structures without introducing artificially length, we start from the following observation, based on Monte Carlo simulations. Kinetic Monte-Carlo simula-

tions of atom deposition [18], with repulsive 1st and attractive 2nd neighbour interactions, shows that interaction up to the second neighbours results in atom clustering, . Including such 2nd neighbour interaction in Equation (1.5) does not leads to KS equation but also to a wave equation.

While the KS equation also has a velocity form displayed by Equation (1.2), it is interesting to investigate a velocity analog of Equation (1.5) which can be written:

$$\dot{x_i} = v_i \tag{1.6}$$

$$m_i\dot{v_i} = \alpha(v_{i-1} - 2v_i + v_{i+1}) + \beta(v_{i-2} - 2v_i + v_{i+2}) \tag{1.7}$$

where $\alpha > 0, \beta < 0$ are the coefficients of the velocity interactions under dynamics of particles : if 2 particles collide, they will cross over so they exchange their velocity that influences on their acceleration. Hence, the mass is conserved. More details of this model will be exposed in Chapter 3.

1.3 The mathematical problem

1.3.1 Sticky particle model for pressureless gas

A sticky particle model method is studied in many researches. It describes the one-dimensional model of pressureless gases at a discrete level by a finite collection of particles that get stuck together after they collide with conservation of mass and momentum. In particular, if 2 particles collide, they create a single particle, whose mass is the sum of the previous two, and the rate calculated to maintain the momentum.
m

At a continuous level, this scalar conservation laws can be shown to be the pressureless Euler system

$$\begin{cases} \partial_t \rho + \partial_x(\rho u) & = 0 \\ \partial_t(\rho u) + \partial_x(\rho u^2) & = 0 \end{cases} \qquad (x,t) \in \mathbb{R} \times (0, +\infty) \tag{1.8}$$

with the initial condition

$$\begin{cases} \rho(x,0) & = \rho^{in}(x) \\ u(x,0) & = u^{in}(x) \end{cases} \tag{1.9}$$

where $\rho(t,x)$ is density field and $u(t,x)$ velocity field. The first equation is for the conservation of mass and the second one for momentum.

For smooth solutions of (1.8), we can obtain the inviscid Burgers equation

$$\partial_t u + \partial_x \left(\frac{u^2}{2} \right) = 0. \tag{1.10}$$

and the solutions satisfy initial condition

$$u(x,0) = u^{in}(x)$$

However, the smooth solutions of the invisced Burgers equation are not suitable for general data. The obvious question is that how to find the correct solutions of this system, first for approximate solutions. This problem have been investigated in many contributions. Bouchut's approach in [3] is to construct exact solutions, with nonnegative ρ and a well-defined velocity field u deduced from momentum $q = \rho u$, in case of particles system and of Riemann problem with special initial data and these solution satisfy the entropy conditions

$$\partial_t \left(\rho U(u) \right) + \partial_x \left(\rho u U(u) \right) \leq 0 \tag{1.11}$$

for all smooth convex functions U.

After that, Grenier [31] and Rykov, Weinan, Sinai [32] proved the global exsistence of measure solutions of system (1.8, 1.9, 1.11) by taking the limits of the discrete particle evolution ρ_n when the number of particles tends to $+\infty$ with bounded mass and initial velocities. Brenier and Grenier [4] then improved this approach with nondecreasing initial condition and general fluxes. We also refer the other approaches by Bouchut and James [33], Poupaud and Rascle [34], Sever [35], Berthelin [5]. The following section introduces the model for the viscous version.

1.3.2 The new sticky particle model for pressureless gases dynamics with small viscosity

A further step is reached in including a viscous term in the Euler system (1.8) [21, 36]. A new sticky particle model, in which we consider interaction force between particles, is proposed in Chapter 4. From this model, we can recover to the system dynamics of pressureless gases with viscosity

$$\begin{cases} \partial_t \rho + \partial_x(\rho u) & = 0 \\ \partial_t(\rho u) + \partial_x(\rho u^2) & = \alpha \partial_{xx} u(t,x) \end{cases} \qquad (x,t) \in \mathbb{R} \times (0,+\infty) \tag{1.12}$$

with the initial condition (1.9).

Chapter 2

The previous particle models concern KS equation

2.1 Introduction

In physics, the motion of particles describe the physical phenomena involved in solid, liquid and gas phases. In this thesis, we consider the motion of N particles in one-dimension line. The particles usually are numbered by integer i, $i = 1, ..., N$ such that the position of particle $x_i < x_j$ then $i < j$. We also label $P_i(t) = (m_i(t), x_i(t), v_i(t), m_i(t)\dot{v}_i(t))$ for each element with its mass, position, velocity and affection force, where $\dot{v}_i(t)$ is the time derivative of $v_i(t)$ and $t \geq 0$. We have definition of momentum of particle $p_i(t) = m_i(t)v_i(t)$.

In the dynamical system, the particles move with initial condition $P_i(0) = (m_i, x_i, v_i, m_i\dot{v}_i)$, with $x_1 < ... < x_n$. The system obeys mass conservation if

$$\sum_{i=1}^{n} m_i = \sum_{i=1}^{n} m_i(t), \quad \text{for} \quad t \geq 0,$$

and momentum conservation if

$$\sum_{i=1}^{n} m_i v_i = \sum_{i=1}^{n} m_i(t)v_i(t), \quad \text{for} \quad t \geq 0.$$

When particle has collision, that makes a shock and its velocity may change. In sticky particle model, when shocks occur, the particles which have the same position will stick together into one particle. The velocity of this particle is defined such that it satisfies

momentum conservation. More details are reported in the section of sticky particle model for pressureless gas dynamics.

2.2 Rost-Krug model

2.2.1 Introduction

We consider a dynamical particle model proposed by Rost, Krug [2]. The particles move on the line and exhibits spatiotemporal chaotic motion described by the Kuramoto-Sivashinsky(KS) equation. It has some symmetry properties of the one-dimensional KS equation.

Let us label the particles by an integer number i, for each particle:
- Mass : $m_i(t) = m = 1$
- Position at time t : $x_i(t)$
- Momentum at time t : $p_i(t)$. Note that since $m_i(t) = 1$ for all time, $p_i(t)$ is velocity, too.
- Distance between two particles : $\xi_i(t) = x_i(t) - x_{i-1}(t) \in [0, 1)$
- Velocity at time t : $u(x_i(t), t) = p_i(t)$

Moreover, the velocity field $u(x, t)$ is defined as a sequence of straight lines connecting the points $(x_i(t), p_i(t))$

$$u(x,t) = \frac{p_i(t)(x - x_{i-1}(t)) + p_{i-1}(t)(x_i(t) - x)}{x_i(t) - x_{i-1}(t)},\ x \in [x_{i-1}(t), x_i(t)) \tag{2.1}$$

then, we have $u(x_i(t), t) = p_i(t)$.

Within this model, two cases occur :

- The collision is the case that when $x_i(t) = x_{i-1}(t)$, two neighboring particles colliding and then being replaced by a new particle ($m = 1$) at the position $x(t) = x_i(t) = x_{i-1}(t)$ with the new velocity

$$p(t) = \frac{\xi_{i-1}(t)p_{i-1}(t) + \xi_{i+1}(t)p_i(t)}{\xi_{i-1}(t) + \xi_{i+1}(t)}.$$

- Case of creation is that when $\xi_i(t) = x_i(t) - x_{i-1}(t) = 1$, two adjacent particles reaches a maximal distance and then the new particle is created at the position $x(t) = \frac{x_{i-1}(t)+x_i(t)}{2}$ with the new velocity

$$p(t) = \frac{p_{i-1}(t) + p_i(t)}{2}.$$

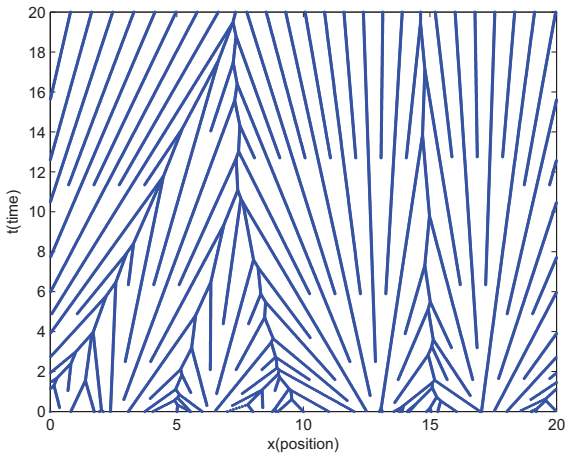

Figure 2.1: Example of the particle trajectories with periodic boundary condition.

2.2.2 The new momenta

The new momenta of particles in two cases are given by following lemma.

Lemma 2.2.1. *For all a, b, in the both cases,* $\int_a^b u(x,t)dx$ *is unchanged if only if the new momentums are*

$$p = \frac{\xi_{i-1}p_{i-1} + \xi_{i+1}p_i}{\xi_{i-1} + \xi_{i+1}} \qquad \textit{in case of collision} \tag{2.2}$$

$$p = \beta p_{i-1} + (1-\beta)p_i \qquad \textit{in case of creation.} \tag{2.3}$$

In Rost-Krug model, $\beta = \frac{1}{2}$.

Proof.

- Assume that (2.1) and (2.2). For each $a < b$, let $a = x_{ia}, b = x_{ib}$. We have

$$\int_{x_{i-1}}^{x_i} u(x,t)dx = \frac{1}{2}(x_i - x_{i-1})(p_i + p_{i+1}),$$

then,

$$\int_{x_{ia}}^{x_{ib}} u(x,t)dx = \frac{1}{2}\sum_{i=ia+1}^{i=ib}(x_i - x_{i-1})(p_i + p_{i+1})$$

In the case of creation, we have $p = \beta p_{i-1} + (1-\beta)p_i$ and $x = \beta x_{i-1} + (1-\beta)x_i$. So (p, x) lies on the previous line segment from (x_{i-1}, p_{i-1}) to (x_i, p_i). Therefore $u(x,t)$ is unchanged on $[x_{i-1}, x_i)$

In the case of collision, we have $(x = x_i = x_{i-1})$. Let us consider the integral of $u(x,t)$ before replacing new particle

$$\begin{aligned}\int_{x_{i-2}}^{x_{i+1}} u(x,t)dx &= \frac{1}{2}(x_{i-1} - x_{i-2})(p_{i-2} + p_{i-1}) + \frac{1}{2}(x_{i+1} - x_i)(p_i + p_{i+1}) \\ &= \frac{1}{2}\xi_{i-1}(p_{i-2} + p_{i-1}) + \frac{1}{2}\xi_{i+1}(p_i + p_{i+1})\end{aligned}$$

and after replacing new particle

$$\begin{aligned}
\int_{x_{i-2}}^{x_{i+1}} u(x,t)dx &= \frac{1}{2}(x-x_{i-2})(p_{i-2}+p) + \frac{1}{2}(x_{i+1}-x)(p+p_{i+1}) \\
&= \frac{1}{2}\xi_{i-1}(p_{i-2} + \frac{\xi_{i-1}p_{i-1}+\xi_{i+1}p_i}{\xi_{i-1}+\xi_{i+1}}) \\
&\quad + \frac{1}{2}\xi_{i+1}(\frac{\xi_{i-1}p_{i-1}+\xi_{i+1}p_i}{\xi_{i-1}+\xi_{i+1}} + p_{i+1}) \\
&= \frac{1}{2}\xi_{i-1}p_{i-2} + \frac{1}{2}\left(\frac{\xi_{i-1}^2 p_{i-1} + \xi_{i-1}\xi_{i+1}p_i}{\xi_{i-1}+\xi_{i+1}}\right) + \frac{1}{2}\xi_{i+1}p_{i+1} \\
&\quad + \frac{1}{2}\left(\frac{\xi_{i-1}\xi_{i+1}p_{i-1} + \xi_{i+1}^2 p_i}{\xi_{i-1}+\xi_{i+1}}\right) \\
&= \frac{1}{2}\xi_{i-1}p_{i-2} + \frac{1}{2}\xi_{i-1}p_{i-1} + \frac{1}{2}\xi_{i+1}p_i + \frac{1}{2}\xi_{i+1}p_{i+1} \\
&= \frac{1}{2}\xi_{i-1}(p_{i-2}+p_{i-1}) + \frac{1}{2}\xi_{i+1}(p_i+p_{i+1}).
\end{aligned}$$

Hence, $\int_{x_{ia}}^{x_{ib}} u(x,t)dx$ is unchanged.

- Assume that for all a, b, in both cases $\int_{x_{ia}}^{x_{ib}} u(x,t)dx$ is unchanged.

In the case of creation, $x = \beta x_{i-1} + (1-\beta)x_i$. We have before creating new particle

$$\int_{x_{i-1}}^{x_i} u(x,t)dx = \frac{1}{2}(x_i - x_{i-1})(p_i + p_{i+1})$$

and after creation

$$\int_{x_{i-1}}^{x_i} u(x,t)dx = \frac{1}{2}(x-x_{i-1})(p_{i-1}+p) + \frac{1}{2}(x_i - x)(p_i + p).$$

Since $\int_{x_{ia}}^{x_{ib}} u(x,t)dx$ is unchanged, we get

$$(x_i - x_{i-1})(p_i + p_{i+1}) = (x-x_{i-1})(p_{i-1}+p) + (x_i - x)(p_i + p).$$

Notice that $x = \beta x_{i-1} + (1-\beta)x_i$, then

$$\begin{aligned}
(x_i - x_{i-1})(p_i + p_{i+1}) &= (1-\beta)(x_i - x_{i-1})(p_{i-1}+p) + \beta(x_i - x_{i-1})(p_i + p) \\
p_i + p_{i+1} &= (1-\beta)(p_{i-1}+p) + \beta(p_i + p) \\
p &= (1-\beta)p_i + \beta p_{i-1}
\end{aligned}$$

In the case of collision, $x_i = x_{i-1}$. We have before collision

$$\int_{x_{i-2}}^{x_{i+1}} u(x,t)dx = \frac{1}{2}\xi_{i-1}(p_{i-2}+p_{i-1}) + \frac{1}{2}\xi_{i+1}(p_i+p_{i+1})$$

and after collision

$$\int_{x_{i-2}}^{x_{i+1}} u(x,t)dx = \frac{1}{2}\xi_{i-1}(p_{i-2}+p) + \frac{1}{2}\xi_{i+1}(p+p_{i+1}).$$

Since $\int_{x_{ia}}^{x_{ib}} u(x,t)dx$ is unchanged, so

$$\begin{aligned}\xi_{i-1}(p_{i-2}+p_{i-1}) + \xi_{i+1}(p_i+p_{i+1}) &= \xi_{i-1}(p_{i-2}+p) + \xi_{i+1}(p+p_{i+1})\\ \xi_{i-1}p_{i-1} + \xi_{i+1} &= \xi_{i-1}p + \xi_{i+1}p\\ p &= \frac{\xi_{i-1}p_{i-1} + \xi_{i+1}p_i}{\xi_{i-1}+\xi_{i+1}}.\end{aligned}$$

□

2.2.3 Particle model for Burgers' equation

2.2.3.1 Burgers' equation

First, we introduce the simple model that connects the constructed model with Burgers' equation.

There are some conditions within this model:

- without acceleration ($\ddot{x}_i = 0$)
- $m_i = 1$
- $\dot{x}_i = p_i, \dot{p}_i = 0$
- velocity field $u(x,t)$

$$u(x,t) = \frac{p_i(t)(x - x_{i-1}(t)) + p_{i-1}(t)(x_i(t) - x)}{x_i(t) - x_{i-1}(t)}, \qquad \forall x \in [x_{i-1}(t), x_i(t))$$

In case of no collision and no creation, taking the derivative with respect to time $u(x,t)$, we have

$$\begin{aligned}u_t(x,t) = &\frac{(x_i(t) - x_{i-1}(t))\left[\dot{p}_i(t)x - \dot{p}_i(t)x_{i-1}(t) - p_i(t)\dot{x}_{i-1}(t)\right]}{\left[x_i(t) - x_{i-1}(t)\right]^2}\\ &+ \frac{(x_i(t) - x_{i-1}(t))\left[\dot{p}_{i-1}(t)x_i(t) + p_{i-1}(t)\dot{x}_i(t) - \dot{p}_{i-1}(t)x\right]}{\left[x_i(t) - x_{i-1}(t)\right]^2}\\ &- \frac{(\dot{x}_i(t) - \dot{x}_{i-1}(t))\left[p_i(t)(x - x_{i-1}(t)) + p_{i-1}(t)(x_i(t) - x)\right]}{\left[x_i(t) - x_{i-1}(t)\right]^2}\end{aligned}$$

Since $\dot{p}_i = 0$, then

$$u_t(x,t) = \frac{[-p_i(t)\dot{x}_{i-1}(t)]}{x_i(t) - x_{i-1}(t)} + \frac{[p_{i-1}(t)\dot{x}_i(t)]}{x_i(t) - x_{i-1}(t)} - \frac{(\dot{x}_i(t) - \dot{x}_{i-1}(t))}{x_i(t) - x_{i-1}(t)}u(x,t)$$

and $\dot{x}_i = p_i$, so

$$\begin{aligned} u_t(x,t) &= \frac{-p_i(t)p_{i-1}(t)}{x_i(t) - x_{i-1}(t)} + \frac{p_{i-1}(t)p_i(t)}{x_i(t) - x_{i-1}(t)} - \frac{\dot{x}_i(t) - \dot{x}_{i-1}(t)}{x_i(t) - x_{i-1}(t)}u(x,t) \\ &= -\frac{\dot{x}_i(t) - \dot{x}_{i-1}(t)}{x_i(t) - x_{i-1}(t)}u(x,t) \end{aligned}$$

Moreover, we have

$$\partial_x u(x,t) = \frac{p_i(t) - p_{i-1}(t)}{x_i(t) - x_{i-1}(t)} = \frac{\dot{x}_i(t) - \dot{x}_{i-1}(t)}{x_i(t) - x_{i-1}(t)}$$

At the result,

$$u_t(x,t) = -\partial_x u(x,t)u(x,t)$$

or

$$u_t(x,t) + \partial_x u(x,t)u(x,t) = 0 \quad \text{(Burgers's equation)} \tag{2.4}$$

2.2.3.2 The particle trajectories

By using Matlab, we obtain a typical portrait of the particle trajectories in the model for Burgers' equation. The idea for constructing this program is explained in appendix. The particle momenta at starting ($t = 0$) are $1, -1, 1, -1, ...$ Notice that there is periodic boundary conditions, so the velocities are the same at the boundary. Then, we also see the momenta of these particles and their height in two later figures. In this example, we put $\alpha = 1$.

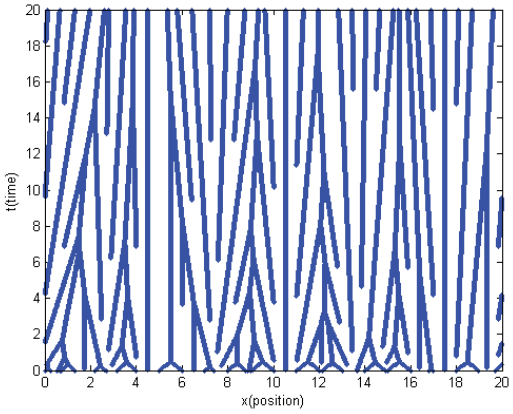

Figure 2.2: The particle trajectories in model for Burgers' equation.

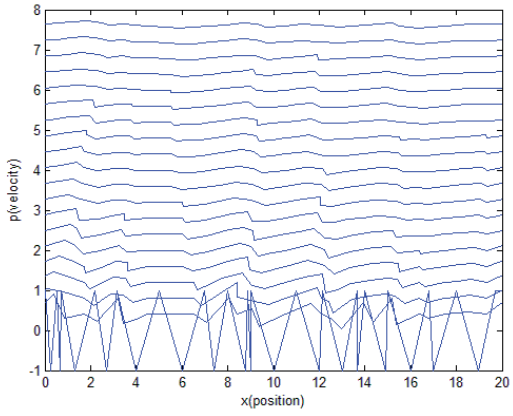

Figure 2.3: The velocity for the same numerical simulation.

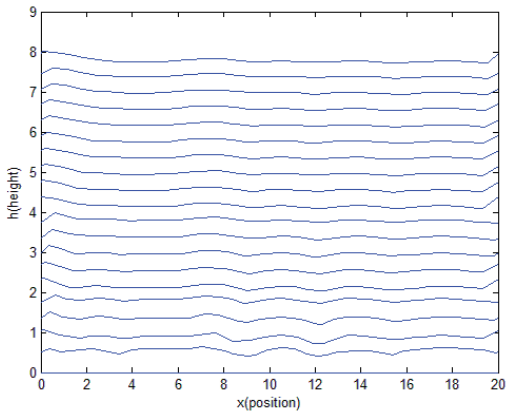

Figure 2.4: And the height function $h(x,t)$.

We have above three figures show trajectories, the velocity field and interface height. The figure 2.2 displays the particles move straight until they have collision. The velocity field in figure 2.3 has relaxation after collision, then it tends to constant after time.

2.2.4 The chaotic particle model

2.2.4.1 Some characteristics of the chaotic particle model

In this model, there are some characteristics:
- $m_i = 1$
- $\dot{x}_i = p_i$
- The force $\dot{p}_i = \xi_i - \xi_{i+1} = (x_i - x_{i-1}) - (x_{i+1} - x_i) = 2x_i - x_{i-1} - x_{i+1}$
- And the velocity field $u(x,t)$

$$u(x,t) = \frac{p_i(t)(x - x_{i-1}(t)) + p_{i-1}(t)(x_i(t) - x)}{x_i(t) - x_{i-1}(t)}, \qquad \forall x \in [x_{i-1}(t), x_i(t))$$

In case of no collision and no creation, taking the derivative with respect to time $u(x,t)$, we have

$$u_t(x,t) = \frac{\dot{p}_i(t)(x - x_{i-1}(t)) - p_i(t)\dot{x}_{i-1}(t) + \dot{p}_{i-1}(t)(x_i(t) - x) + p_{i-1}(t)\dot{x}_i(t)}{x_i(t) - x_{i-1}(t)} - \partial_x u(x,t)u(x,t)$$

or

$$u_t(x,t) + \partial_x u(x,t)u(x,t) = \frac{\dot{p}_i(t)(x - x_{i-1}(t)) + \dot{p}_{i-1}(t)(x_i(t) - x)}{x_i(t) - x_{i-1}(t)} \tag{2.5}$$

2.2.4.2 The particle trajectories

In this section, The particle trajectories are characterized. At $t = 0$, the momenta are zeros. Notice that there is periodic boundary conditions,thus $u(0,t) = u(L,t)$. Then, we also see the momenta of these particles and their height in two later figures. Let momenta be zero at $t = 0$.

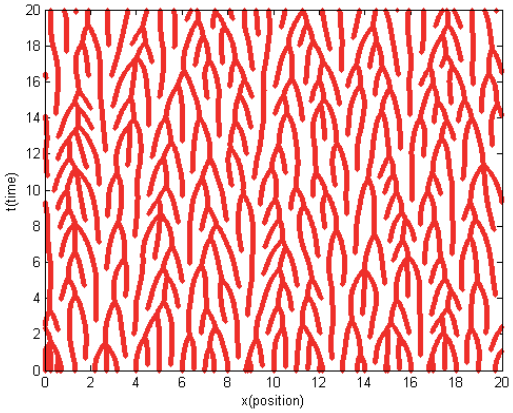

Figure 2.5: The particle trajectories in chaotic model.

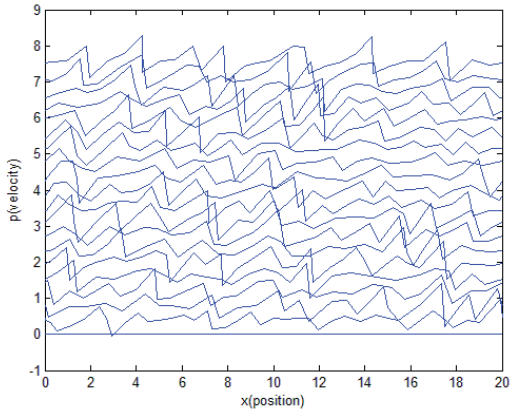

Figure 2.6: The velocity of particles in chaotic model.

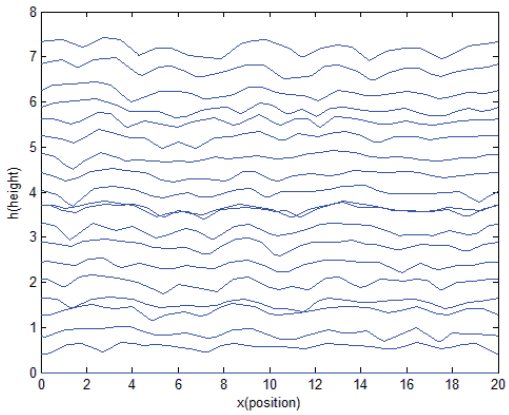

Figure 2.7: The interface height of particles in chaotic model.

The particles trajectories were identified as the minimum points of cellular structures in KS equation. The velocity is unstable under the repulsive force and the interface height shows cellular characteristic.

2.2.5 Simulation on number of particles

2.2.5.1 Number of particles in the model for Burgers equation

In the model was constructed, we see that there are two cases may occur, the case of creation and the case of collision. Therefore, the number of particles in this model may be changed according to time or not have conservation. We watched for what happened with particles in above section and following is estimation the number of these particles at time by time $N(t)$.

We put α to be the distance for case of creation, L to be is a part of length's box (notice that there is periodic boundary condition, so the same phenomenon at the left and the right box), $N0$ is number of particles at time $t = 0$ or number of particles at starting, $N(0)$, $P0$ is momenta of these particles at starting.

Now we consider some examples for different values of α. In the model, we begin with $N0$ particles and $P0 = (1, -1, 1, -1, ...)$ and consider for the time being $T = 30$ and $L = 20$.

Example 1 This is the case for $\alpha = 1$. Some following figures show the number of particles in the model for Burgers equation according to time.

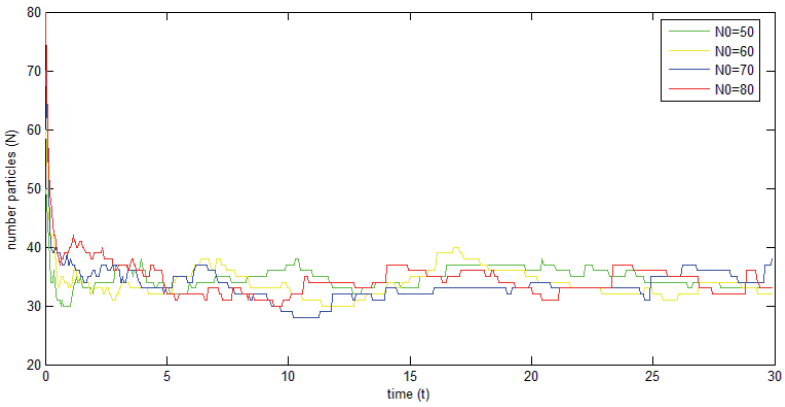

Figure 2.8: The number of particles in the model for Burgers equation with $N0 = 50, 60, 70, 80$.

We can see that, although starting with many or less than of particles, we also have $N(30) \in [29, 38]$ at the end. So we can hope that the number of particles will be around in small interval after a long time (oscillate but be stable in this interval). We continue to consider some similar examples with α smaller and see what we hope if it is real.

Example 2 This is the case for $\alpha = 0.9$. Some following figures show the number of particles in the model for Burgers equation according to time.

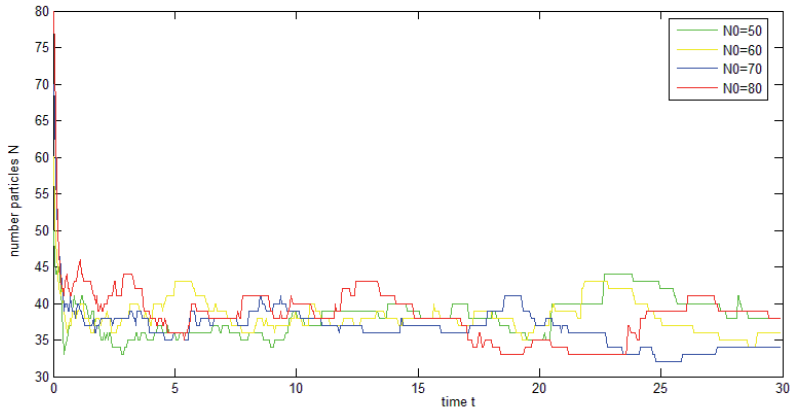

Figure 2.9: The number of particles in the model for Burgers equation with $N0 = 50, 60, 70, 80$.

In this example, we also have $N(30) \in [34, 38]$ at the end. The final number of particle does not depend on the initial number of particle.

Example 3 This is the case for $\alpha = 0.7$. Some following figures show the number of particles in the model for Burgers equation according to time.

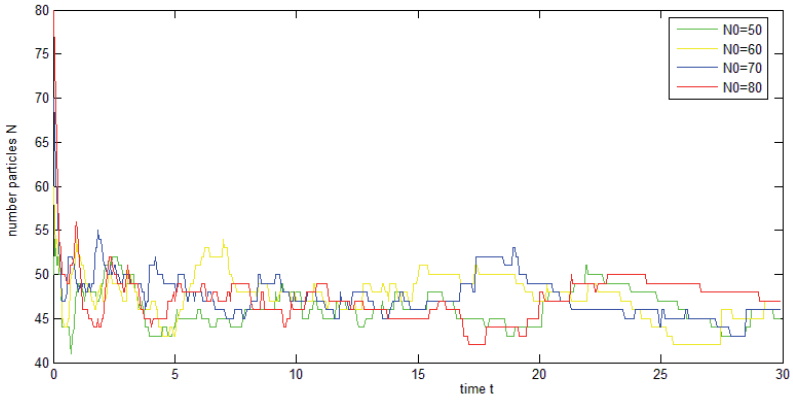

Figure 2.10: The number of particles in the model for Burgers equation with $N0 = 50, 60, 70, 80$.

In this example, we also have $N(30) \in [42, 47]$ at the end.

Example 4 This is the case for $\alpha = 0.5$. Some following figures show the number of particles in the model for Burgers equation according to time.

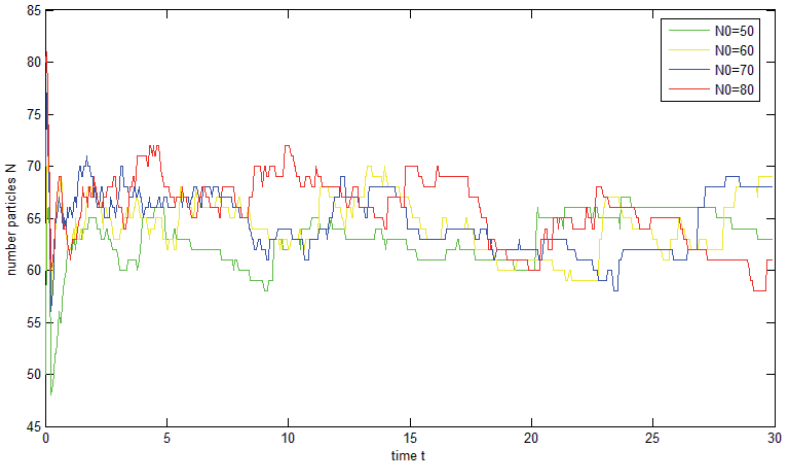

Figure 2.11: The number of particles in the model for Burgers equation with $N0 = 50, 60, 70, 80$.

In this example, we also have $N(30) \in [61, 77]$ at the end.
The final number of particle is stable, does not depend on initial number of particle, but depends on the strength of force.

Average number of particles In this section, we present the previous examples in other view with average numbers of particles corresponding α.

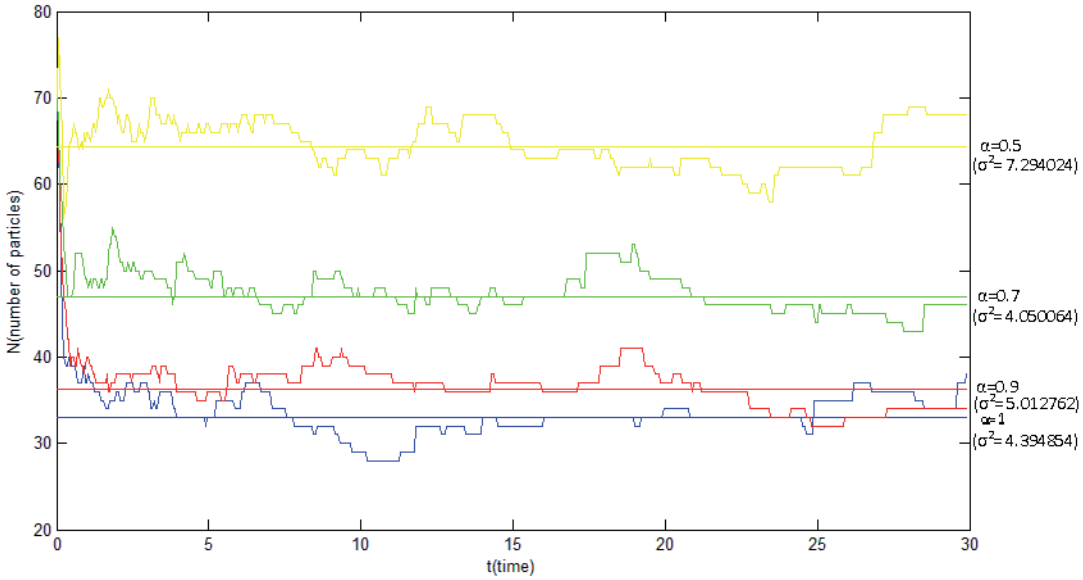

Figure 2.12: The average numbers of particles in the model for Burgers equation with $N0 = 70$.

Remarks

(i) From these examples, we may assume that for each positive α and L, there exist $N_1 < N_2$ and t_0 such that $N(t) \in [N_1, N_2]$ for all $t \geq t_0$ where $|N_2 - N_1|$ is small enough - $N(t)$ is number of particles at time t .

(ii) Notice that, when α is smaller, average $N(T)$ is larger and perhaps more unstable that is the distance $|N_2 - N_1|$ is larger.

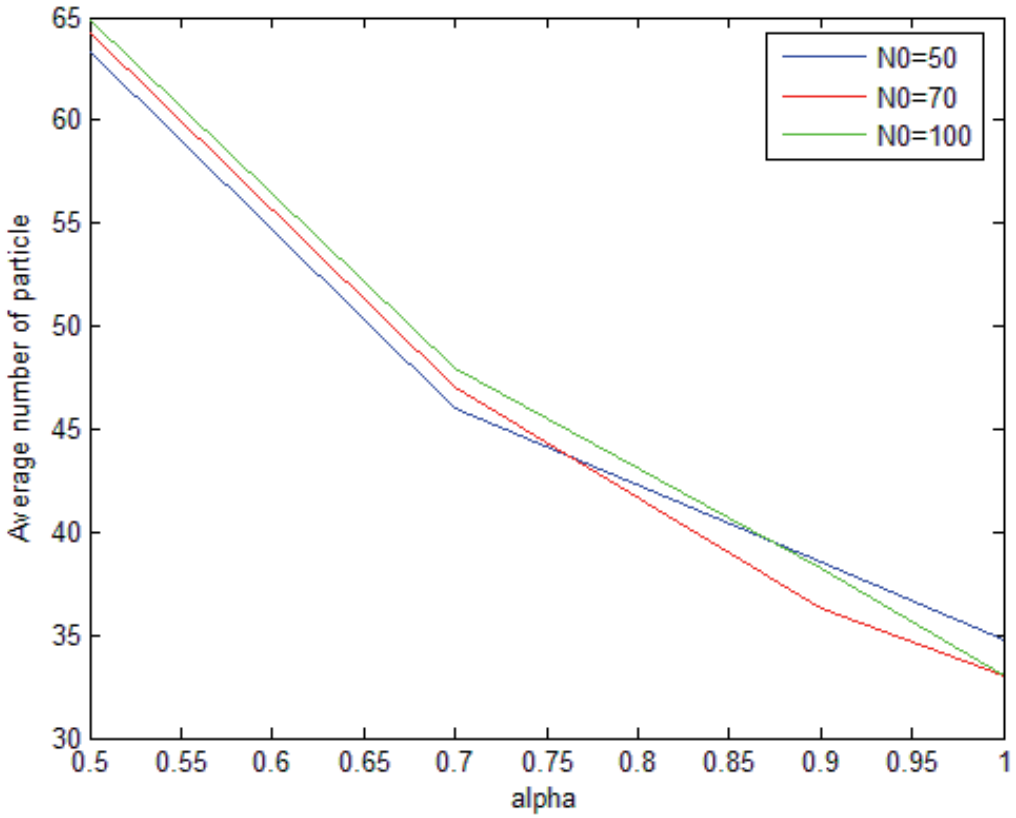

Figure 2.13: The comparison the average numbers of particles in three previous examples. We can see that they are nearly same.

2.2.5.2 Number of particles in the chaotic model

In this section, we also investigate the effect of damping the number of the particles for the chaotic model on the remaining particle at the end of run.

We put α to be the distance for case of creation, L to be is a part of length's box (notice that there is periodic boundary condition, so the same phenomenon at the left and the right box), $N0$ is number of particles at time $t = 0$ or number of particles at starting, $N(0)$, $P0$ is momenta of these particles at starting.
Now we consider some examples that are different from α. In the model, we begin with $N0$ particles and momenta of particles are zero. We consider for the time being $T = 30$ and $L = 20$.

Example 1 This is the case for $\alpha = 1$.

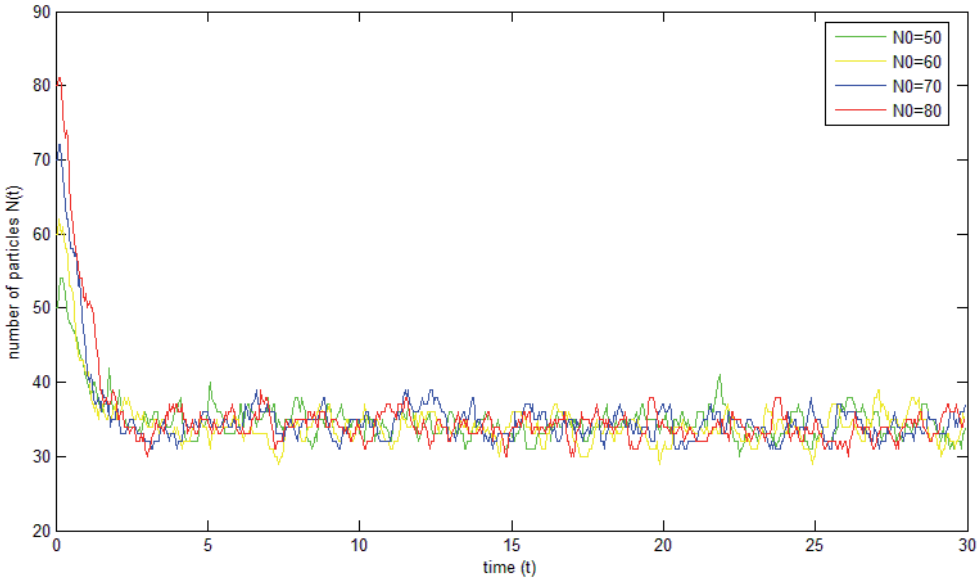

Figure 2.14: The number of particles in the chaotic model with $N0 = 50, 60, 70, 80$.

We have $N(T) \in [30, 37]$ at the end and we can also hope that the number of particles will be around in small interval after a long time. We continue to consider some similar examples with α smaller and see what happened.

Example 2 This is the case for $\alpha = 0.9$.

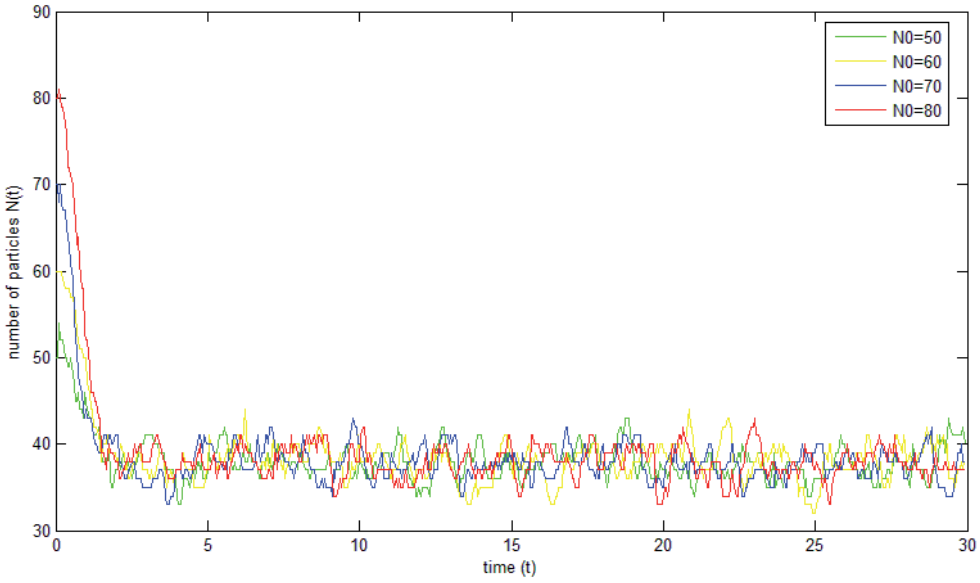

Figure 2.15: The number of particles in the chaotic model with $N0 = 50, 60, 70, 80$.

In this example, we also have $N(T) \in [38, 40]$ at the end.

Example 3 This is the case for $\alpha = 0.7$. Some following figures show the number of particles in the chaotic model according to time.

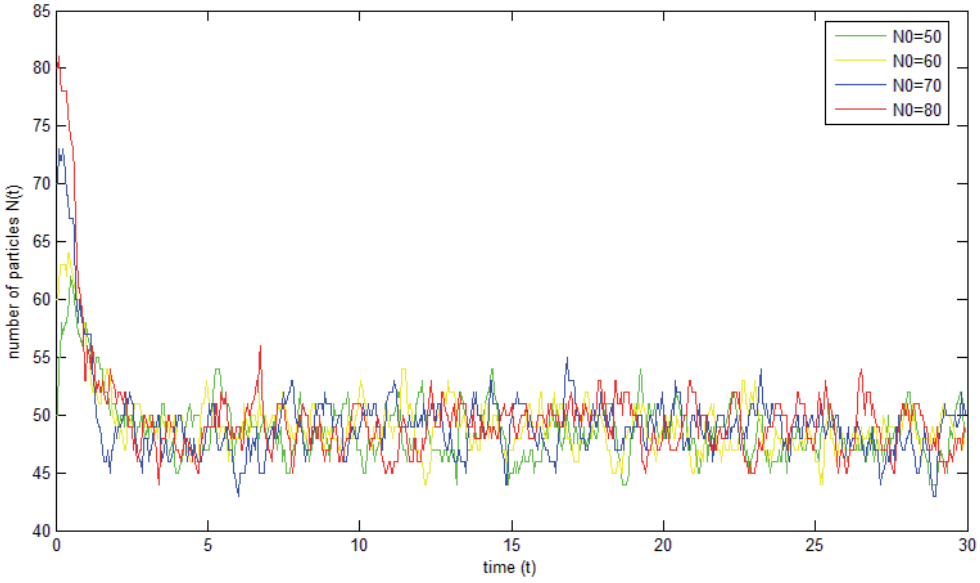

Figure 2.16: The number of particles in the chaotic model with $N0 = 50, 60, 70, 80$.

In this example, we also have $N(30) \in [47, 54]$ at the end.

Example 4 This is the case for $\alpha = 0.5$.

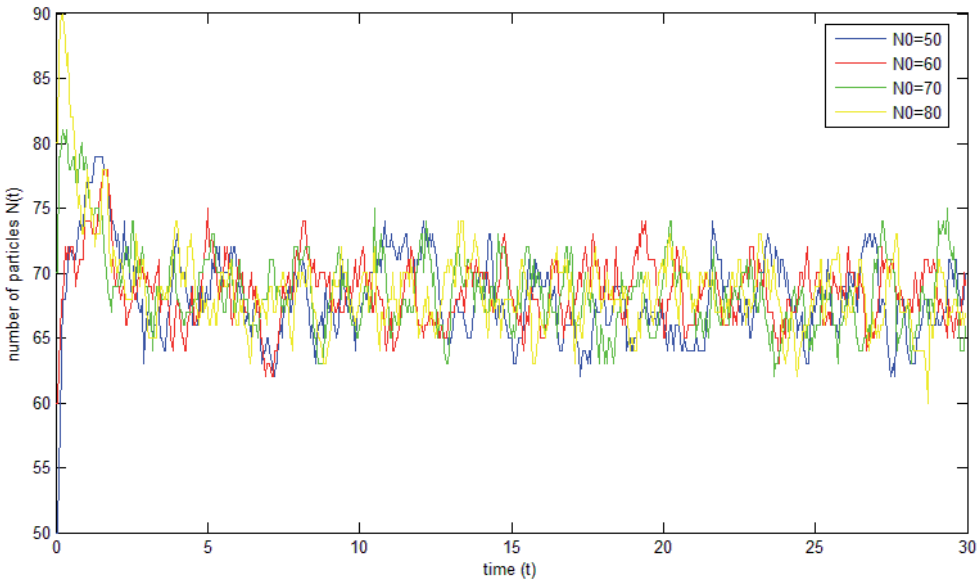

Figure 2.17: The number of particles in the chaotic model with $N0 = 50, 60, 70, 80$.

In this example, we also have $N(30) \in [66, 70]$ at the end.

Average number of particles In this section, similarly with the model for Burgers' equation, we present the number of particles in other view with its average corresponding α.

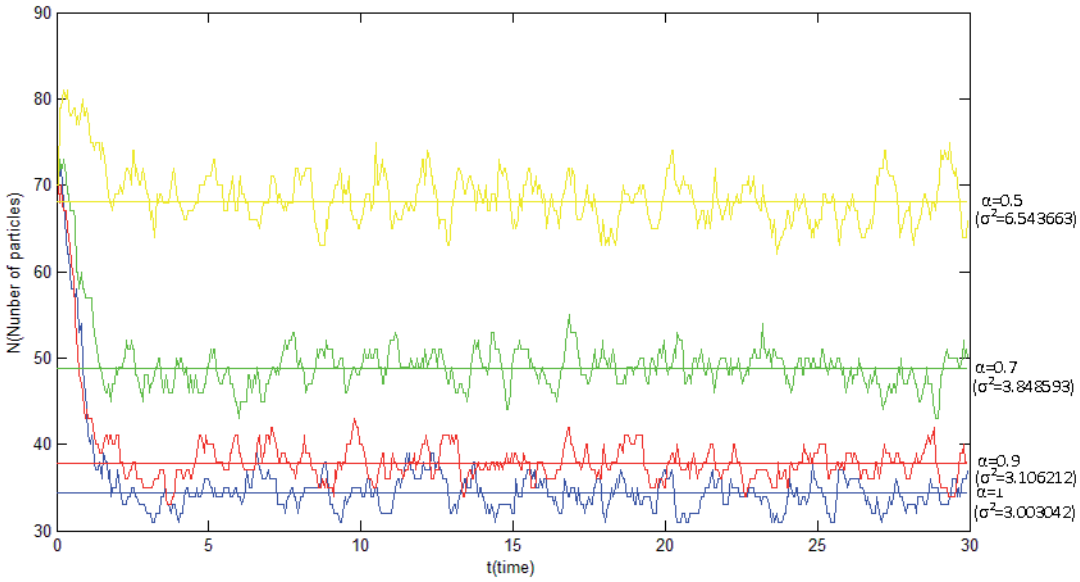

Figure 2.18: The average numbers of particles in the chaotic model with $N0 = 70$.

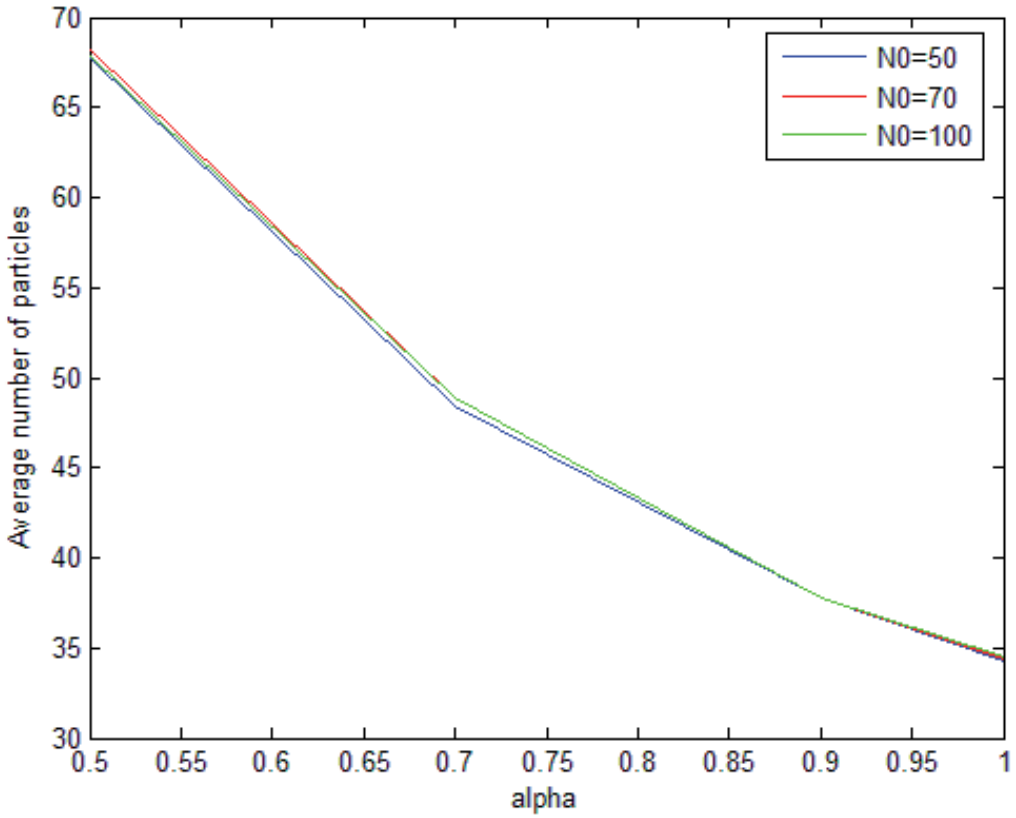

Figure 2.19: The comparison the average numbers of particles in three previous examples. We can see that they are almost same.

Conclusion In the chaotic model, there is similar phenomena as Burgers model but the number of particles are more unstable, it is easier to change in a short time. Following data are the average number of particles and the variance we get from two models.

Model	Burgers' equation			Chaotic		
N_0 / α	50	70	100	50	70	100
1	34.77	33.044	32.97	34.314	34.342	34.456
0.9	38.588	36.292	38.254	37.73	37.8	37.826
0.7	46.066	46.994	47.97	48.364	48.848	48.848
0.5	63.274	64.258	64.88	67.73	68.132	67.838

Figure 2.20: The average number of particles $\bar{N}$.

Model	Burgers' equation			Chaotic		
N_0 / α	50	70	100	50	70	100
1	2.337776	4.394854	1.932966	3.061527	3.003042	2.569202
0.9	5.509275	5.012762	1.765014	3.143387	3.106212	2.292309
0.7	3.083812	4.050064	7.744589	4.16784	3.848593	4.089074
0.5	4.419764	7.294024	5.869339	7.215531	6.543663	5.899555

Figure 2.21: The variance σ^2.

2.3 Bohr-Pikovsky model with anomalous diffusion

To consider the connection with particle model in the Kuramoto-Sivashinsky equation, Bohr and Pikovsky [6] showed the numerical simulation of particle displacement that lead to anomalous diffusion in KS equation.

2.3.1 Definition for particle model

Let us consider KS equation in one-dimension with velocity version

$$\partial_t u(t,x) + u\partial_x u(t,x) = -\partial_{xx} u - \partial_{xxxx} u. \tag{2.6}$$

The particle at position x in model have the velocity $u(t,x)$. Denote $r(t)$ be trajectory of a particle. It must satisfy

$$\partial_t r(t) = u(t, r(t)). \tag{2.7}$$

The anomalous diffusion in KS equation was proved by considering average the square of displacement $[\Delta r(t)]^2$ over the starting time t'

$$\left\langle [\Delta r(t)]^2 \right\rangle = \left\langle [r(t'+t) - r(t')]^2 \right\rangle. \tag{2.8}$$

2.3.2 Numerical results

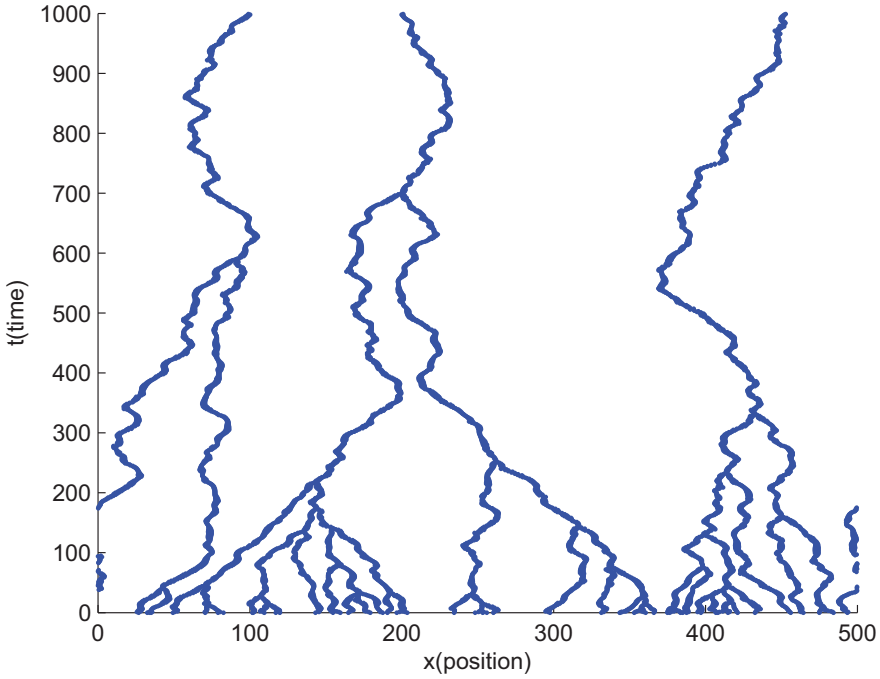

Figure 2.22: The anomalous diffusion in KS equation by following 50 'walking' particles.

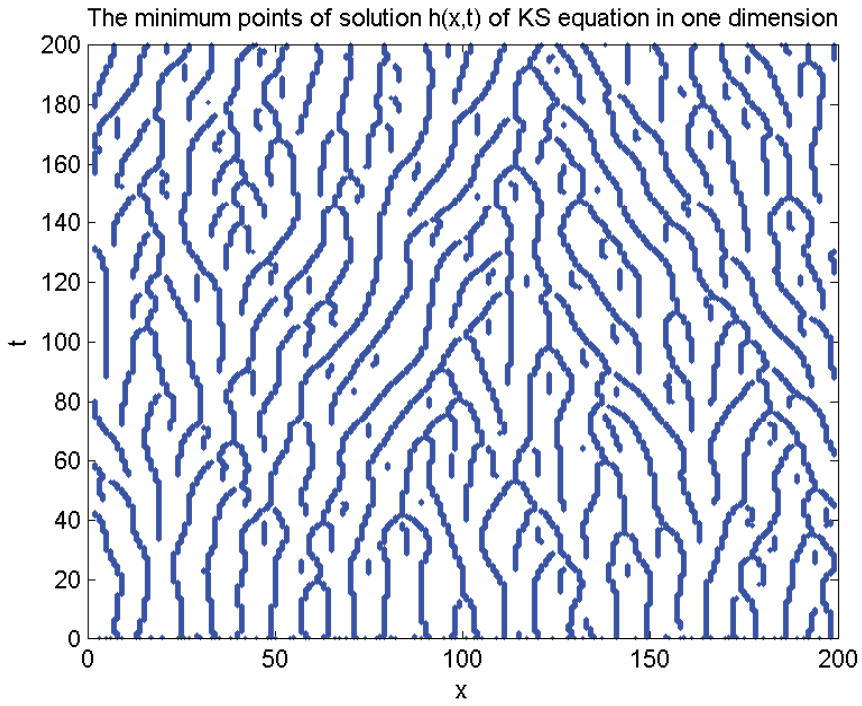

Figure 2.23: The minimum points of KS evolution time.

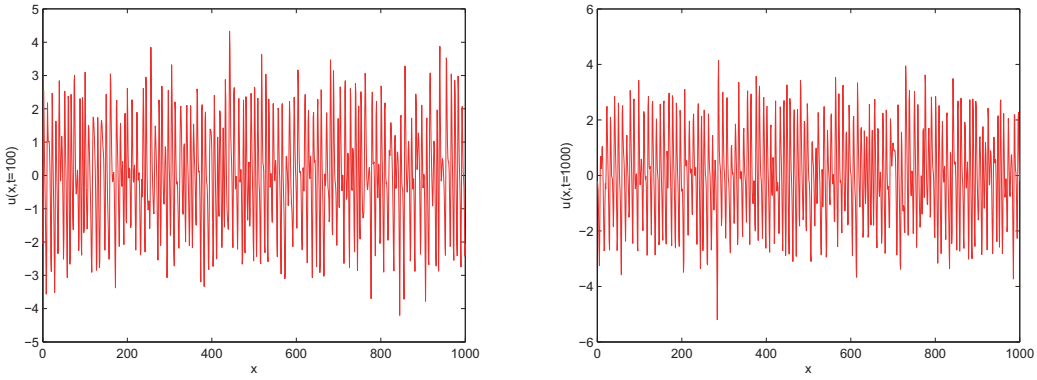

Figure 2.24: The velocity field of KS equation with length size $L = 1000$. Left: $T = 100$. Right: $T = 1000$

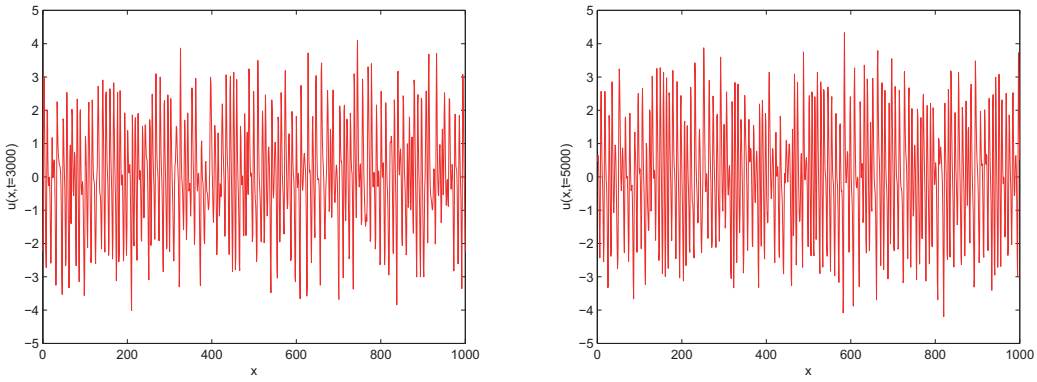

Figure 2.25: The velocity field of KS equation with length size $L = 1000$. Left: $T = 3000$. Right: $T = 5000$

Chapter 3

The new model for Kuramoto-Sivashinsky equation

3.1 The new model for Kuramoto-Sivashinsky equation

3.1.1 Introduction

We will consider the motion of N particles in line with periodic boundary condition and the size of system is L. We describe the i-th particle by its weight $m_i(t)$, position $x_i(t)$, velocity or momentum $v_i(t)$, and acceleration or force $a_i(t)$ at time $t \in [0, T]$. For this model, the particle dynamics has initial condition (m_i, x_i, v_i) where $m_i = 1, x_i = i\frac{L}{N}, v_i$ get random value for all $1 < i < N$. Moreover, we consider particles moving with the velocity changing due to first and second neighbor velocity interactions such that

$$\begin{cases} v_i(t) & = \dot{x}_i(t) \\ a_i(t) & = \dot{v}_i(t) = \alpha(v_{i-1}(t) - 2v_i(t) + v_{i+1}(t)) + \beta(v_{i-2}(t) - 2v_i(t) + v_{i+2}(t)) \end{cases}$$

where α, β are coefficients to be precised later. We define a continuous velocity field as a sequence of straight lines connecting the points $(x_i(t), v_i(t))$

$$u(t, x) = \frac{v_i(t)(x - x_{i-1}(t)) + v_{i-1}(t)(x_i(t) - x)}{x_i(t) - x_{i-1}(t)} \text{ for } x \in [x_{i-1}(t), x_i(t))$$

From there, we define the height field as in KS equation such that $u(t, x) = -\partial_x h(t, x)$. The feature of this dynamic is that when two neighbor particles reach collision, they do not stick together nor make annihilation. They are crossing and the system status is updated.

As long as the particles do not meet, they move at the velocity $v_i(t)$. We assume that at time t_0, there exists j such that $x_j(t_0) = x_{j+1}(t_0)$ and $x_j(t_0) < x_{j+1}(t_0)$for all $t < t_0$. This effects on system since after that we have $v_j(t_0+) = v_{j+1}(t_0)$ and $v_{j+1}(t_0+) = v_j(t_0)$. Therefore the velocity of neighbor particles will exchange bringing about influence on acceleration. The i-index must be changed by its position-order to suit the order in definition of force.
We note that by this feature, the number of particle N is constant and the mass of each of particle is always 1.

3.1.2 Particle models

3.1.2.1 Particle model for zero-pressure gas

We know that the particle motion without forces ($\alpha = \beta = 0$), coupled with sticky particles dynamics, yields to the system of pressureless gases (see [30, 31, 32, 33]):

$$\partial_t \rho + \partial_x(\rho u) = 0, \qquad \partial_t(\rho u) + \partial_x(\rho u^2) = 0$$

where ρ is density and u velocity of gas. First equation is for mass conservation and second one for momentum conservation. If $\rho(x,t)$ and $u(x,t)$ are smooth solutions, then we get the Burgers equation for u by multiplying the first one by u and subtracting it to second one

$$\partial_t u + u\partial_x u = 0.$$

In this case, we consider the particle motion which is described by

$$v_i(t) = \dot{x}_i(t), \qquad a_i(t) = \dot{v}_i(t) = 0.$$

The particles move without force ($\alpha = \beta = 0$) so that the velocity of the particles is constant until collision. When a collision occur, the involved particles stick together to create a new particle, with mass equal to the sum of preceding masses, and velocity computed such that the momentum is preserved. That implies the global conservation of mass and momentum. When there is no collision, the velocity field $u(x,t)$ satisfies Burgers equation. It is easy to see by taking derivative with respect to time on formula of $u(x,t)$. We cannot get that is always true since $\partial_t u(t_-, x) \neq \partial_t u(t_+, x)$ while collision.

A variant of this model, with $\beta = 0$ and $\alpha > 0$ will be studied in Chapter 4.

3.1.2.2 Particle model for Kuramoto-Sivashinsky equation

In this section, we consider the particle model with interaction force within both first and second neighbors ($\alpha, \beta \neq 0$). The introduction of the second neighbor interaction is

motivated by a remark from [18], where it is shown that, in a different context, quasi-periodic structures can be obtained by taking into account such interactions.

$$\begin{cases} v_i(t) &= \dot{x}_i(t) \\ \dot{v}_i(t) &= \alpha(v_{i-1}(t) - 2v_i(t) + v_{i+1}(t)) + \beta(v_{i-2}(t) - 2v_i(t) + v_{i+2}(t)). \end{cases}$$

Assuming $\alpha > 0$ makes an attractive force between next neighbors and its discrete form connects to the second order derivative or viscosity term in KS equation. Similarly, the β term relates the fourth derivative term. It is clearly evidenced by rewriting the force as following

$$\dot{v}_i(t) = (\alpha+4\beta)(v_{i-1}(t)-2v_i(t)+v_{i+1}(t))+\beta(v_{i-2}(t)-6v_{i-1}+4v_i(t)-6v_{i+1}+v_{i+2}(t)). \quad (3.1)$$

To link to KS equation, where the coefficients in front of both second and fourth order derivatives are negative, several conditions will be needed on α and β, as we will see below. It will turn out that the particle model has attraction to first neighbor and repulsion to second one.

The dynamics of collisions is supposed to be elastic, in order to keep the total number of particles constant. This is similar to the Rost-Krug model [2] where particle system in which the interaction force is defined by limit of potential

$$v_i = 2x_i - x_{i-1} - x_{i+1}$$

with annihilation and creation of particles without mass conservation. Some results given in Chapter 2 show that this procedure approximately preserves the particle number. However, it is impossible to recover the KS equation, especially the fourth derivative terms.

In the following part we propose a hyperbolic scaling function X that connects the model with KS equation and we also consider some simulations on this model. The hyperbolic scaling is usually given by

$$x_i(t) = \frac{1}{\varepsilon} X(\varepsilon t, \varepsilon i). \quad (3.2)$$

The function X introduced in (3.2) is actually the flow of the particle system, in the sense that $x = X(t, x_0)$ is the position at time t of a particle that was at time 0 in position x_0. Therefore it has to be understood that there are initial N particles equally disposed at positions i/L, $i = 1, \ldots, N$, and the scaling means that we are interested in long time evolution ($t \sim 1/\varepsilon$), and high density of particles ($\sim 1/\varepsilon$), since in this context, ε is L/N,

where N is the number of particles, and L the length of the interval.
We introduce the new variables

$$\tau = \varepsilon t, \qquad y = \varepsilon x.$$

From any (smooth) function $g(t,x)$, we can define a scaled function $f(\tau, y)$ by writing

$$f(\tau, y) = g\left(\frac{\tau}{\varepsilon}, \frac{X(\tau, y)}{\varepsilon}\right), \tag{3.3}$$

For instance, suppose that there exists a function $v(t,x)$ such that for each i one has $v_i(t) = v\big(t, x_i(t)\big)$. Then using the scaled variables, we can define a function $u(\tau, y)$ so that we have obviously

$$v_i(t) = v\big(t, x_i(t)\big) = u(\varepsilon t, \varepsilon x_i(t)) = u\big(\varepsilon t, X(\varepsilon t, \varepsilon i)\big), \tag{3.4}$$

the hyperbolic scaling is designed to preserve the velocities. On the other hand, we have also, by using the usual chain rule,

$$v_i(t) = \dot{x}_i(t) = \partial_\tau X(\varepsilon t, \varepsilon i). \tag{3.5}$$

From (3.4) and (3.5) we deduce

$$\dot{v}_i(t) = \varepsilon \partial_\tau u + \partial_y u \varepsilon \partial_\tau X = \varepsilon(\partial_\tau u + u \partial_y u). \tag{3.6}$$

With this scaling, we obtain the usual Burgers term. If one wishes to obtain $\lambda u \partial_x u$ as in Kuramoto's paper, the scaling should be $\tau = \varepsilon t, \quad y = \lambda \varepsilon x$.
On the other hand, we can write

$$v_{i-1}(t) - v_i(t) = v\big(t, x_{i-1}(t)\big) - v\big(t, x_i(t)\big) = \big(x_{i-1}(t) - x_i(t)\big)\partial_x v + \frac{\big(x_{i-1}(t) - x_i(t)\big)^2}{2}\partial_{xx} v + \cdots,$$

with

$$x_{i-1}(t) - x_i(t) = \frac{1}{\varepsilon}\big(- \varepsilon \partial_y X + \frac{\varepsilon^2}{2}\partial_{yy} X + \cdots.$$

$$v_{i-1}(t) - v_i(t) = -\partial_y X \partial_x v + (\partial_y X)^2 \partial_{xx} v + \varepsilon\big(\partial_{yy} X \partial_x v - \partial_y X\, \partial_{yy} X\big) + \cdots,$$

Rewriting this for $v_{i+1} - v_i$, and taking care of the signs in front of $\partial_y X$, we get

$$v_{i-1} - 2v_i + v_{i+1} = (\partial_y X)^2 \partial_{xx} v + \varepsilon \partial_{yy} X \partial_x v + \cdots.$$

From the definition of u (3.4), we obtain

$$\partial_y u = \frac{1}{\varepsilon}\partial_x v\, \partial_y X, \qquad \partial_{yy} u = \frac{1}{\varepsilon^2}\partial_{xx} v (\partial_y X)^2 + \frac{1}{\varepsilon}\partial_x v\, \partial_{yy} X,$$

so that

$$v_{i-1} - 2v_i + v_{i+1} = \varepsilon^2 \partial_{yy} u + \frac{\varepsilon^4}{12} \partial_{yyyy} u + \cdots . \tag{3.7}$$

Similarly, we also obtain

$$v_{i-2}(t) - 6v_{i-1}(t) + 4v_i(t) - 6v_{i+1}(t) + v_{i+2}(t) = \varepsilon^4 \partial_{yyyy} u + \cdots .$$

This kind of relation holds for any pair of functions related by (3.3). Recalling now (3.6), we see that we can simplify by ε the velocity equation, and get

$$\begin{aligned} (\partial_\tau u + u\partial_y u)(\tau, y_i) &= \varepsilon(\alpha + 4\beta)\partial_{yy} u(\tau, y_i) + (\alpha + 4\beta)\frac{\varepsilon^3}{12}\partial_{yyyy} u(\tau, y_i) + \beta\varepsilon^2 \partial_{yyyy} u(\tau, y_i) \\ &= \varepsilon \left[(\alpha + 4\beta)\partial_{yy} u + \varepsilon^2 \big(\frac{\alpha}{12} + \frac{4\beta}{3}\big)\partial_{yyyy} u \right]. \end{aligned} \tag{3.8}$$

where y_i denotes $X(\tau, \varepsilon i)$.

In this form, it is clear that when $\varepsilon \to 0$ (recall it means high density and long time scale), formally, this equation tends to the Burgers equation. Therefore to observe more complex phenomena, one has to rescale the microscopic forces, hence α and β. Setting for instance $\alpha_\varepsilon = \alpha/\varepsilon$ and $\beta_\varepsilon = \beta/\varepsilon$ leads to an asymptotic behavior following the the KS equation

$$(\partial_\tau u + u\partial_y u)(\tau, y_i) = \nu_2 \partial_{yy} u(\tau, y_i) + \nu_4 \partial_{yyyy} u(\tau, y_i),$$

with the following values for ν_2 and ν_4:

$$\nu_2 = \alpha + 4\beta, \qquad \nu_4 = \varepsilon^2 \big(\frac{\alpha}{12} + \frac{4\beta}{3}\big). \tag{3.9}$$

This means that for fixed values of α and β, we recover for small ε, the long time dynamics for which ν_2 is dominating. If one wishes to observe the KS-like behavior on a given time interval for some ε then for $\varepsilon/10$, one has to rescale the coefficients by a factor 10.

Notice that, since for the KS equation we must have $\nu_2 < 0$ and $\nu_4 < 0$, we find the required conditions on α, β: $\alpha + 4\beta < 0$ gives $\nu_2 < 0$, which in turns imply $\alpha/12 + 4\beta/3 < 0$, that is $\nu_4 < 0$. Since we have assumed $\alpha > 0$, we get finally

$$0 < \alpha < -4\beta.$$

In the converse way, to obtain given values for ν_2 and ν_4, α and β can be rescaled as

$$\alpha = \frac{4}{3}\nu_2 - \frac{4\nu_4}{\varepsilon^2}, \qquad \beta = \frac{\nu_4}{\varepsilon^2} - \frac{\nu_2}{12}. \tag{3.10}$$

This possibility was not investigated in the present chapter, where fixed values for the microscopic forces are used.

3.2 Simulation results

3.2.1 The general view of the particle model

In this part, there are some figures about particle trajectory, velocity field.

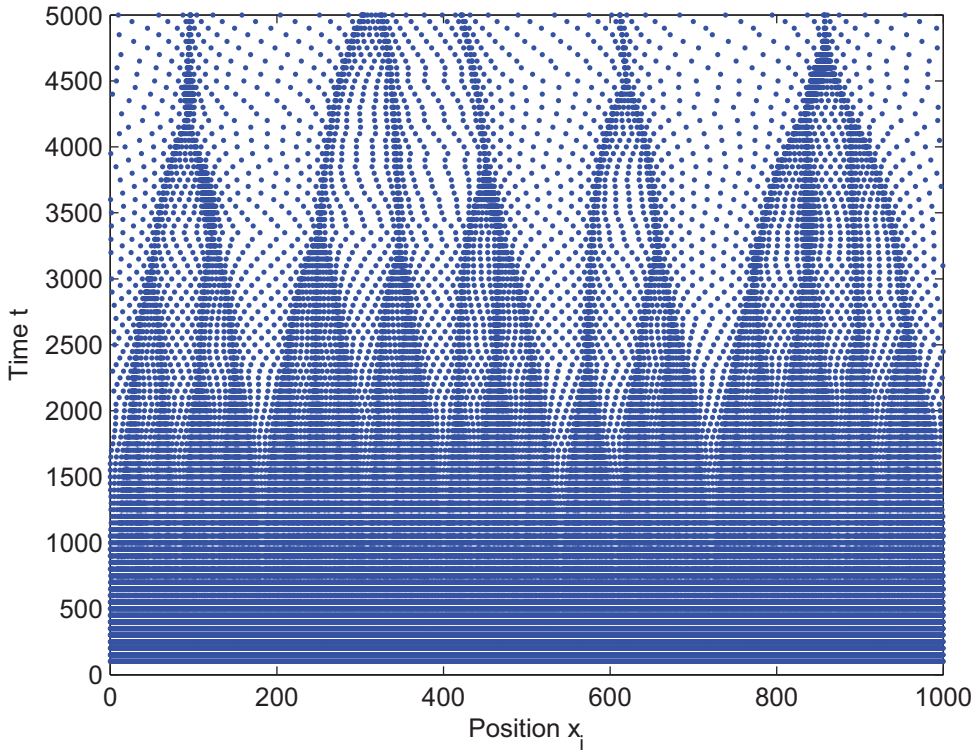

Figure 3.1: Trajectories of particles on line.

The figure (3.1) shows the trajectories of 100000 particles in time $T = 5000$. The system size $L = 1000$ and the coefficients $\alpha = 3.5, \beta = -1$. The particles aggregate to big particles after long time. In the figure (3.1), the time period for each step is a little long (50). So in order to see more details and investigate the KS regime in the model, we have following example

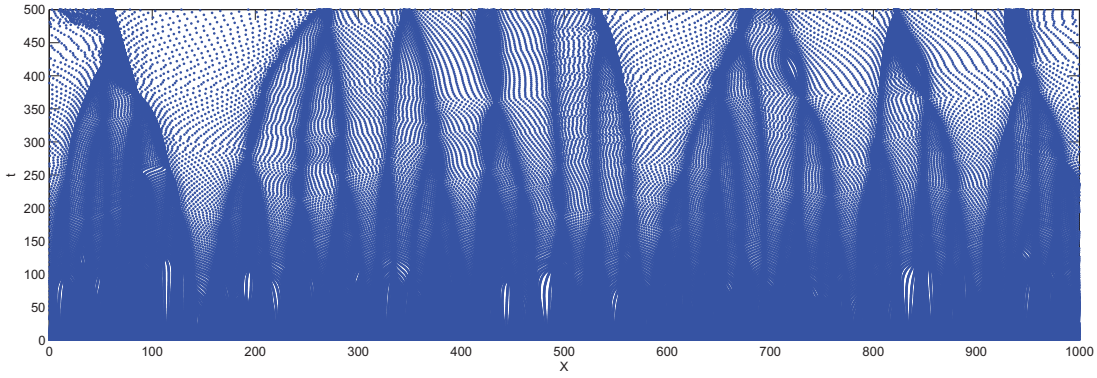

Figure 3.2: The trajectory of particles shows chaotic regime.

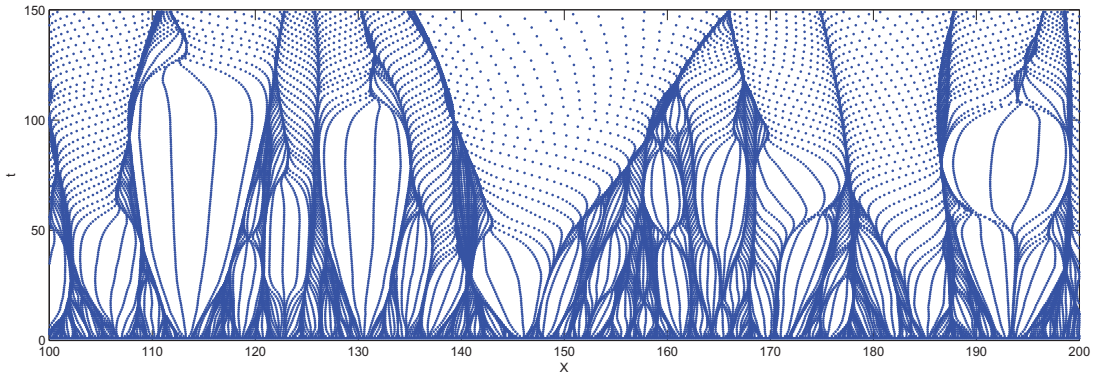

Figure 3.3: Zoom out of the trajectory of particles where $x \in [100, 200]$.

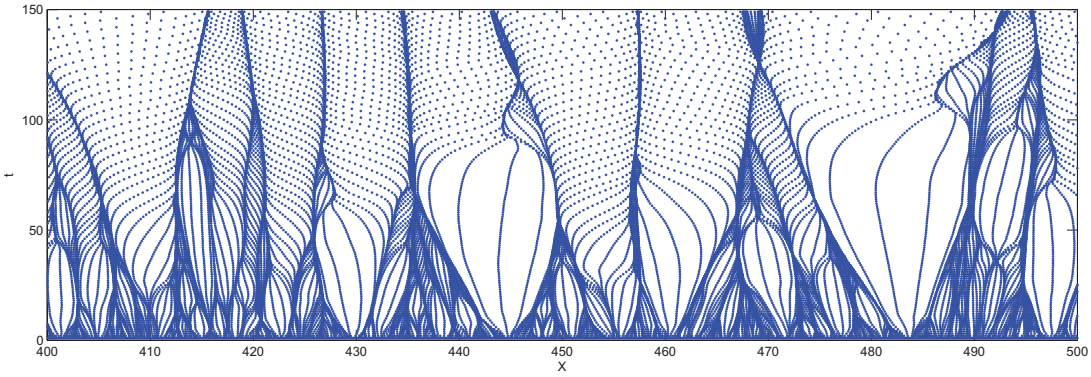

Figure 3.4: Zoom out of the trajectory of particles where $x \in [400, 500]$.

The figure (3.2) shows the trajectories of 10000 particle on line. The figure (3.3), (3.4) are parts of the trajectories of particles where $x \in [100, 200], [400, 500]$ and $t \in [0, 150]$ (thank to refer appendix for full zoom out of figure (3.2)). The system size $L = 1000$ and the coefficients $\alpha = 3, \beta = -1$. The trajectory shows chaotic regime in KS equation. Some particles collide in big particle, others separate to create new big particle. It corresponds to cellular structure in KS equation. Let recall the minimum points revolution of the KS equation in figure (3.5) in which cells annihilation and splitting . In some times, there are two minima get stick together or appearing new minima between two. The main particles is considered as minimum points. The particles tend to aggregate after long time but in former they obtain chaotic regime as figure (3.3), (3.4).

The minimum points are corresponding to the cellular structure. The merging of two minima is like the collision procedure and new cell respectively creation.

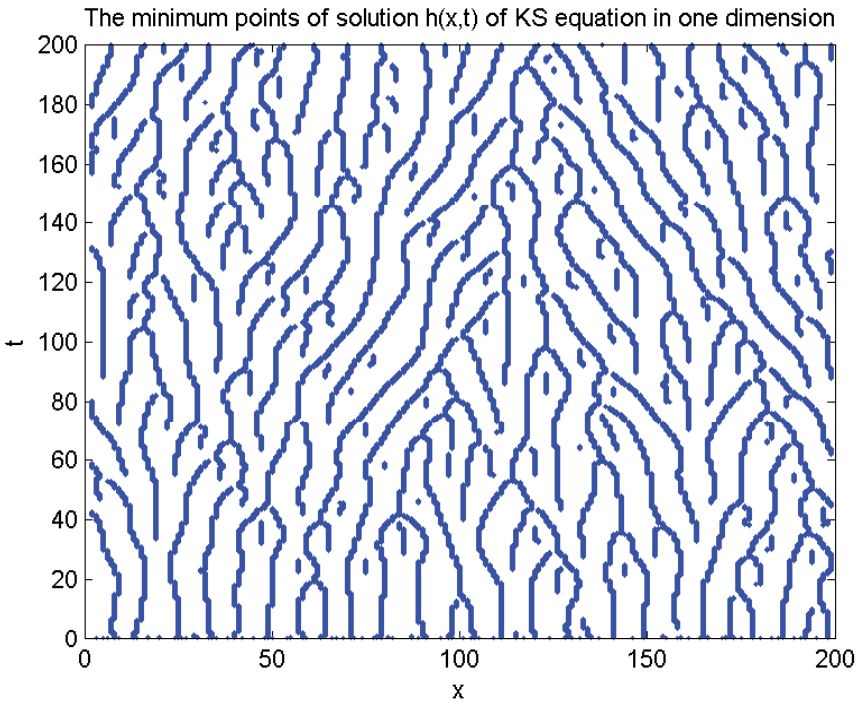
The minimum points of solution h(x,t) of KS equation in one dimension
t
x
0
20
40
60
80
100
120
140
160
180
200
0
50
100
150
200

Figure 3.5:

Velocity field.

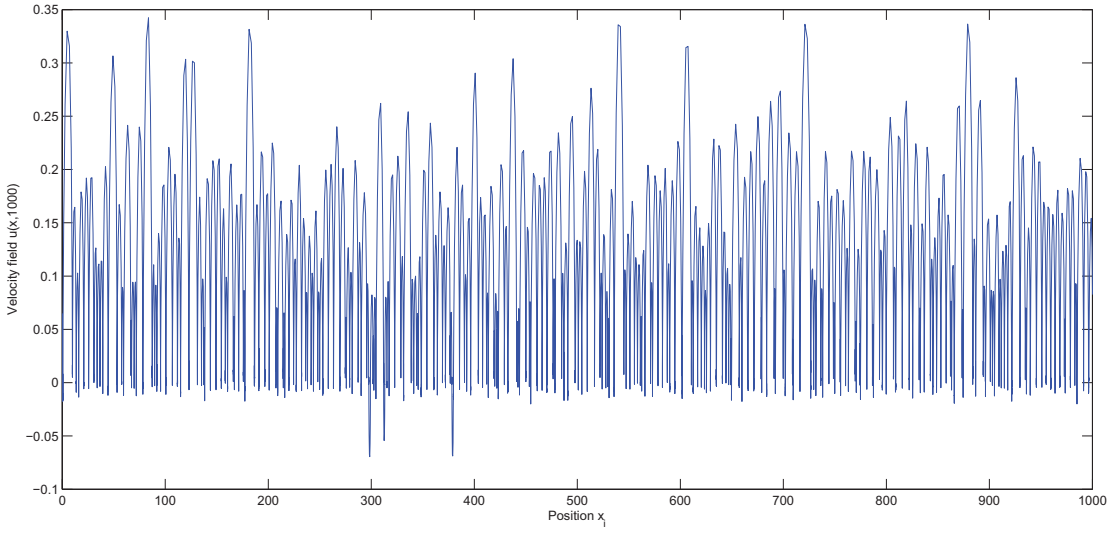

Figure 3.6: And the velocity field.

The figure (3.6) is an example of velocity field at time $t = 1000$ corresponding to figure (3.1). The mean velocity remains close to zero, due to the high number of big particles with almost zero velocity.
The following figures (3.7) and (3.8) give the average velocity field over 50 runs for 2 different value of coupling α, ie. $\alpha = 3$ and 3.5 at early and late time $t = 10$ and 100.

For $\alpha = 3$, the oscillatory behavior is smooth. This effect is less pronounced for $\alpha = 3.5$.

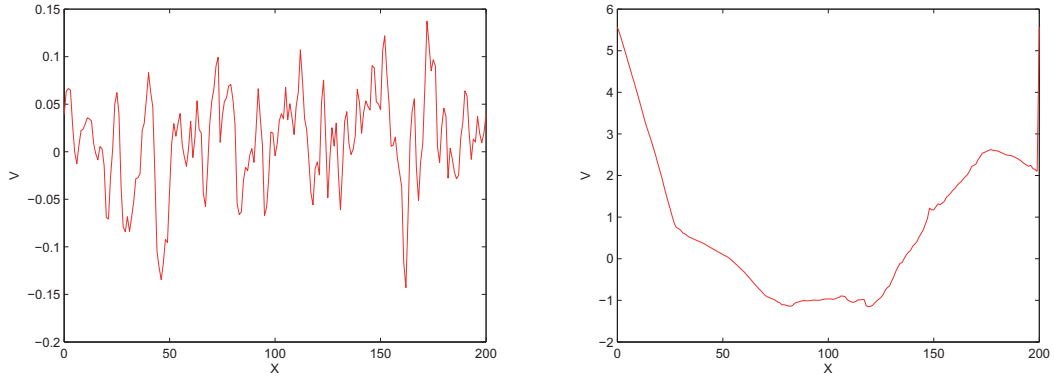

Figure 3.7: Average of velocity field. The system size $L = 200, \alpha = 3, \beta = -1, dt = 0.001$. Initial velocity is random value in $[-0.5, 0.5]$, average over 50 runs. $T = 10, 100$.

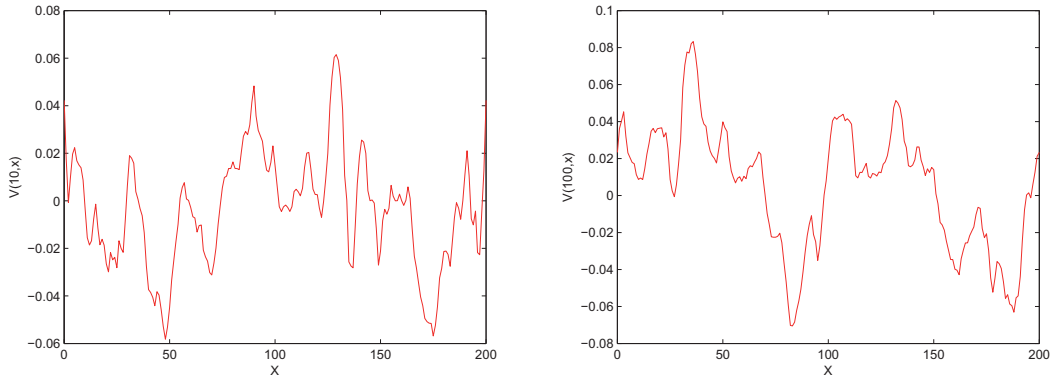

Figure 3.8: Average of velocity field. The system size $L = 200, \alpha = 3.5, \beta = -1, dt = 0.001$. Initial velocity is random value in $[-0.5, 0.5]$, average over 50 runs. $T = 10, 100$.

3.2.2 Powerspectrum

First, we recall the definition of powerspectrum

$$S(k) = L \langle ||\widehat{u}_k|| \rangle$$

where the angular brackets denote average over time t and $\widehat{u}_k$ is Fourier transform of velocity u.
The erosion process described by the linear equation

$$\partial_t u = \nu_2 \partial_{xx} u + \nu_4 \partial_{xxxx} u \tag{3.11}$$

where $\nu_2, \nu_4 < 0$. The solutions of (3.11) has form

$$u(x,t) = ce^{\sigma t + ikx}.$$

So, we imply

$$\begin{aligned} c\sigma e^{\sigma t+ikx} &= -\nu_2 ck^2 e^{\sigma t+ikx} + \nu_4 ck^4 e^{\sigma t+ikx} \\ \sigma &= -\nu_2 k^2 + \nu_4 k^4 \end{aligned}$$

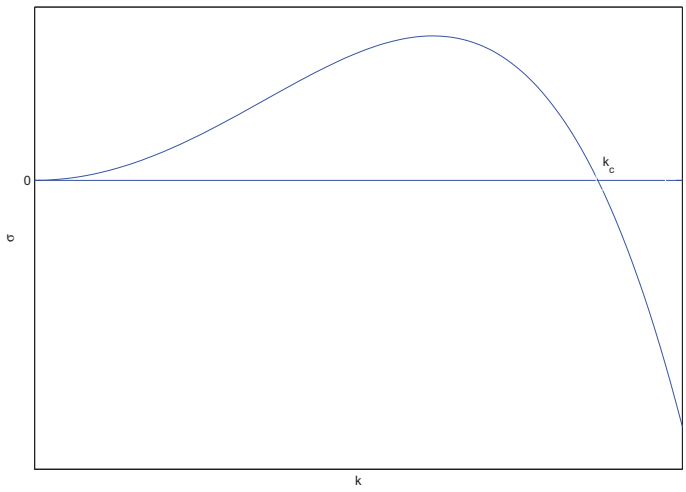

Figure 3.9: Rate evolution.

To obtain k_c, we can not use the estimation of ν_2, ν_4 as (3.9) because in fact, the value ε changes in time. We can see the figure trajectory of particles: after a long time,

many particles aggregate to become some big particles, then the scaling value ε must be increased. Comparing the formula of force

$$\dot{v}_i(t) = (\alpha + 4\beta)(v_{i-1}(t) - 2v_i(t) + v_{i+1}(t)) + \beta(v_{i-2}(t) - 6v_{i-1} + 4v_i(t) - 6v_{i+1} + v_{i+2}(t)).$$

and (3.11), we choose

$$\nu_2 = \alpha + 4\beta, \nu_4 = \beta,$$

then

$$k_c = \sqrt{\frac{\alpha + 4\beta}{\beta}}.$$

The powerspectrum are calculated for the different defined α values $(2.5, 3, 3.5, 3.8)$ and for the different system size but with $\varepsilon = 0.1$ the particle number is changed accordingly and they are displayed in figures (3.10) to (3.12).

3.2.2.1 Length size 256

The parameters are chosen using $\varepsilon = 0.1$, so there are 2560 particles and discrete Fourier points, $\beta = -1, T = 100, \Delta t = 0.001$. Initial velocity is random value in $[-0.1, 0.1]$. Average over 80 times.

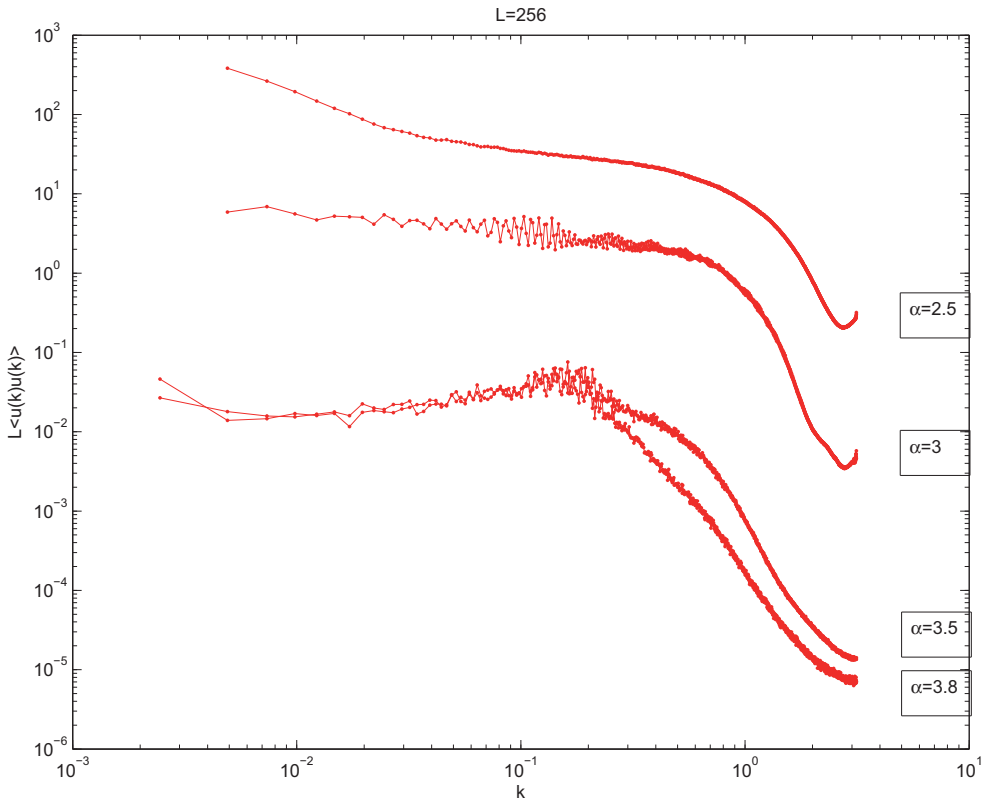

Figure 3.10: The powerspectrum with system size $L = 256$.

3.2.2.2 Length size 512

The parameters are chosen using $\varepsilon = 0.1$, so there are 5120 particles and discrete Fourier points, $\beta = -1, T = 100, \Delta t = 0.001$. Initial velocity is random value in $[-0.1, 0.1]$. Average over 80 times.

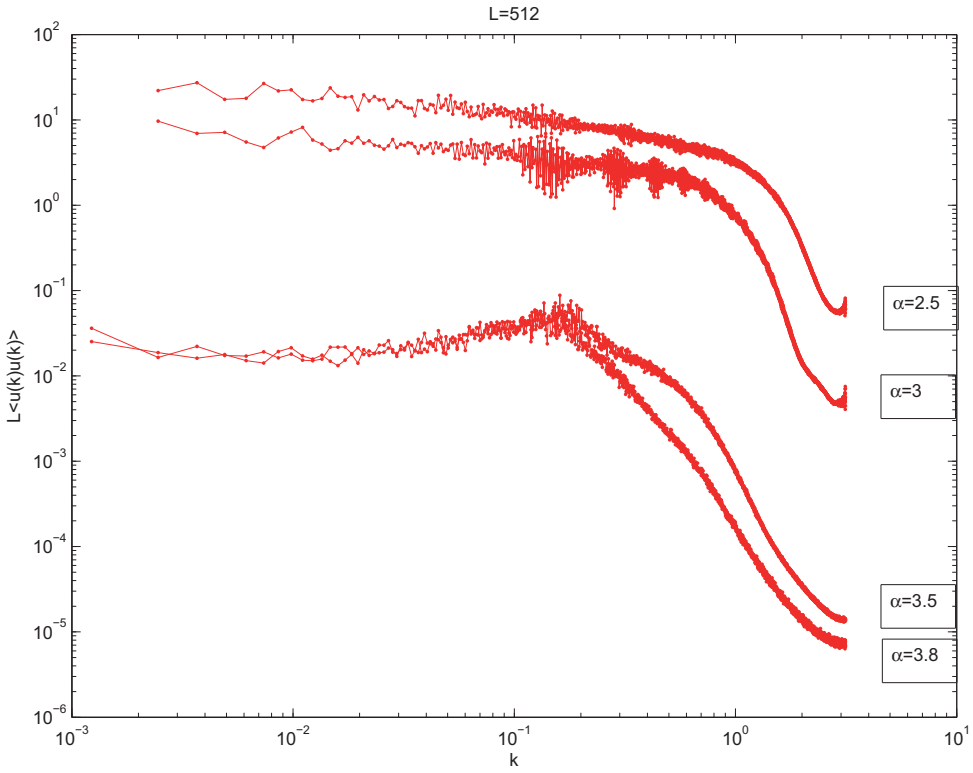

Figure 3.11: The powerspectrum with system size $L = 512$.

3.2.2.3 Length size 1024

The parameters are chosen using $\varepsilon = 0.1$, so there are 10240 particles and discrete Fourier points, $\beta = -1, T = 100, \Delta t = 0.001$. Initial velocity is random value in $[-0.1, 0.1]$. Average over 80 times.

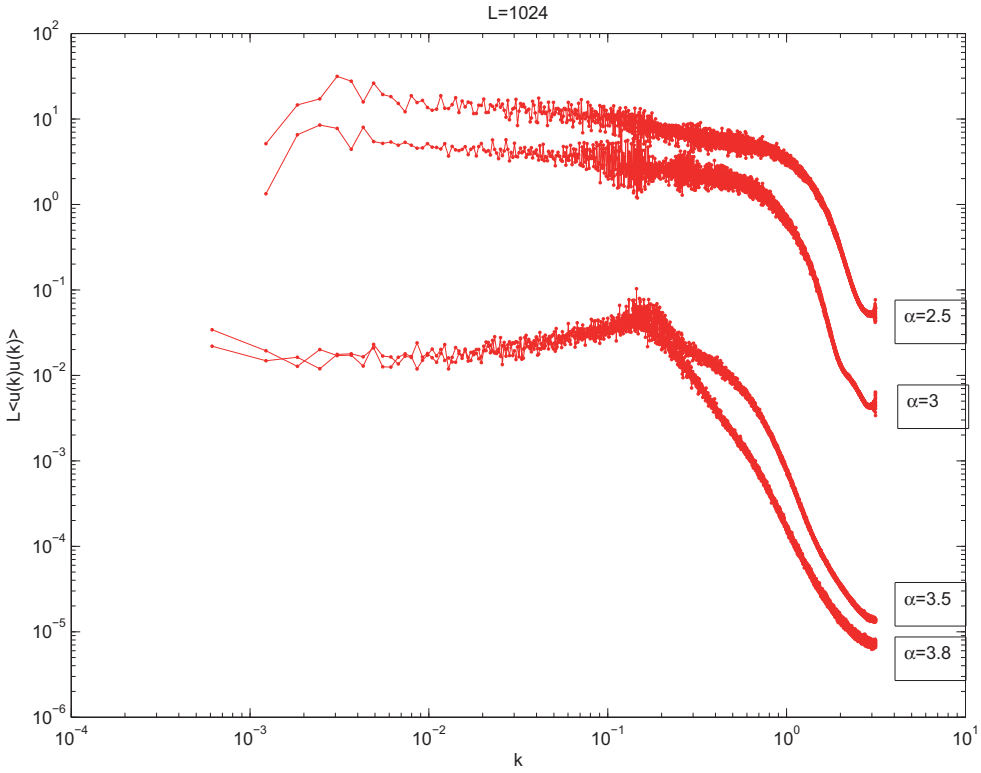

Figure 3.12: The powerspectrum with system size $L = 1024$.

Conclusion for powerspectrum

Let k_s be typical wavenumber obtained from figures above. We consider following tables.

α, β	Wavenumber k_s	Wavelength l_s	Wavenumber k_c	Wavelength l_c
$2.5, -1$	1	6.2832	1.2247	5.1302
$3, -1$	0.9	6.9813	1.0000	6.2832
$3.5, -1$	0.4	15.7080	0.7071	8.8858
$3.8, -1$	0.2	31.4159	0.4472	14.0496

Simulated values are closed to predicted one for small α coupling values while the wavelength increases when increasing α above 3.
We can observe that the k-value of the slope change is decreasing when increasing α when comparing fig. 3.10, 3.11, 3.12. Moreover, the increase of simulation size with ε identical, does not change the k-value of the slope change. It means that the smallest size is large enough for preventing boundary effect. This is also favored by periodic boundary conditions.

3.2.3 Variance of velocity

The variance of velocity is written as

$$I_v^2(t,L) =< (v(t)-\bar{v})^2 > \qquad \text{where} \qquad \bar{v} = \frac{1}{N}\sum_{i=1}^{N} v_i(t).$$

It is a measure of the roughness of the velocity field. Moreover it characterize its growth mode. It is calculated for 2 large size $L = 1024$ and 2048 for the four α values.

3.2.3.1 Length size 1024

The parameters are chosen that $\varepsilon = 1$, so there are 1024 particles, $\beta = -1, T = 1000, \Delta t = 0.001$. Initial velocity is random value in $[-0.1, 0.1]$. Average over 50 times.

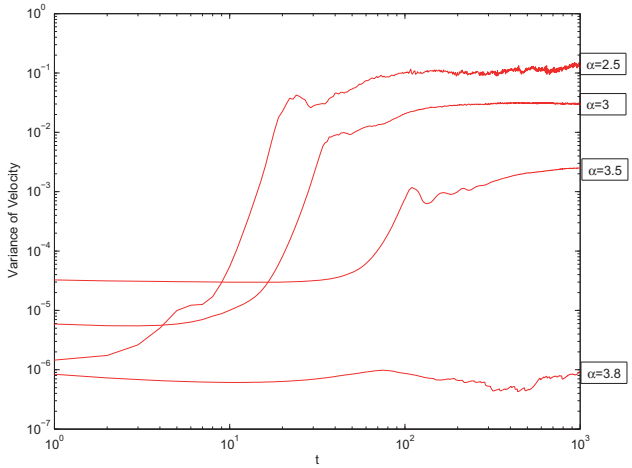

Figure 3.13: The velocity interface width with system size $L = 1024$.

We see that with $\alpha = 3.8$, the velocity interface is almost flat. It takes longer time to reach saturation regime. Therefore in order to estimate saturation time and investigate its behavior, the calculations are performed up to $T = 10^4$ for $\alpha = 3.8$.

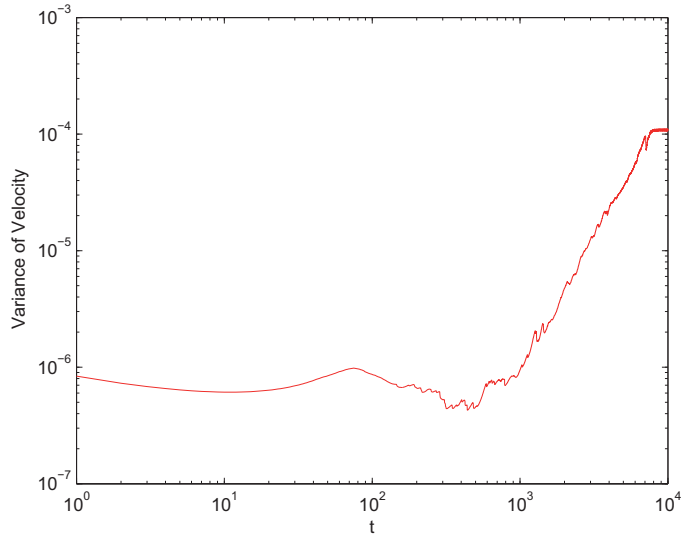

Figure 3.14: The velocity interface width with $\alpha = 3.8$.

3.2.3.2 Length size 2048

The parameters are chosen that $\varepsilon = 1$, so there are 2048 particles, $\beta = -1, T = 1000, \Delta t = 0.001$. Initial velocity is random value in $[-0.1, 0.1]$. Average over 50 times.

We see that with $\alpha = 3.8$, the velocity interface is almost flat. It takes longer time to reach saturation regime, which is not reached at $T = 10^4$ for $\alpha = 3.8$.

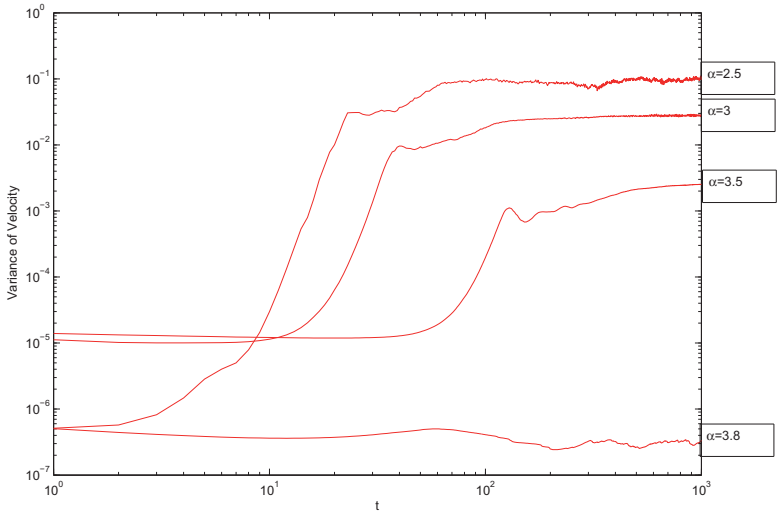

Figure 3.15: The velocity interface width with system size $L = 2048$.

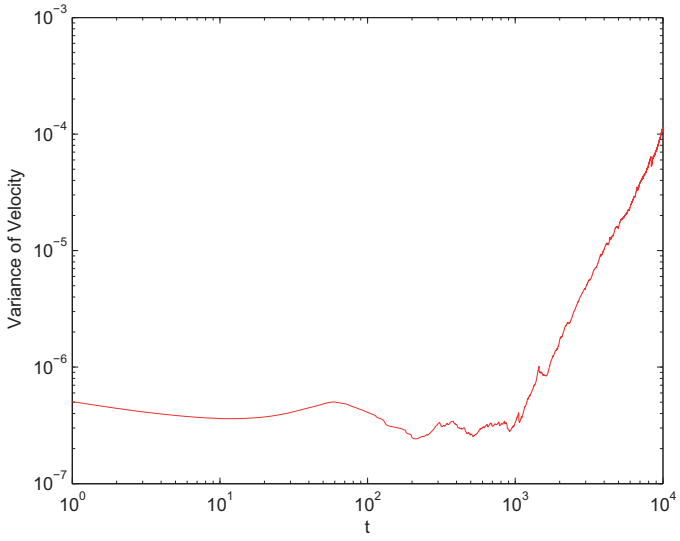

Figure 3.16: The velocity interface width with $\alpha = 3.8$.

Conclusion for the variance of velocity. The velocity field interface width shows a primary stable phase which is increasing duration when increasing α. This is followed by an unstable behavior at an exponential rate. Then a stable regime is reached in a form of a plateau, for which the height is decreased when increasing α. This behavior is not dependent on the system size but depends on the α-value.

3.2.4 Height interface width

The height interface width is defined by

$$W^2(t,L) =< (h(t) - \bar{h})^2 > \quad \text{where} \quad \bar{h} = \frac{1}{N}\sum_{i=1}^{N} h_i(t) \quad \text{and} \quad \partial_x h_i(t) = u_i(t).$$

It measures the roughness of the interface defined by the function $h_i(t)$

3.2.4.1 Length size 1024

The parameters are chosen $\varepsilon = 1$, so there are 1024 particles, $\beta = -1, T = 1000, \Delta t = 0.001$. Initial velocity is random value in $[-0.1, 0.1]$. Average over 50 times.

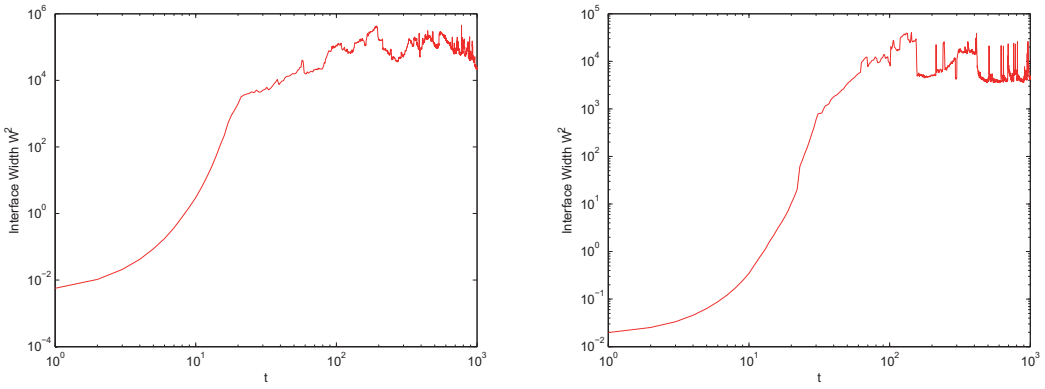

Figure 3.17: Left: $\alpha = 2.5$. Right: $\alpha = 3$.

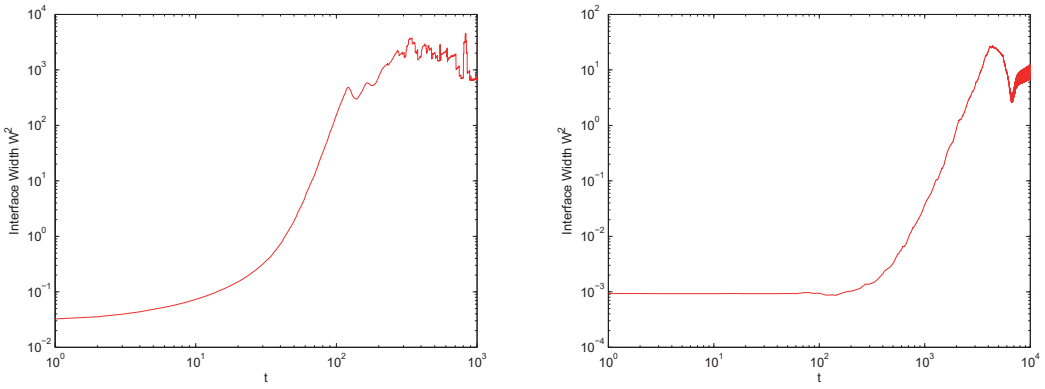

Figure 3.18: Left: $\alpha = 3.5$. Right: $\alpha = 3.8$.

3.2.4.2 Length size 2048

The parameters are chosen $\varepsilon = 1$, so there are 2048 particles, $\beta = -1, T = 1000, \Delta t = 0.001$. Initial velocity is random value in $[-0.1, 0.1]$. Average over 50 times.

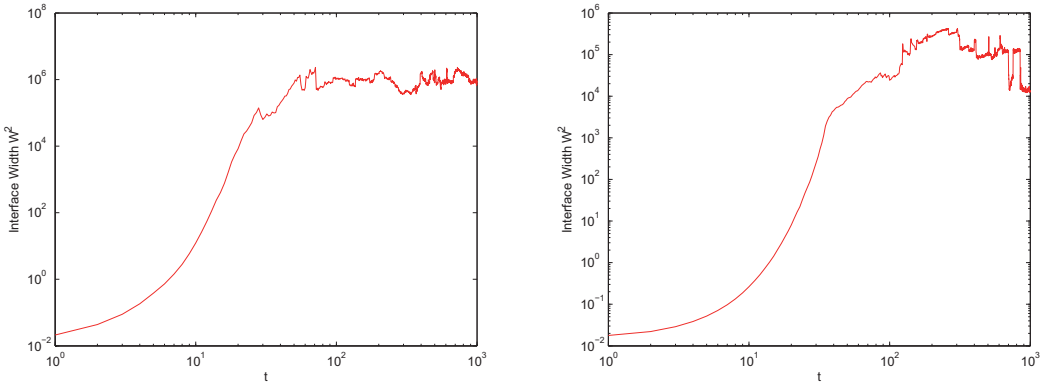

Figure 3.19: Left: $\alpha = 2.5$. Right: $\alpha = 3$.

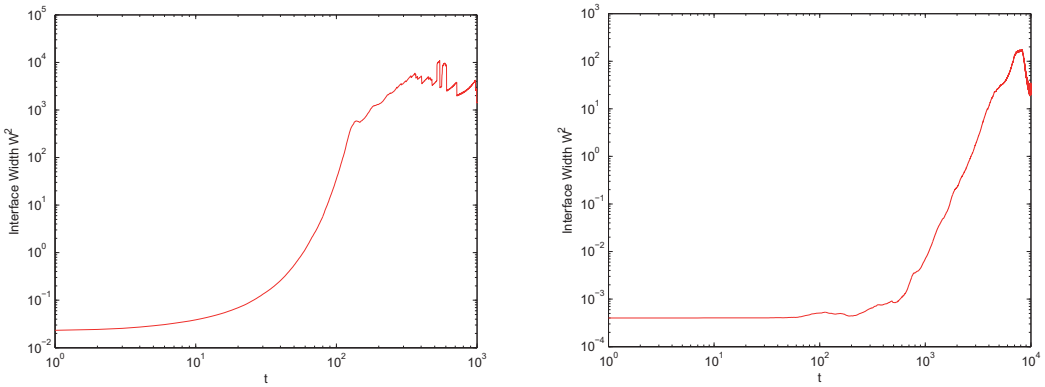

Figure 3.20: Left: $\alpha = 3.5$. Right: $\alpha = 3.8$.

Conclusion for height interface width

For $t < t^*$, the interface width increase exponentially as $W \sim \exp(\lambda t)$ after some time delay which depends on the α-value. For $t > t^*$, W still increases but at a smaller rate close to a saturation behavior. We also see that the height interface width W does not change so much when we increase the length size L. As for velocity interface width, the height interface width shows an increasing duration of the primary stable phase prior to the exponential increasing phase. The cross over time t^* is then also increasing. The magnitude of the saturation plateau is decreasing when α is increasing above $\alpha = 3$. As pointed out by Khang *et al*[25], a signature of the KS behavior is given by the height interface width $w(L,t)$:

$$w(L,t) \equiv \sqrt{\frac{1}{L}\sum_{i=1}^{L}[h(i,t) - \overline{h}(t)]^2}.$$

where h is the interface height. Especially, it is also observed that the interface width displays a crossover regime at a characteristic time t^*: for $t < t^*$, the width $w(L,t)$ increases exponentially as $w(L,t) \propto \exp\left(\frac{\nu_2 t}{l_c^2}\right)$, while for $t > t^*$, $w(L,t)$ still increases but at a considerably smaller rate than an exponential function. Figure 3.17 on the right shows a typical plot of $w(L,t)$ for L =1024 and $\alpha = 3$ and $\beta = -1$.

The values of $t*$ are very close in both situations except for the highest α-value, while the λ-parameters are very different, by roughly a factor 10. The crossover time is around 40. The rate of instability issued from direct simulation [25] is $t^* = l_c^2/|\nu_2| \approx 39$. Using the particle model and fitting the exponential increase in the Figure 3.17 using $w(L,t) \propto e^{\lambda t}$, one find $\lambda = 0.289$, far from the expected value ν_2/l_c^2=0.025.

The following table gives the value of parameters $\lambda and t^*$. s subscript refers to values deduced from graphics and c values comes from analytical values.

α, β	Exponential rate λ_s	Saturation time t_s^*
2.5,-1	0.6215	20
3, -1	0.2893	40
3.5, -1	0.0889	100
3.8, -1	0.0026	3000

α, β	Exponential rate $\lambda_c = \frac{\lvert\nu_2\rvert}{l_c^2}$	Saturation time $t_c^* = \frac{l_c^2}{\lvert\nu_2\rvert}$
2.5,-1	0.0380	26
3, -1	0.0253	39
3.5, -1	0.0127	79
3.8, -1	0.0051	197

3.2.5 Mean square displacement

The mean square displacement of particle trajectory is written as

$$\sigma^2 =< (y(t) - y(0))^2 >_L \qquad \text{where} \qquad \dot{y}(t) = u(y(t), t).$$

$\dot{y}(t)$ is the velocity of the particle at the position $y(t)$.

3.2.5.1 Length size 1024

The parameters are chosen that $\varepsilon = 1$, so there are 1024 particles, $\beta = -1, T = 1000, \Delta t = 0.001$. Initial velocity is random value in $[-0.1, 0.1]$. Average over 50 times.

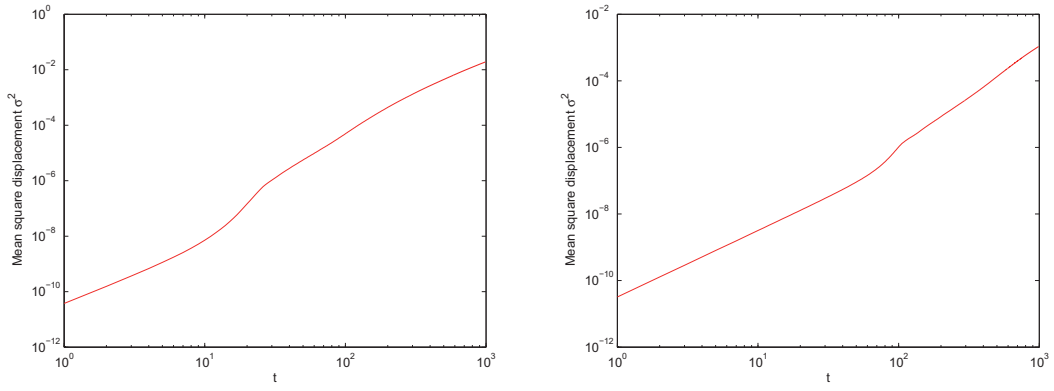

Figure 3.21: Left: $\alpha = 3$. Right: $\alpha = 3.5$.

3.2.5.2 Length size 2048

The parameters are chosen that $\varepsilon = 1$, so there are 2048 particles, $\beta = -1, T = 1000, \Delta t = 0.001$. Initial velocity is random value in $[-0.1, 0.1]$. Average over 50 times. **Remarks** The mean square of the tracer particle's displacement grows with time $\sigma^2 \sim t^{8/3}$ for $\alpha = 3$ and $\sigma^2 \sim t^2$ for $\alpha = 3.5$, and it is not dependant on the length zize. Moreover, the crossover time between the regimes is the same as $t*$ for height interface width.

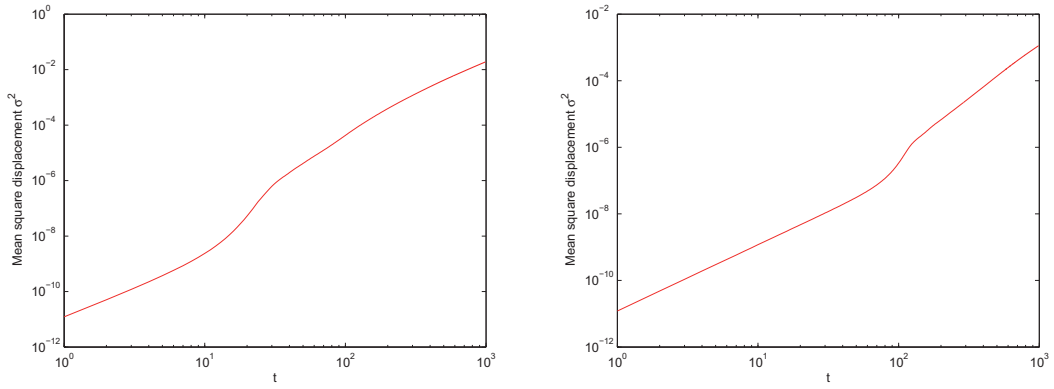

Figure 3.22: Left: $\alpha = 3$. Right: $\alpha = 3.5$.

3.2.6 Conclusions

The first information that can be extracted from the present model is the particle trajectory in the fluid. Figure 3.1 display a set of trajectories for 100000 particles submitted to equation KS force (3.1) on a system of size $L = 1000$ with $\alpha = 3.5$ and $\beta = -1$. Set of trajectories are converging for forming a cluster during a time, after which some trajectories are leaving the cluster. The initial convergence is consistent with trajectories issued from the direct resolution of the KS equation [6].

The interface height $h(x,t)$ is obtained by integrating $u(x,t) = -\partial_x h(x,t)$. The oscillatory behavior is clearly visible and it is consistent with the KS length scale $l_c = 2\pi\sqrt{\dfrac{\beta}{\alpha + 4\beta}}$, which gives l_c=6.2 for $\alpha = 3$ and $\beta = -1$.
The evolution of the height interface width is consistent with the one predicted by the KS theory [25]. a two step evolution starting with an exponential increase is observed, followed by a quasi-saturating regime.

Chapter 4

A sticky particles model for viscous pressureless gases

4.1 Introduction

We investigate here a variant of the preceding models, which approximates the system of viscous pressureless gases. We consider only attractive forces between nearest neighbours, and the collision dynamics is now sticky, which means that two colliding particles result in a single one, with mass and momentum conservation. Sticky particles dynamics without interaction leads to the pressureless gases system

$$\partial_t \rho + \partial_x(\rho u) = 0, \qquad \partial_t(\rho u) + \partial_x(\rho u^2) = 0,$$

where ρ is the gas density, and u its velocity, see [3, 4]. A specific feature of this model is that the sticky particles dynamics leads directly to a distribution solution for the pressureless gases. When an interaction force is present, this is no longer the case, and some specific time and space scalings have to be performed in order to obtain the viscous pressureless gases system

$$\partial_t \rho + \partial_x(\rho u) = 0 \tag{4.1}$$

$$\partial_t(\rho u) + \partial_x(\rho u^2) = \alpha \partial_{xx} u \tag{4.2}$$

$$\rho(.,0) = \rho^{in}, u(.,0) = u^{in} \tag{4.3}$$

4.2 The particle dynamics

Consider initially N particles on the real line, the observation time $T > 0$ and label the particles by integers $0 \leq i \leq N$. Then, for each of particle we define functions of time t:

- mass : $m_i(t)$
- position at time t : $x_i(t)$
- velocity at time t : $v_i(t) = \dot{x}_i(t)$
- acceleration at time t : $a_i(t) = \dot{v}_i(t) = \ddot{x}_i(t)$

where $1 \leq i \leq N$, $t \in [0, T]$. We have $x_i(t) \in [0, 1]$ since we study a finite system with periodic boundary condition on a system of size 1. We define $\varepsilon = 1/N$.

For this model, we consider particles moving with the velocity changing in time. The principle is as following: for fixed N, that is fixed ε, as long as the particles do not meet, they move accordingly to the dynamics

$$\dot{x}_i^\varepsilon(t) = v_i^\varepsilon(t), \qquad m_i^\varepsilon(t)\dot{v}_i^\varepsilon(t) = \alpha_\varepsilon(v_{i-1}^\varepsilon(t) - 2v_i^\varepsilon(t) + v_{i+1}^\varepsilon(t)).$$

The coefficient α_ε is positive, and is the strength of the interaction. Sometimes we drop the ε dependence when the context is clear.

The dynamics of collisions is defined as follows. We assume that at time t_0, there exists j such that $x_j(t_0) = x_k(t_0)$ and $x_j(t_0) \neq x_k(t_0)$ for all $t < t_0$. Note that there is a finite number of shocks because particles coalesce together. Put $A = \{j \in [1, I] : x_j(t_0) = x_k(t_0)\}(k = \min(A))$. The new velocity after sticking is given by

$$v_k'(t_0) = \frac{\sum\limits_{j\in A} m_j v_j(t_0)}{\sum\limits_{j\in A} m_j}.$$

where $v_i'(t)$ is the velocity after shock. Therefore, the momentum is conserved

$$(\sum_{j\in A} m_j)v_k'(t_0) = \sum_{j\in A} m_j v_j(t_0).$$

The new particle get the new mass by the total mass of stuck particles

$$m_k(t_0) = \sum_{j\in A} m_j.$$

We also note that after collision, the i-index must be changed by its position-order to suit the order in the definition of force.

In this model, we define a continuous velocity field as a sequence of straight lines connecting the points $(x_i^\varepsilon(t), v_i^\varepsilon(t))$

$$v^\varepsilon(x,t) = \frac{v_i^\varepsilon(t)(x - x_{i-1}^\varepsilon(t)) + v_{i-1}^\varepsilon(t)(x_i^\varepsilon(t) - x)}{x_i^\varepsilon(t) - x_{i-1}^\varepsilon(t)} \quad \text{for } x \in [x_{i-1}^\varepsilon(t), x_i^\varepsilon(t)). \tag{4.4}$$

4.3 Towards the continuous model

We have the definition of the empirical density function $\rho_\varepsilon(x,t)$ and momentum $\rho_\varepsilon v_\varepsilon(x,t)$ given by

$$\begin{aligned} \rho_\varepsilon(x,t) &= \frac{1}{N}\sum_{i=1}^{N} m_i^\varepsilon(t)\delta(x-x_i^\varepsilon(t)), \\ q_\varepsilon(x,t) &= \frac{1}{N}\sum_{i=1}^{N} m_i^\varepsilon(t)v_i^\varepsilon(t)\delta(x-x_i^\varepsilon(t)). \end{aligned} \tag{4.5}$$

Notice that we kept the notation $m_i^\varepsilon(t)$ to be consistent with the dynamics, but in these formulas particles have mass 1, and are counted with repetition if collisions have occured. These quantities are defined in the sense of distribution: for any test function $\varphi \in C^\infty([0,1]\times[0,T))$, periodic in space and compactly supported in time,

$$\langle \rho_\varepsilon, \varphi\rangle = \frac{1}{N}\int_0^T \sum_{i=1}^{N} m_i^\varepsilon(t)\varphi(x_i^\varepsilon(t),t)dt, \qquad \langle q_\varepsilon, \varphi\rangle = \frac{1}{N}\int_0^T \sum_{i=1}^{N} m_i^\varepsilon(t)v_i^\varepsilon(t)\varphi(x_i^\varepsilon(t),t)dt.$$

To study the limit as $\varepsilon \to 0$ of the system, we need to perform the same hyperbolic scaling as in Chapter 3, which we describe in more details here. Starting from the velocity field (4.4), we introduce the scaled velocity u_ε and the scaled flow X_ε by

$$\begin{aligned} v_\varepsilon(t,x) &= u_\varepsilon(\varepsilon t, \varepsilon x), \\ \partial_s X_\varepsilon(s,y) &= u_\varepsilon\big(s, X_\varepsilon(s,y)\big), \quad X_\varepsilon(0,y) = y. \end{aligned} \tag{4.6}$$

A straightforward computation shows that the hyperbolic scaling is given by

$$x_i^\varepsilon(t) = \frac{1}{\varepsilon}X_\varepsilon(\varepsilon t, \varepsilon i). \tag{4.7}$$

It has to be understood that there are initial N particles equally disposed at positions i/L, $i = 1,\dots,N$. The scaling means that we are interested in long times ($t \sim 1/\varepsilon$), and high density of particles ($\sim 1/\varepsilon$).

The rescaled functions obtained from ρ_ε and q_ε in (4.5) are defined by

$$\langle \rho^*, \varphi\rangle = \varepsilon^2\langle \rho, \varphi_\varepsilon\rangle, \qquad \langle q^*, \varphi\rangle = \varepsilon^2\langle q, \varphi_\varepsilon\rangle.$$

Using the fact that $\varepsilon = 1/N$, and performing the variable change $\tau = \varepsilon t$ in the time

integrals, we have

$$\begin{aligned}
\langle \rho^*, \varphi \rangle &= \sum_i \int m_i(t) \varphi\big(\tau, X_\varepsilon(\tau, \varepsilon i)\big)\, d\tau, \\
\langle q^*, \varphi \rangle &= \varepsilon \sum_i \int m_i(t) v_i^\varepsilon(t) \varphi\big(\varepsilon t, \varepsilon x_i^\varepsilon(t)\big)\, dt \\
&= \varepsilon \sum_i \int m_i(t) v_\varepsilon(t, x_i^\varepsilon(t)) \varphi\big(\varepsilon t, \varepsilon x_i^\varepsilon(t)\big)\, dt \\
&= \varepsilon \sum_i \int m_i(t) u_\varepsilon(\varepsilon t, \varepsilon x_i^\varepsilon(t)) \varphi\big(\varepsilon t, \varepsilon x_i^\varepsilon(t)\big)\, dt \\
&= \sum_i \int m_i(t) u_\varepsilon(\tau, X_\varepsilon(\tau, \varepsilon i)) \varphi\big(\tau, X_\varepsilon(\tau, \varepsilon i)\big)\, d\tau.
\end{aligned}$$

Thus for $\varepsilon > 0$, ρ_ε^* and q_ε^* are defined in terms of the variables $\tau = \varepsilon t$, $y = \varepsilon x$, and in some sense $q_\varepsilon^* = \rho_\varepsilon^* u_\varepsilon$.

Proposition 4.3.1. *For $\varepsilon > 0$, $(\rho_\varepsilon^*, q_\varepsilon^*)$ are solutions of the system in sense of distribution,*

$$\partial_\tau \rho_\varepsilon^* + \partial_y q_\varepsilon^* = 0 \tag{4.8}$$

$$\partial_\tau q_\varepsilon^* + \partial_y (\rho_\varepsilon u_\varepsilon^2) = S_\varepsilon \tag{4.9}$$

where S_ε^* is the distribution defined by

$$\langle S_\varepsilon^*, \varphi \rangle = \varepsilon \int \sum_i m_i(t) \frac{d}{d\tau} \big[u_\varepsilon\big(\tau, X_\varepsilon(\tau, \varepsilon i)\big)\big]\, \varphi\big(\tau, X_\varepsilon(\tau, \varepsilon i)\big)\, d\tau.$$

Proof. For each $\varepsilon > 0$, for any $\varphi \in C^\infty([0, L] \times [0, T))$

$$\begin{aligned}
\langle \partial_\tau \rho_\varepsilon^*, \varphi \rangle &= -\langle \rho_\varepsilon^*, \partial_\tau \varphi \rangle \\
&= -\varepsilon^2 \int \sum_i m_i(t) \partial_\tau \varphi(\varepsilon t, \varepsilon x_i^\varepsilon(t))\, dt = -\varepsilon \int \sum_i m_i(t) \partial_\tau \varphi\big(\tau, X_\varepsilon(\tau, \varepsilon i)\big)\, d\tau \\
&= -\varepsilon \int \sum_i m_i(t) \frac{d}{d\tau}\big[\varphi\big]\, d\tau + \varepsilon \int \sum_i m_i(t) \partial_s X_\varepsilon(\tau, \varepsilon i) \partial_y \varphi\big(\tau, X_\varepsilon(\tau, \varepsilon i)\big)\, d\tau
\end{aligned}$$

Since φ is compactly supported in time, the first term of the right-hand side in the preceding equation vanishes, we use (4.6), and we obtain $-N\langle q_\varepsilon, \varphi \rangle$. When collisions occur, these computations can be justified as in Bouchut's paper [3], by writing the mass balance at each collision time, which are in finite number.

Let us consider the second equation.

$$\begin{aligned}
\langle \partial_\tau q_\varepsilon^*, \varphi\rangle &= -\langle q_\varepsilon^*, \partial_\tau\varphi\rangle \\
&= -\varepsilon^2 \int \sum_i m_i(t) v_\varepsilon(t, x_i^\varepsilon(t)) \partial_\tau\varphi(\varepsilon t, \varepsilon x_i^\varepsilon(t))\, dt \\
&= -\varepsilon \int \sum_i m_i(t) u_\varepsilon\big(\tau, X_\varepsilon(\tau,\varepsilon i)\big) \partial_\tau\varphi\big(\tau, X_\varepsilon(\tau,\varepsilon i)\big)\, d\tau \\
&= -\varepsilon \int \sum_i m_i(t) u_\varepsilon\big(\tau, X_\varepsilon(\tau,\varepsilon i)\big) \frac{d}{d\tau}\big[\varphi\big(\tau, X_\varepsilon(\tau,\varepsilon i)\big)\big]\, d\tau \\
&\quad + \varepsilon \int \sum_i m_i(t) u_\varepsilon^2\big(\tau, X_\varepsilon(\tau,\varepsilon i)\big) \partial_y\varphi\big(\tau, X_\varepsilon(\tau,\varepsilon i)\big)\, d\tau \\
&= -\varepsilon \int \sum_i m_i(t) \frac{d}{d\tau}\left[(u_\varepsilon\varphi)\big(\tau, X_\varepsilon(\tau,\varepsilon i)\big)\right]\, d\tau \\
&\quad + \varepsilon \int \sum_i m_i(t) \varphi\big(\tau, X_\varepsilon(\tau,\varepsilon i)\big) \frac{d}{d\tau}\left[u_\varepsilon\big(\tau, X_\varepsilon(\tau,\varepsilon i)\big)\right]\, d\tau \\
&\quad + \varepsilon \int \sum_i m_i(t) u_\varepsilon^2\big(\tau, X_\varepsilon(\tau,\varepsilon i)\big) \partial_y\varphi\big(\tau, X_\varepsilon(\tau,\varepsilon i)\big)\, d\tau
\end{aligned}$$

Using the same remark as before, we have m_i is a constant between collisions, which are in finite number. Thus the conservation of momentum at each collision time implies that the first term in the right-hand side is zero. The second term defines S_ε,and the third one is $-N\langle \partial_y(\rho_\varepsilon^* u_\varepsilon^2), \varphi\rangle$. □

We turn now to the following formal result of consistency for the particle system.

Theorem 4.3.1. *Assume that the scaled distributions ρ_ε^*, q_ε^* converge towards ρ and q, and that the velocity field u_ε converges to some smooth enough u, and let X by the associated flow. Assume finally that we have $\alpha_\varepsilon = \alpha/\varepsilon$, for some $\alpha > 0$. Then (ρ, u) are distributional solutions of the system*

$$\partial_\tau\rho + \partial_y(\rho u) = 0 \tag{4.10}$$

$$\partial_\tau(\rho u) + \partial_y(\rho u^2) = \alpha\partial_{yy} u \tag{4.11}$$

Proof. First, we observe that by the convergence assumptions, we have in the sense of distributions

$$\partial_\tau\rho_\varepsilon^* + \partial_y(\rho_\varepsilon^* u_\varepsilon) \to \partial_\tau\rho + \partial_y(\rho u)$$

and

$$\partial_\tau(\rho_\varepsilon^* u_\varepsilon) + \partial_y(\rho_\varepsilon^* u_\varepsilon^2) \to \partial_\tau(\rho u) + \partial_y(\rho u^2).$$

when $\varepsilon \to 0$. Thus we prove (4.11) by using the following lemma on hyperbolic scaling and recalling the definition of S_ε^*.

Lemma 4.3.2. *For each $\varepsilon > 0$,*

$$\varphi(\tau, X(\tau, X(\tau, \varepsilon(i+1)) - 2\varphi(\tau, X(\tau, \varepsilon i)) + \varphi(\tau, X(\tau, \varepsilon(i-1))) = \varepsilon^2 \partial_{yy}\varphi(\tau, X(\tau, \varepsilon i)) + o(\varepsilon^2).$$

The proof of this lemma consists in a sequence of tedious but straightforward computations.

We turn now to the study of S^*_ε. Going back to the definition of u_ε, we first notice that, with $\tau = \varepsilon t$,

$$\begin{aligned}\varepsilon \frac{d}{d\tau}\left[u_\varepsilon\big(\tau, X_\varepsilon(\tau, \varepsilon i)\big)\right] = \dot v_i^\varepsilon(t) &= \frac{\alpha_\varepsilon}{m_i}\left(v_{i+1}^\varepsilon(t) - 2v_i^\varepsilon(t) + v_{i-1}^\varepsilon(t)\right) \\ &= \frac{\alpha_\varepsilon}{m_i}\left(u_\varepsilon\big(\tau, X_\varepsilon(\tau, \varepsilon(i+1)\big) - 2u_\varepsilon\big(\tau, X_\varepsilon(\tau, \varepsilon i\big) + u_\varepsilon\big(\tau, X_\varepsilon(\tau, \varepsilon(i1)\big)\right),\end{aligned}$$

where we have used the definition of the interaction force. Thus S^*_ε can be rewritten

$$\begin{aligned}\langle S^*_\varepsilon, \varphi\rangle \;=\; & \alpha_\varepsilon \sum_i \int \left(u_\varepsilon(\tau, X_\varepsilon(\tau, \varepsilon(i+1)) - 2u_\varepsilon(\tau, X_\varepsilon(\tau, \varepsilon i)) + u_\varepsilon(\tau, X_\varepsilon(\tau, \varepsilon(i-1)))\right) \\ & \times \varphi\big(\tau, X_\varepsilon(\tau, \varepsilon i)\big)\, d\tau,\end{aligned}$$

which can be rewritten by switching the indices and using periodicity

$$\begin{aligned}\langle S^*_\varepsilon, \varphi\rangle \;=\; & \alpha_\varepsilon \sum_i \int \left(\varphi(\tau, X_\varepsilon(\tau, \varepsilon(i+1)) - 2\varphi(\tau, X_\varepsilon(\tau, \varepsilon i)) + \varphi(\tau, X_\varepsilon(\tau, \varepsilon(i-1)))\right) \\ & \times u_\varepsilon\big(\tau, X_\varepsilon(\tau, \varepsilon i)\big)\, d\tau.\end{aligned}$$

We write $\langle S^*_\varepsilon, \varphi\rangle = \langle S^*_\varepsilon - S^0_\varepsilon, \varphi\rangle + \langle S^0_\varepsilon, \varphi\rangle$, where S^0_ε is defined as S^*_ε, but with X_ε replaced by X.

We apply lemma 4.3.2 to φ, and get

$$\langle S^0_\varepsilon, \varphi\rangle = \alpha_\varepsilon \sum_i \varepsilon^2 \int u(\tau, X(\tau, \varepsilon i))\left[\partial_{yy}\psi\big(\tau, X(\tau, \varepsilon i)\big) + o(\varepsilon^2)\right] d\tau.$$

The sum over i can be replaced by an integral on y using the quadrature formula $\sum_i \varepsilon\chi(\varepsilon i) \sim \int \chi(y)\, dy + o(\varepsilon)$, so that, recalling that $\alpha_\varepsilon = \alpha/\varepsilon$,

$$\langle S^0_\varepsilon, \varphi\rangle = \alpha \int_{]0,\infty[} \int_0^1 u(\tau, X(\tau, y))\left[\partial_{yy}\psi\big(\varepsilon t, X(\tau, y)\big) + o(\varepsilon^2)\right] d\tau\, dy.$$

Finally, we notice that $S^*_\varepsilon - S^0_\varepsilon \to 0$ when $\varepsilon \to 0$, thus together with the preceding formula for S^0_ε one gets for $\varepsilon \to 0$ that $S^*_\varepsilon \to S$ defined by

$$\langle S, \varphi\rangle = \alpha \int_{]0,\infty[} \int_L u\big(\tau, X(\tau, y)\big)\left[\partial_{yy}\psi\big(\tau, X(\tau, y)\big)\right] d\tau\, dy,$$

that is $S = \alpha\partial_{yy}u$.

4.4 Estimates on the velocity in the particle model

The particles are numbered in such a way that $i < j \Rightarrow x_i \leq x_j$. For theoretical results, the number of particles remains constant, so that there may be several indices $i_1, \dots, i_k$ such that $x_{i_1} = \cdots = x_{i_k}$. For practical computations, one has to renumber the particles, thus the total number decreases. Recall that, following Grenier [31], one has the following estimates for the sticky particles dynamics:

$$x_i(t) < x_j(t) \quad \Longrightarrow \quad v_j(t) - v_i(t) \leq \frac{x_j(t) - x_i(t)}{t} \text{ and } v_j(t) - v_i(t) \geq -\frac{2A}{t}, \qquad (4.12)$$

assuming that the support of ρ^0 lies in $[-A, A]$. The first estimate is the discrete analogue of the OSL estimate at the continuous level, namely $\partial_y u \leq 1/t$, the second one corresponds to a bounded variation estimate.

To prove the OSL estimate in (4.12), first notice that, if particles i and j never encounter collisions between 0 and t, then one has $0 > x_i^0 - x_j^0 = x_i(t) - tv_i(t) - x_j(t) + tv_j(t)$, and the estimate is optimal. Now, *ab absurdo*, if one has $x_i(t) = x_j(t)$ and $v_j - v_i > (x_j - x_i)/t$, then for $h > 0$ small enough to ensure that no collision occur, we get

$$x_i(t+h) - x_j(t+h) = x_i(t) + hv_i(t) - x_j(t) + hv_j(t) < \big(x_i(t) - x_j(t)\big)\big(1 + \frac{h}{t}\big) = 0.$$

Therefore, two particles that coincide at time t are separated at time $t+h$, which contradicts the sticky particle dynamics. In the same way, the BV estimate holds true when no collisions occur, since $t(v_j - v_i) = x_j - x_i - (x_j^0 - x_i^0) \geq -2A$, and the same contradiction argument gives the general estimate.

The numerical scheme for the scalar pressureless gases system with viscous was considered by Boudin and Mathiaud in [21]. They proposed the upwind diffusive scheme for density and velocity that satisfy one-side Lipschitz (OSL) condition which is required for the duality solution. In this work, we also consider this system in view of particle model which is introduced as above. For estimates with attractive force, we do not obtain exact OSL estimate but BV norm estimate. This is enough to get compactness, hence convergence. This will be checked in lemma 4.4.1.

Now we introduce some notations. Let $\Delta t > 0$, time step $t^n = n\Delta t$, $v_i^n = v_i(t^n)$, L is the system size and I is the number of particle. We denote the density and velocity ρ_i^n, u_i^n which are respected the approximation of solutions of (4.1,4.2,4.3) at time $n\Delta t \in [0, T]$ and coordinate $x_i(n\Delta t)$. Assume that the periodic initial data $u^{in}, \rho^{in}(u^0, \rho^0) \in C^1([0, L])$. First we consider lemma (4.4.1) for BV norm estimate on velocity field of particles.

Lemma 4.4.1. *For any $n \geq 0$, we have*
$TV(v^n) \leq TV(u^0)$ where $TV(u) = \sum_i |\Delta u_{i+1/2}|$ is the discrete BV norm of $u = (u_i)_i$.

Proof. . For the BV norm estimate, since we have a finite number of collisions, we can first check with Δt small enough such that there are no collisions until $t^n + \Delta t$. Thus we compute

$$v_i^* = v_i^n + \frac{\alpha \Delta t}{m_i}\big(v_{i+1}^n - 2v_i^n + v_{i-1}^n\big).$$

We introduce the so-called incremental coefficients

$$C_{i+1/2} = D_{i+1/2} = \frac{\alpha \Delta t}{m_i} \geq 0, \tag{4.13}$$

so that the preceding relation becomes

$$v_i^* = C_{i+1/2} v_{i+1}^n + \Big(1 - D_{i+1/2} - C_{i+1/2}\Big) v_i^n + D_{i-1/2} v_{i-1}^n.$$

It is clear that, provided $1 - D_{i+1/2} - C_{i+1/2} \geq 0$, we have a convex combination on the right-hand side, which gives readily the maximum principle for v_i^*. Since $m_i \geq 1$ for all i, this is satisfied if

$$2\alpha \Delta t \leq 1. \tag{4.14}$$

To get BV estimates, we set $\Delta v_{i+1/2} = v_{i+1} - v_i$, so that we can write

$$\Delta v_{i+1/2}^* = \Delta v_{i+1/2}^n + \frac{\alpha \Delta t}{m_{i+1}} \Delta v_{i+3/2}^n - \alpha \Delta t \Big(\frac{1}{m_i} + \frac{1}{m_{i+1}}\Big) \Delta v_{i+1/2}^n + \frac{\alpha \Delta t}{m_i} \Delta v_{i-1/2}^n. \tag{4.15}$$

Using the same incremental coefficients (4.13), we can rewrite (4.15) as

$$\Delta v_{i+1/2}^* = C_{i+3/2} \Delta v_{i+3/2}^* + \Big(1 - D_{i+1/2} - C_{i+1/2}\Big) \Delta v_{i+1/2}^* + D_{i-1/2} \Delta v_{i-1/2}^*. \tag{4.16}$$

Under condition (4.14), all coefficients in (4.16) are nonnegative, so that

$$|\Delta v_{i+1/2}^*| \leq C_{i+3/2} |\Delta v_{i+3/2}^*| + \Big(1 - D_{i+1/2} - C_{i+1/2}\Big) |\Delta v_{i+1/2}^*| + D_{i-1/2} |\Delta v_{i-1/2}^*|.$$

In the definition of the BV norm, a telescopic summation is involved, so that we get

$$TV(v^*) \leq TV(v^n).$$

Hence when no collisions occur, we have the maximum principle as well as a (local in time) BV estimate for u.

Now we consider a collision time t, assuming that u^* stands for the velocities at t^-, and denoting the post-collisional velocities by u'. The maximum principle is strightforward, since for all i u'_i is convex combination of the pre-collisonal velocities:

$$v'_i = \frac{\sum_j m_j v_j^*}{\sum_j m_j} \in [\min(v_j^*)_j, \max(v_j^*)_j].$$

Concerning the BV estimate, we notice that, for a binary collision between i and $i+1$ (the generalization is obvious), indexing the outgoing particle velocity with index i,

$$|v'_{i+2} - v'_i| \leq |v^*_{i+2} - v^*_{i+1}| + \frac{m_i}{m_i + m_{i+1}} |v^*_{i+1} - v^*_i| \leq |v^*_{i+2} - v^*_{i+1}| + |v^*_{i+1} - v^*_i|$$

since $\dfrac{m_i}{m_i + m_{i+1}} < 1$.

Iterating this method must lead to maximum principle and BV estimate such as

$$\|v^n\|_\infty \leq \|u^0\|_\infty, \qquad TV(v^n) \leq TV(u^0),$$

for a "theoretical" scheme where for a given Δt, u^{n+1} is computed from u^n by iterating the preceding steps a finite number of times on one time step.
Assume that at t^n, one has $TV(v^n) = \sum_i |v_{i+1}(t^n) - v_i(t^n)\| \leq TV(v^0)$. Up to the first collision time, say $t^* > t^n$, we can apply the Euler scheme described above, and let Δt go to zero. This will lead to $TV(v(t^*_-) \leq TV(v^n)$. Since collisions decrease the TV norm, as we have seen before, we have after collision $TV(v(t^*_+) \leq TV(v^n)$. To obtain the estimate for any given $T > 0$, we proceed step by step since we have a finite number of collisions. □

Theorem 4.4.2. *Let $v = (v_i)_i$ is the velocity field of particle model and u_ε is the scaled function of v. Then there exists u in $BV([0, L])$ that $u_\varepsilon \to u$ when $\varepsilon \to 0$.*

Proof. Applying the scaling (**??**), which defines the function u_ε by (**??**), we have

$$\begin{aligned} \textstyle\sum_i |v_{i+1}(t) - v_i(t)| &= \sum_i \left| u_\varepsilon\left(\varepsilon t, X\big(\varepsilon t, \varepsilon(i+1)\big)\right) - u_\varepsilon\left(\varepsilon t, X\big(\varepsilon t, \varepsilon i\big)\right)\right| \\ &= \varepsilon \sum_i \frac{\left| u_\varepsilon\left(\tau, X\big(\tau, \varepsilon(i+1)\big)\right) - u_\varepsilon\left(\tau, X\big(\tau, \varepsilon i\big)\right)\right|}{\varepsilon}. \end{aligned}$$

By the same quadrature formula we already used in theorem 4.3, this should go to

$$\int |\partial_y u(\tau, y)|\, dy = TV(u(\tau, .)).$$

From this we can get the decrease of the TV norm by lemma 4.4.1, hence the compactness that is enough to get convergence.

4.5 Numerical illustration

We illustrate here the behavior of the particle system for two values of N (hence of ε). Notice that, as noticed for instance in [36], solution to the viscous pressureless gases system are smooth, and that, provided ρ remains positive, the velocity is solution to the Burgers-like equation

$$\partial_\tau u + u\partial_y u = \frac{\alpha}{\rho}\partial_{yy} u.$$

Initial datum for velocity is a sine function with five oscillations on $[0, 1]$

$$u^0(x) = \frac{1}{2}(1.1 + \sin(10\pi)),$$

and the particles are regularly disposed in $[0, 1]$.

The particles tend to concentrate on five aggregates which increase and propagate in time. This is illustrated in figure 4.1, for an initial number of particles $N = 10000$, and $\alpha_\varepsilon = 500$ (which corresponds somehow to $\alpha = 0.05$).

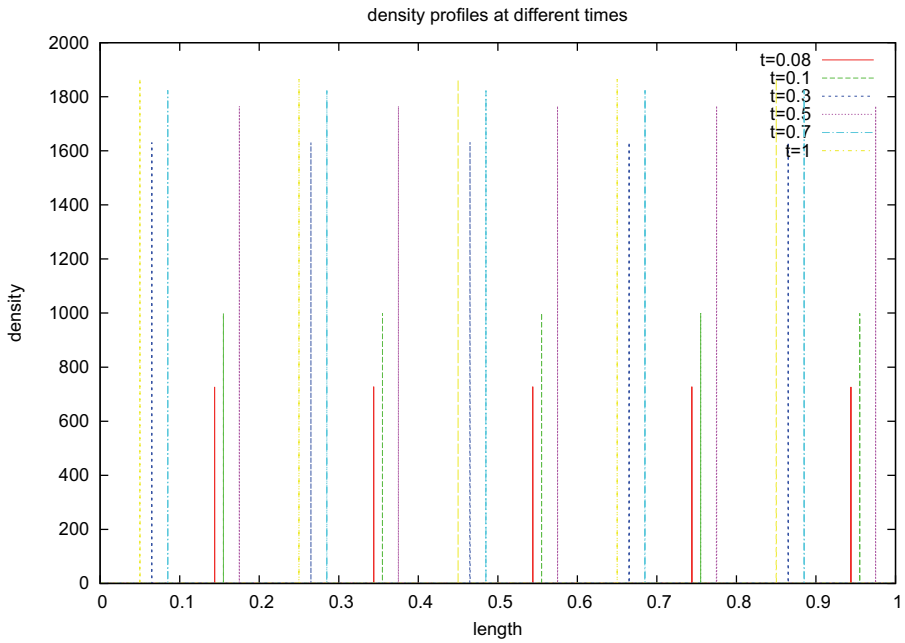

Figure 4.1: $N = 10000$, $\alpha_\varepsilon = 500$

Now we compare the velocity profiles at fixed times, for $N = 10000$ and $N = 100000$ particles, that is $\varepsilon = 10^{-5}$ and $\varepsilon = 10^{-6}$. Accordingly, the two values of α_ε are respectively $\alpha_\varepsilon = 500$ and $\alpha_\varepsilon = 5000$. Figures 4.2 and 4.3 show the corresponding velocity profiles. We notice a very similar behavior between the two computations, the sharper form of the

profiles in Figure 4.3 likely results from a better numerical diffusion due to the higher number of particles.

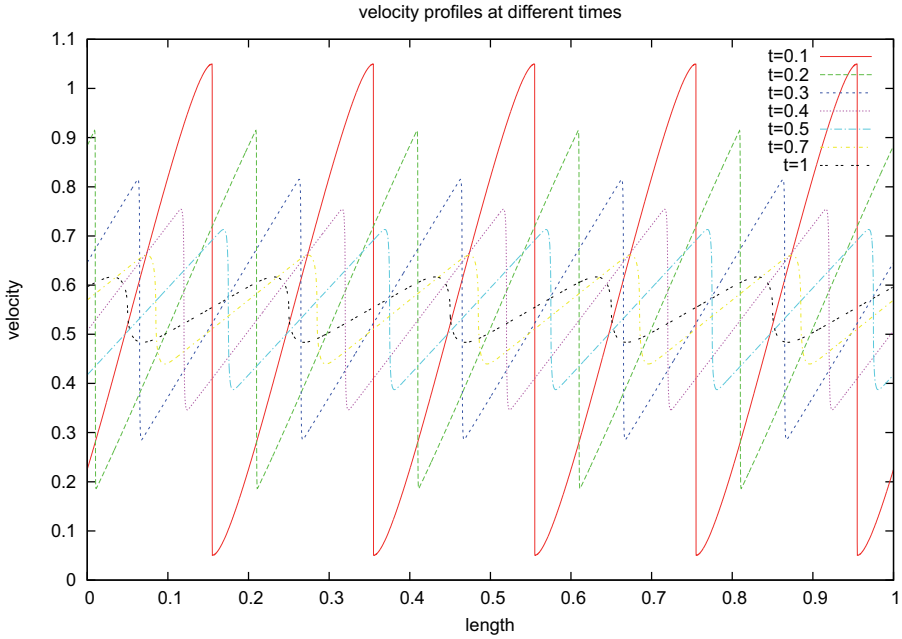

Figure 4.2: $N = 10000$, $\alpha_\varepsilon = 500$

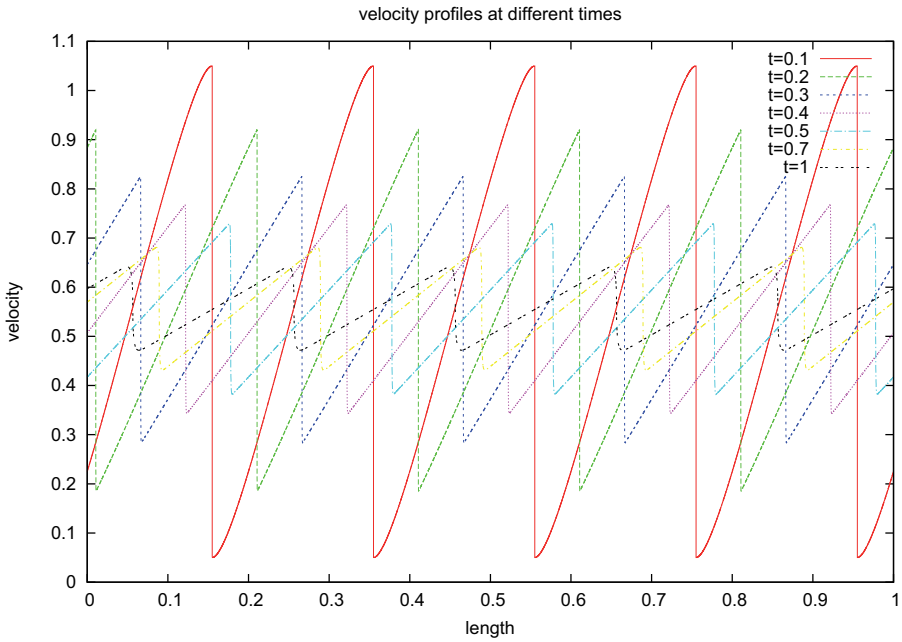

Figure 4.3: $N = 100000$, $\alpha_\varepsilon = 5000$

Appendix A

Appendix

Lemma A.0.1. *For each L is the size of the system. We have*

$$\int_0^L u(x,t)dx = \frac{1}{2}\sum_i (x_i - x_{i-1})(p_i + p_{i+1})$$

where $u(x,t)$ is defined

$$u(x,t) = \frac{p_i(t)(x - x_{i-1}(t)) + p_{i-1}(t)(x_i(t) - x)}{x_i(t) - x_{i-1}(t)}$$

Proof.
We have

$$\begin{aligned}
\int_{x_{i-1}}^{x_i} u(x,t)dx &= \frac{1}{2}\left(\frac{p_i - p_{i-1}}{x_i - x_{i-1}}\right) x^2\Big|_{x_{i-1}}^{x_i} + \left(\frac{p_{i-1}x_i - p_i x_{i-1}}{x_i - x_{i-1}}\right) x\Big|_{x_{i-1}}^{x_i} \\
&= \frac{1}{2}(p_i - p_{i-1})(x_i - x_{i-1}) + p_{i-1}x_i - p_i x_{i-1} \\
&= \frac{1}{2}(p_i x_i + p_i x_{i-1} - p_{i-1}x_i - p_{i-1}x_{i-1}) + p_{i-1}x_i - p_i x_{i-1} \\
&= \frac{1}{2}(p_i x_i - p_i x_{i-1} + p_{i-1}x_i - p_{i-1}x_{i-1}) \\
&= \frac{1}{2}(x_i - x_{i-1})(p_i + p_{i+1})
\end{aligned}$$

Hence

$$\int_0^L u(x,t)dx = \frac{1}{2}\sum_i (x_i - x_{i-1})(p_i + p_{i+1})$$

□

Lemma A.0.2. *Put function $v(x)$ as the right hand side of* (4.1)

$$v(x) = \frac{\dot{p}_i(x - x_{i-1}) + \dot{p}_{i-1}(x_i - x)}{x_i - x_{i-1}}$$

with

$\dot{x}_i = p_i$

$\dot{p}_i = \xi_i - \xi_{i+1} = (x_i - x_{i-1}) - (x_{i+1} - x_i) = 2x_i - x_{i-1} - x_{i+1}$

then,

$$\int_{x_{ia}}^{x_{ib}} v(x)dx = \frac{1}{2} \sum_{i=ia+1}^{i=ib} (x_i^2 - x_{i-1}^2 - x_i x_{i+1} - x_i x_{i-2} + x_{i-1} x_{i+1} + x_{i-1} x_{i-2})$$

Proof.

Rewrite the function $v(x)$,

$$v(x) = \frac{\dot{p}_i - \dot{p}_{i-1}}{x_i - x_{i-1}} x + \frac{\dot{p}_{i-1} x_i - \dot{p}_i x_{i-1}}{x_i - x_{i-1}}.$$

Taking integral this function in interval $[x_{i-1}, x_i]$

$$\begin{aligned}
\int_{x_{i-1}}^{x_i} v(x)dx &= \frac{1}{2} \left(\frac{\dot{p}_i - \dot{p}_{i-1}}{x_i - x_{i-1}} \right) x^2 \Big|_{x_{i-1}}^{x_i} + \left(\frac{\dot{p}_{i-1} x_i - \dot{p}_i x_{i-1}}{x_i - x_{i-1}} \right) x \Big|_{x_{i-1}}^{x_i} \\
&= \frac{1}{2} (\dot{p}_i - \dot{p}_{i-1})(x_i - x_{i-1}) + \dot{p}_{i-1} x_i - \dot{p}_i x_{i-1} \\
&= \frac{1}{2} (\dot{p}_i x_i + \dot{p}_i x_{i-1} - \dot{p}_{i-1} x_i - \dot{p}_{i-1} x_{i-1}) + \dot{p}_{i-1} x_i - \dot{p}_i x_{i-1} \\
&= \frac{1}{2} (\dot{p}_i x_i - \dot{p}_i x_{i-1} + \dot{p}_{i-1} x_i - \dot{p}_{i-1} x_{i-1}) \\
&= \frac{1}{2} (x_i - x_{i-1})(\dot{p}_i + \dot{p}_{i+1}),
\end{aligned}$$

then, we get

$$\begin{aligned}
\int_{x_{ia}}^{x_{ib}} v(x)dx &= \frac{1}{2} \sum_{i=ia+1}^{i=ib} (x_i - x_{i-1})(\dot{p}_i + \dot{p}_{i+1}) \\
&= \frac{1}{2} \sum_{i=ia+1}^{i=ib} (x_i - x_{i-1})(2x_i - x_{i-1} - x_{i+1} + 2x_{i-1} - x_{i-2} - x_i) \\
&= \frac{1}{2} \sum_{i=ia+1}^{i=ib} (x_i - x_{i-1})(x_i + x_{i-1} - x_{i+1} - x_{i-2}) \\
&= \frac{1}{2} \sum_{i=ia+1}^{i=ib} (x_i^2 - x_{i-1}^2 - x_i x_{i+1} - x_i x_{i-2} + x_{i-1} x_{i+1} + x_{i-1} x_{i-2}).
\end{aligned}$$

□

A.1 Explanation of the matlab program for simulation

A.1.1 The trajectories of particles

In this program, we consider the motions of n particles which depend on time t. We have the position of the particle at time t is $x_i(t)$ and its velocity is $p_i(t)$. Since the position $x_i(t)$ depends on $p_i(t)$, so in the program, we also find $p_i(t)$ after each step.
The following conditions are necessary for the simulation.
(i) The position of particle:
We have

$$\dot{x}_i(t) = p_i(t)$$

and

$$x_i(t+\varepsilon) \approx x_i(t) + \varepsilon \dot{x}_i(t),$$

thus

$$x_i(t+\varepsilon) \approx x_i(t) + \varepsilon p_i(t). \tag{A.1}$$

(ii) The velocity of particle:
We can see that in order to find the position $x_i(t+\varepsilon)$ on the next steps of time, we need to know its velocity which is different from two models.
- In the particle model for Burgers' equation, we have

$$\dot{p}_i(t) = 0,$$

so

$$p_i(t+\varepsilon) = p_i(t). \tag{A.2}$$

- In the chaotic model, we have

$$\dot{p}_i(t) = 2x_i(t) - x_{i+1}(t) - x_{i-1}(t), \tag{A.3}$$

so

$$p_i(t+\varepsilon) \approx p_i(t) + \varepsilon(2x_i(t) - x_{i+1}(t) - x_{i-1}(t)). \tag{A.4}$$

(iii) The collision:
This condition make an effect on the models. If two neighboring particles (x_i and x_{i+1}) collide, then they are replaced by a single one (with mass $m = 1$). We have its new

position and velocity as following

$$x(t) = x_i(t) = x_{i+1}(t)$$
$$p(t) = \frac{[x_i(t) - x_{i-1}(t)]p_i(t) + [x_{i+2}(t) - x_{i+1}(t)]p_{i+1}(t)}{x_{i+2}(t) - x_{i-1}(t)}$$

(iv) The creation:
If the distance between two neighboring particles is α, then there is new particle created at the position

$$x(t) = \frac{1}{2}(x_i(t) + x_{i+1}(t))$$

and its velocity is

$$p(t) = \frac{1}{2}(p_i(t) + p_{i+i}(t))$$

(v) The starting condition:
We begin the program with n_0 particles as a random vector $x(0) = (x_1(0), ..., x_{n_0}(0))$ such that

- $x_i \in [a, b]$
- $x_i < x_{i+1}$
- $\xi_i = x_{i+1} - x_i \in (0, \alpha)$

We also put a random velocity vector $p(0) = (p_1(0), ..., p_{n_0}(0))$ at the beginning. Then, we chose ε small enough, we can calculate $x_i(t)$ and $p_i(t)$ by (7.1), (7.2), (7.4). After each step, the positions $x_i(t)$ are plotted.

A.1.1.1 The velocity

We use the previous program to plot the velocity $p_i(t)$ instead of $x_i(t)$. That portrait is also the velocity field $u(x, t)$

$$u(x,t) = \frac{p_i(t)(x - x_{i-1}(t)) + p_{i-1}(t)(x_i(t) - x)}{x_i(t) - x_{i-1}(t)},\ x \in [x_{i-1}(t), x_i(t))$$

that are the segments from $(x_{i-1}(t), p_{i-1}(t))$ to $(x_i(t), p_i(t))$.

A.1.1.2 The height function

We will plot the value of function $h(x_i, t) = h(x_i(t))$ and begin program with $h(x_1(0)) = 0$. Following is explanation how to compute $h(x_{i+1}(t))$ by $h(x_i(t))$ and $h(x_i(t+\varepsilon))$ by $h(x_i(t))$.

Notice that by previous program, we have $x_i(t)$ and $p_i(t)$ for all i, t.
First, we consider the following equation

$$u(x,t) = -\partial_x h(x,t) \tag{A.5}$$

and get

$$h(x_{i+1},t) - h(x_i,t) = -\int_{x_i}^{x_{i+1}} u(x,t)dx$$
$$h(x_{i+1},t) - h(x_i,t) = -\frac{1}{2}(x_{i+1}(t) - x_i(t))(p_{i+1}(t) + p_i(t))$$

so

$$h(x_{i+1},t) = h(x_i,t) - \frac{1}{2}(x_{i+1}(t) - x_i(t))(p_{i+1}(t) + p_i(t)). \tag{A.6}$$

Second, we must find $h(x_i(t+\varepsilon))$ by $h(x_i(t))$. The equations that characterize for two models are considered in this part.
- *In the model for Burgers equation*:
We replace the Burgers equation (3.1) by (7.5) and get

$$-\partial_{tx} h(x,t) + u(x,t)\partial_x u(x,t) = 0 \quad \text{(Burgers's equation)},$$
$$\partial_x(-\partial_t h(x,t) + \frac{1}{2}(u(x,t))^2) = 0$$

that implies

$$-\partial_t h(x,t) + \frac{1}{2}(u(x,t))^2 = c_t$$
$$\partial_t h(x,t) = \frac{1}{2}(u(x,t))^2 - c_t.$$

Then, we have the approximation

$$h(x,t+\varepsilon) \approx h(x,t) + \frac{1}{2}\varepsilon(u(x,t))^2 - \varepsilon c_t.$$

In the program, we chose ε small enough so that we can ignore εc_t and obtain

$$h(x_i(t+\varepsilon)) \approx h(x_i(t)) + \frac{1}{2}\varepsilon(u(x_i,t))^2$$

$$h(x_i(t+\varepsilon)) \approx h(x_i(t)) + \frac{1}{2}\varepsilon(p_i(t))^2 \tag{A.7}$$

- *In the chaotic model*:
To be simple equation (4.1), put

$$f(x,t) = \frac{\dot{p}_{i+1}(t)(x - x_i(t)) + \dot{p}_i(t)(x_{i+1}(t) - x)}{x_{i+1}(t) - x_i(t)},\ x \in [x_i(t), x_{i+1}(t))$$

and take its integral

$$\int f(x,t)dx = \frac{(\dot{p}_{i+1}(t) - \dot{p}_i(t))}{2(x_{i+1}(t) - x_i(t))}x^2 + \frac{\dot{p}_i(t)x_{i+1}(t) - \dot{p}_{i+1}(t)x_i(t)}{x_{i+1}(t) - x_i(t)}x + c_t.$$

Then, we replace the equation (4.1) by (7.5),

$$-\partial_{tx}h(x,t) + u(x,t)\partial_x u(x,t) = f(x,t)$$
$$\partial_x(-\partial_t h(x,t) + \frac{1}{2}(u(x,t))^2) = f(x,t).$$

that implies

$$-\partial_t h(x,t) + \frac{1}{2}(u(x,t))^2 = \int f(x,t)dx$$
$$\partial_t h(x,t) = \frac{1}{2}(u(x,t))^2 - \int f(x,t)dx.$$

By the similar steps as for Burgers equation, the result is

$$h(x_i(t+\varepsilon)) = h(x_i(t)) + \frac{1}{2}\varepsilon(p_i(t))^2 - \frac{(\dot{p}_{i+1}(t) - \dot{p}_i(t))}{2(x_{i+1}(t) - x_i(t))}\varepsilon x_i^2(t) - \frac{\dot{p}_i(t)x_{i+1}(t) - \dot{p}_{i+1}(t)x_i(t)}{x_{i+1}(t) - x_i(t)}\varepsilon x_i(t).$$

A.2 Trajectory of particles

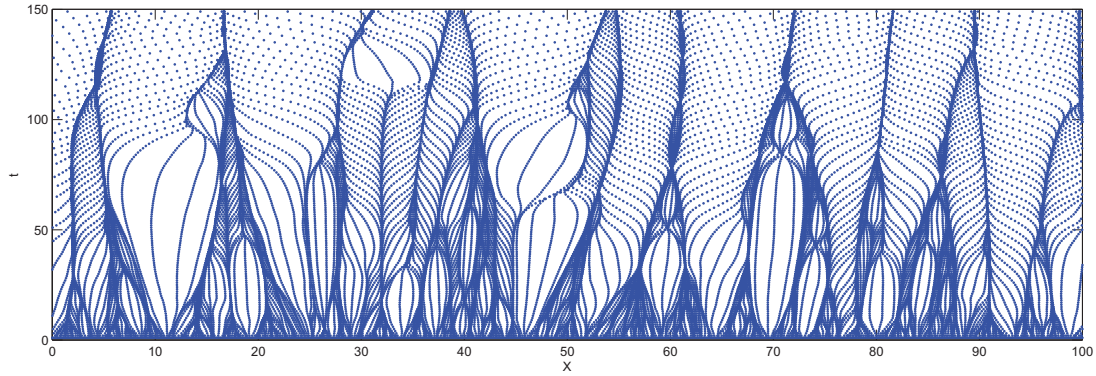

Figure A.1: Zoom out of the trajectory of particles where $x \in [0, 100]$.

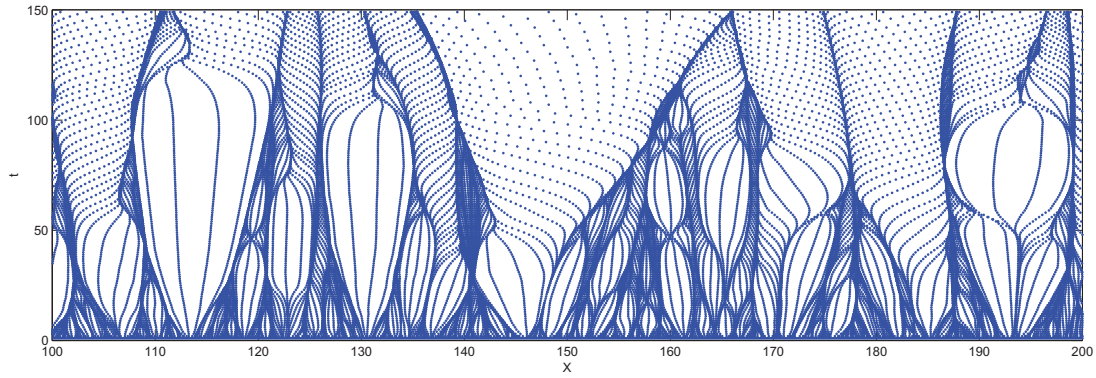

Figure A.2: Zoom out of the trajectory of particles where $x \in [100, 200]$.

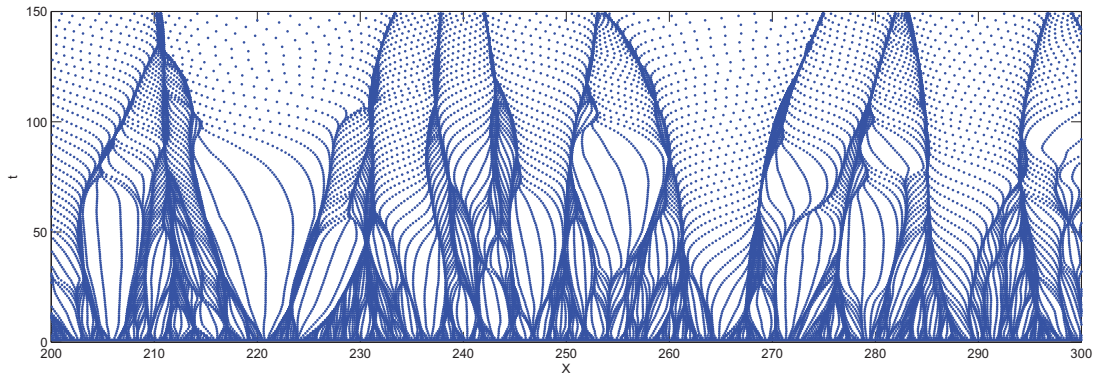

Figure A.3: Zoom out of the trajectory of particles where $x \in [200, 300]$.

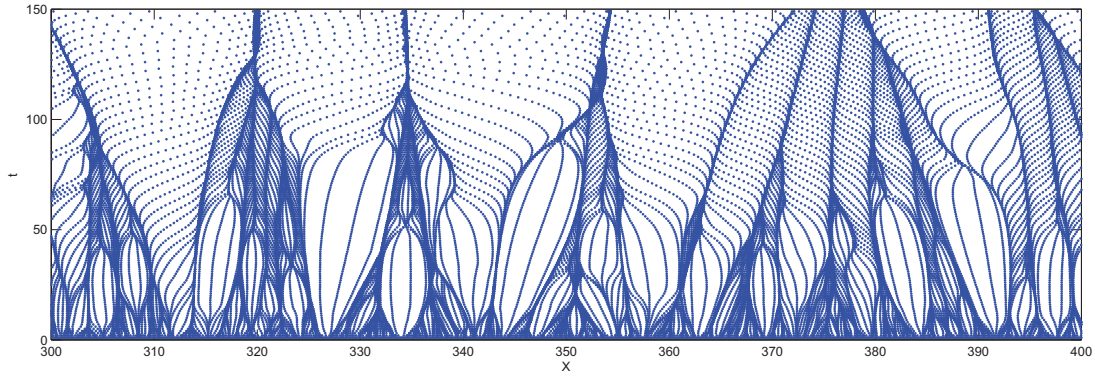

Figure A.4: Zoom out of the trajectory of particles where $x \in [300, 400]$.

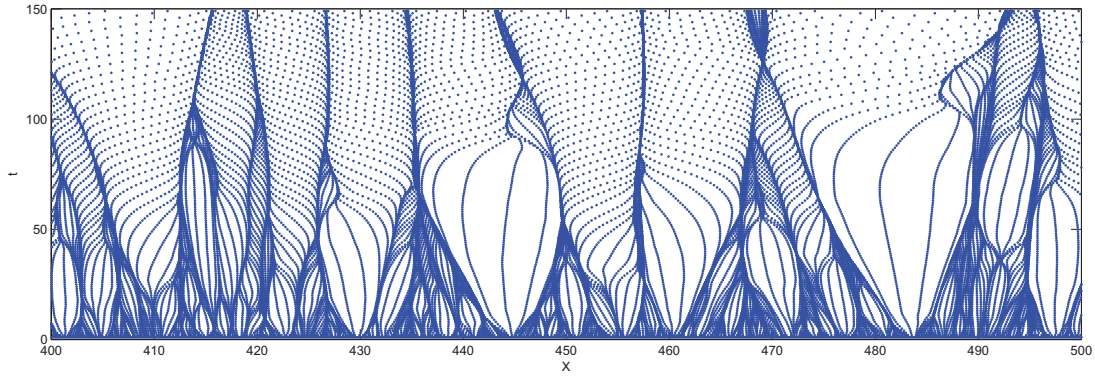

Figure A.5: Zoom out of the trajectory of particles where $x \in [400, 500]$.

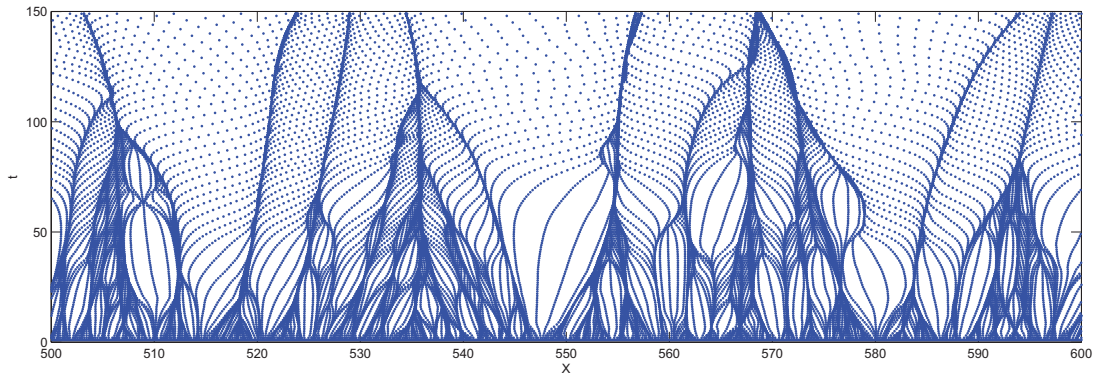

Figure A.6: Zoom out of the trajectory of particles where $x \in [500, 600]$.

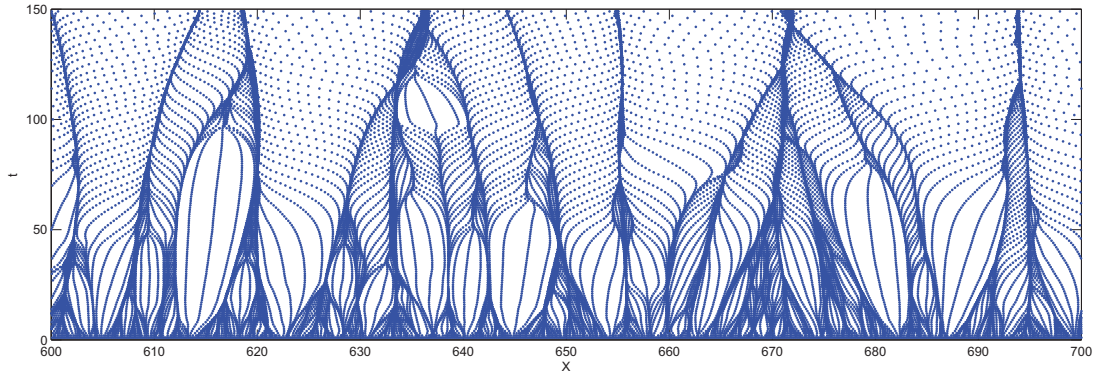

Figure A.7: Zoom out of the trajectory of particles where $x \in [600, 700]$.

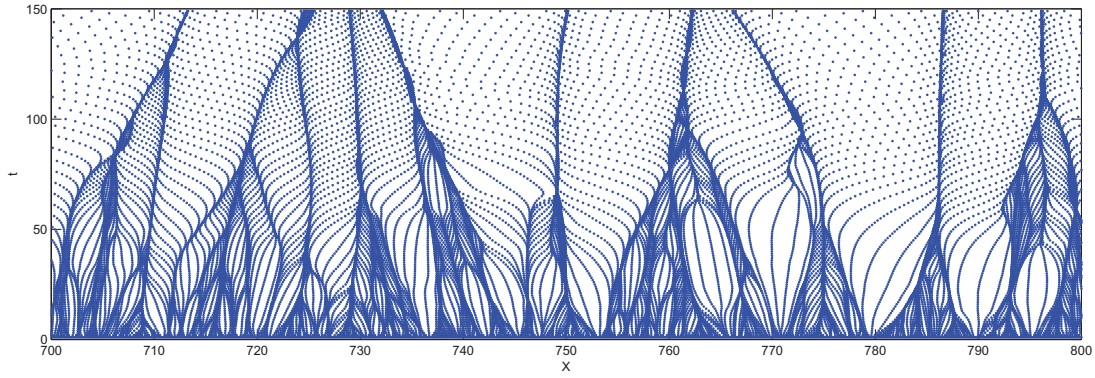

Figure A.8: Zoom out of the trajectory of particles where $x \in [700, 800]$.

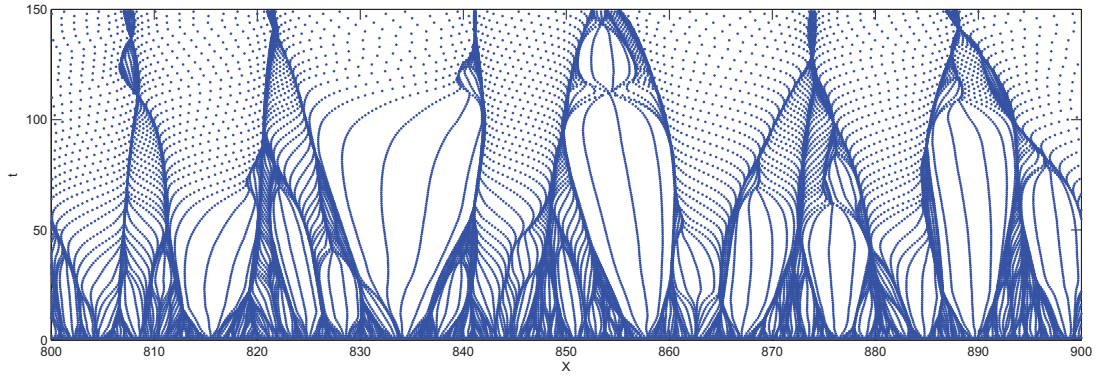

Figure A.9: Zoom out of the trajectory of particles where $x \in [800, 900]$.

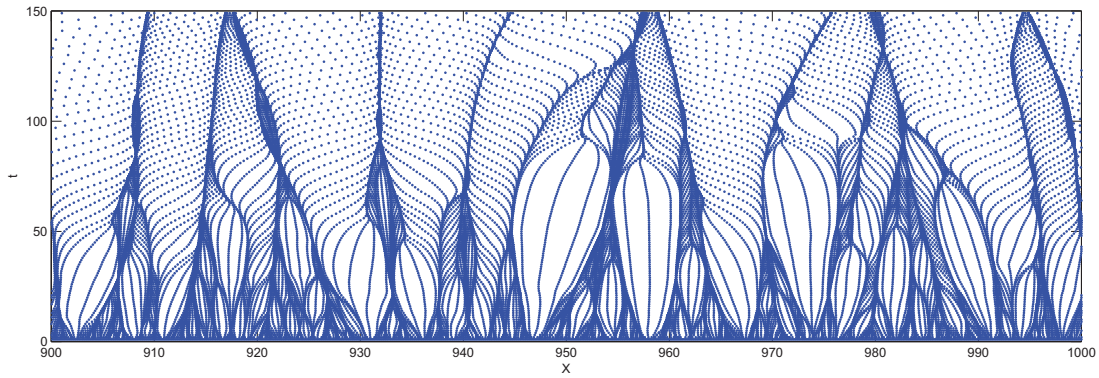

Figure A.10: Zoom out of the trajectory of particles where $x \in [900, 1000]$.

Bibliography

[1] A.L. Barabasi, H.E. Stanley, *Fractal Concepts in Surface Growth* , Cambridge University Press, Cambridge, England, (1995)

[2] M. Rost, J. Krug, *A particle model for Kuramoto-Sivashinsky equation*, *Physica D*, **88** (1995), 1-13

[3] F. Bouchut, *On zero-pressure gas dynamics*, Advances in Kinetic Theory and Computing, Sev. Adv. Math. Appl. Sci., 1994.

[4] Y. Brenier, E. Grenier, *Sticky particles and scalar conservation law*, SIAM J. Numer. Anal., 1998.

[5] F. Berthelin, *Existence and weak stability for a pressureless model with unilateral constraint*, Math. Models Methods Appl. Sci., **12** (2002) 249-272

[6] Tomas Bohr, Arcady Pikovsky, *Anomalous Diffusion in the Kuramoto-Sivashinsky Equation*, Physical review letters **70** (1993) 2892-2895

[7] J. Giannoulis, M. Herrmann, A. Mielke, *Continuum descriptions for the dynamics in discrete lattices: derviation and justification*, Springer, 435–466, (2006)

[8] Michel Peyrard, *Nonlinear dynamics and statistical physics of DNA*, Nonlinearity,**17** (2004) R1-R40

[9] Y. Kuramoto and T. Tsuzuki , *Persistent Propagation of Concentration Waves in Dissipative Media Far from Thermal Equilibrium*, Prog. Theor. Phys. 55, 356 (1976)

[10] Y. Kuramoto and T. Tsuzuki On the Formation of Dissipative Structures in Reaction-Diffusion Systems, Prog. Theor. Phys., **54** (1975) 687-699

[11] Y. Kuramoto and T. Tsuzuki , Supplement Prog. Theor. Phys. 64, 346 (1978)

[12] G. I. Sivashinsky, Acta Astronaut. 6, 569 (1979)

[13] G. I. Sivashinsky, *Nonlinear analysis of hydrodynamic instability in laminar flames - I*, Acta Astronaut. 4, 1177 (1977)

[14] G. I. Sivashinsky, *Instabilities, pattern formation, and turbulence in flames*, *Ann. Rev. Fluid. Mech.*, **15** (1983), 179-199

[15] Hayot F., Jayaprakash C., and Josserand C., *Long-wavelength properties of the Kuramoto-Sivashinsky equation*, Physical Review E., **47** (1993), 911-915

[16] K. Sneppen, J. Krug, M. H. Jensen, C. Jayaprakash, T. Bohr, *Dynamic scaling and crossover analysis for the Kuramoto-Sivashinsky equation*, Physical Review A, **46** (1992), 7351-7354

[17] S. Park, B. Kahng, H. Jeong, and A.-L. Barabisi, *Dynamics of Ripple Formation in Sputter Erosion: Nonlinear Phenomena*, Phys. Rev. Lett., **83** (1999) 3486-3489

[18] Eric S. Hood, Brian H. Toby, and W. H. Weinberg, *Precursor-Mediated Molecular Chemisorption and Thermal Desorption: The Interrelationships among Energetics*, Kinetics, and Adsorbate Lattice Structure, Phys. Rev. Lett., **55** (1985), 2437-2440

[19] S. Zaleski, *A stochastic model for the large scale dynamics of some fluctuating interfaces*, Physica D **34** (1989) 427-438 North-Holland, Amsterdam

[20] Felix Otto, *Optimal bounds on the Kuramoto-Sivashinsky Equation*, Journal of Functional Analysis **257** (2009) 2188-2245

[21] Laurent Boudin, Julien Mathiaud, *A numerical scheme for the scalar pressureless gases system*, HAL (2010)

[22] T.C. Kim, C. M. Ghim, H. J. Kim, D. H. Kim, D.Y. Noh, N. D. Kim, J.W. Chung, J. S. Yang,Y. J. Chang,T.W. Noh, B. Kahng, J.-S. Kim, Kinetic Roughening of Ion-Sputtered Pd(001) surface: Beyond the Kuramoto-Sivashinsky Model, Phys. Rev. Lett. 92 (2004) 246106

[23] S. Park, B. Kahng, H. Jeong, A.-L. Barabasi, Dynamics of Ripple Formation in Sputter Erosion: Nonlinear Phenomena, Phys. Rev. Lett. 83 (1999) 3486-3489

[24] K. B. Lauritsen, R Cuerno, H. A. Makse, Noisy Kuramoto-Sivashinsky equation for an erosion model, Phys. Rev. E. 54 (1996) 3577-3580

[25] B. Kahng, H. Jeong, A.-L. Barabasi, Quantum dot and hole formation in sputter erosion, Appl. Phys. Lett. 78 (2001) 805-807

[26] F. Frost, B. Rauschenbach, Nanostructuring of solid surfaces by ion-beam erosion, Appl. Phys. A 77 (2003) 1-9

[27] G. I. Sivashinsky, On self-turbulization of laminar flame, *Acta Astronautica* **6** (1979) 560-591

[28] J. Krug, Four lectures on the physics of crystal growth, Physica A **313** (2002) 47-82

[29] J. Krug, Kinetic patter formation at solid surfaces, in Collective Dynamics of Nonlinear and Disordered Systems, ed. G. Radons, W. Just, P. Haussler (Springer, Berlin, 2005), 5-37

[30] Ya. B. Zel'dovich, Gravitational instability: An approximate theory for large density perturbations, Astro. Astrophys., **5** (1970) 84-89

[31] E. Grenier, Existence globale pour le systhme des gaz sans pression , C. R. Acad. Sci. Paris Sér. I Math., **321** (1995) 171-174

[32] W. E, Yu. G. Rykov, Ya. G. Sinai, Generalized variational principles, global weak solutions and behavior with random initial data for systems of conservation laws arising in adhesion particle dynamics , Comm. Math. Phys., **177** (1996) 349-380

[33] F. Bouchut, F. James, One-dimensional transport equation with discontinuous coefficients, Non- linear Analysis, TMA, 32 (1998), **7**, 891-933

[34] F. Poupaud, M. Rascle, Mesure solutions to the linear transport equations with nonsmmooth coefficients, Comm. Partial Differential Equations, **22** (1997) 337-358

[35] M. Sever, An existence theorem in the large for zeros-pressure gas dynamics, Differential Interal Equations, **14** (2001) 1077-1092

[36] L. Boudin, A solution with bounded expansion rate to the model of viscous pressureless gases, SIAM J. Math. Anal. **32** (2000) 172-193

[37] G. Wolansky, Dynamics of a system of sticking particles of finite size on the line, Nonlinearity **20** (2007) 2175-2189

Thanh-Tam PHUNG

Vers un modèle particulaire de l'équation de Kuramoto-Sivashinsky

Résumé : (1700 caractères max.)

Dans cette thèse, on étudie des systèmes de particules en interaction dont le comportement est lié à certaines équations aux dérivées partielles lorsque le nombre de particules tend vers l'infini. L'équation de Kuramoto-Sivashinsky modélise par exemple la propagation de certains fronts de flamme, la topographie de la surface d'une couche mince en cours de croissance, et fait apparaître des structures macroscopiques. Un modèle de particules en interaction par un couplage harmonique des vitesses, attractif aux premièx vitesses voisines, répulsive aux secondes voisines, associée à des collisions élastiques, produit des profils de vitesses analogues aux fronts de flamme. On observe également la création et l'annihilation d'agrégats de particules. Un autre modèle, où les particules fusionnent lors des collisions en préservant masse et quantité de mouvement, et avec uniquement attraction au plus proche voisin, permet de retrouver un modèle de type gaz sans pression avec viscosité. Ces modèles sont étudiés théoriquement, en particulier les facteurs de mise à l'échelle des forces d'interaction sont précisés pour obtenir les équations correctes dans la limite du grand nombre de particules. Des simulations numériques confirment la validité et la pertinence des modèles.

Mots clés : modèle particulaire, Kuramoto-Sivashinsky, gaz sans pression

Particle models in connection with Kuramoto-Sivashinsky equation

Résumé : (1700 caractères max.)

This work is concerned by systems of interacting particles, which are linked to partial derivative equations when the particle number becomes large enough. The Kuramoto-Sivashinsky equation is actually modeling as well the front flame propagation as the morphology of growing interfaces, in deposition, for example. Moreover, surface periodical macroscopic structuring is occurring. An interacting particle model through an harmonic velocity coupling, attractive with the first velocity-neighbor and repulsive for the second neighbors, associated with elestic collisions. This model thus provides us with velocity profiles close to those of front flame propagation. Creation and annihilation of particle clusters is also observed. Another model, where particle are merging during collisions, while retaining mass and momentum conservation and with only nearest neighbor attraction, allows to recover a viscous pressureless gas model. These models are studied using mathematical tools. Especially interaction scaling factors are determined for obtaining the suitable equations in the large particle number limit. The numerical simulations confirm the relevance of the models.

Keywords : particle model, Kuramoto-Sivashinsky, pressureless gas

MAPMO & GREMI CNRS-Université d'Orléans